

2017

The Apoptotic and Wallerian Degeneration Pathways Regulate Disease Onset and Progression in the SOD-1G93A Transgenic Mouse Model of ALS

Deanna Belsky

Follow this and additional works at: http://digitalcommons.rockefeller.edu/student_theses_and_dissertations



Part of the [Life Sciences Commons](#)

Recommended Citation

Belsky, Deanna, "The Apoptotic and Wallerian Degeneration Pathways Regulate Disease Onset and Progression in the SOD-1G93A Transgenic Mouse Model of ALS" (2017). *Student Theses and Dissertations*. 387.
http://digitalcommons.rockefeller.edu/student_theses_and_dissertations/387

This Thesis is brought to you for free and open access by Digital Commons @ RU. It has been accepted for inclusion in Student Theses and Dissertations by an authorized administrator of Digital Commons @ RU. For more information, please contact mcsweej@mail.rockefeller.edu.



THE APOPTOTIC AND WALLERIAN DEGENERATION PATHWAYS
REGULATE DISEASE ONSET AND PROGRESSION IN THE *SOD-1*^{G93A}
TRANSGENIC MOUSE MODEL OF ALS

A Thesis Presented to the Faculty of
The Rockefeller University
in Partial Fulfillment of the Requirements for
the degree of Doctor of Philosophy

by
Deanna Belsky

June 2017

THE APOPTOTIC AND WALLERIAN DEGENERATION PATHWAYS
REGULATE DISEASE ONSET AND PROGRESSION IN THE *SOD-1^{G93A}*
TRANSGENIC MOUSE MODEL OF ALS

Deanna Belsky, Ph.D.

The Rockefeller University 2017

Amyotrophic Lateral Sclerosis is a neurodegenerative disorder characterized by progressive muscle denervation, motor axon degeneration and the death of motor neurons. The molecular mechanisms that mediate axon degeneration in ALS remain unknown, but motor neuron cell body death occurs through apoptosis. Genetic deletion of the pro-apoptotic gene *Bax* delays muscle denervation, prolongs disease onset, prevents motor neuron cell death and improves survival in an ALS mouse model. However, the timing and extent of axon degeneration in these mice is unaffected. Here, we examine the role of *Sarm1*, a component of the Wallerian degeneration pathway, and its interaction with the classical apoptotic cascade in ALS. Consistent with previous work, we find that genetic deletion of *Bax* delays symptom onset and extends lifespan of *SOD-1^{G93A}* transgenic mice. In contrast, elimination of *Sarm1* modestly delays axon degeneration at later stages of the disease without affecting lifespan. Genetic block of both pathways delays symptom onset, prolongs survival, and decreases disease burden by significantly reducing, by half, the number of days that mice exhibit disease-related symptoms. Our results demonstrate divergent

and mutually reinforcing roles for the apoptotic and Wallerian degeneration pathways in ALS and suggest the presence of a molecularly distinct pathway that mediates disease progression.

To my family and friends for all their continuous love and support.

Acknowledgments

I, first off, have to thank my mentor, Marc Tessier-Lavigne. While Marc was the president of Rockefeller University, he held many responsibilities beyond his laboratory, but this was never felt within the lab. He always took time to dedicate to his lab and was readily available for scientific discussions to move projects forward. Marc exemplifies an amazing scientist and a phenomenal leader. He enforced scientific rigor with a calm, professional demeanor that was echoed in the members he selected for his laboratory. I am extremely grateful to have been given the opportunity to work alongside such excellent scientists and people for the past five years.

The assortment of people that Marc chose could not have provided a better learning environment. Each member displayed scientific excellence, but much more than that, they also exhibit kindness, helpfulness, and give a reason to come into work every day. A special thank you to Olav, who besides setting up a great lab culture, was instrumental in the completion of my PhD work. From performing the neurological scoring protocol with me, despite his severe allergies to mice, to discussing scientific experiments and results, Olav has been key to helping this project succeed. Thank you to Kim, whose scientific rigor helped better my project in addition to helping create a wonderful working environment.

Thank you to my fellow graduate students, Shaun, Dylan, Andy, and more recently Eliza, Ross, and Ryan for helping me survive the ups and downs of graduate school. A special thanks to Shaun and Dylan for the friendship that

lasted throughout the more difficult times in graduate school. They were always there to listen when things turned for the worse, beyond colleagues; they will continue to be lifelong friends. Thank you to the post docs, Jing, Zhu hao, Nico, Yuya, Dave, Dominik, Nick, and more recently, Jianjin. Thank you to the lab technicians Jinjoo, Alice, and Kate who worked closely with me on this project. Thank you to Devrim and Hiro from the electron microscope facility who took part in this work and guided me in my analysis of electron microscopy. Thank you to Kaye and Allison in the bioimaging facility for all of their help and guidance in processing confocal images.

Thank you to those in the Dean's Office for selecting me to be a part of the Rockefeller graduate school community, Sid, Emily, Marta, Kristen, Cris, and Stephanie. The mitigation of the bureaucratic system made it easier to give back to the community and concentrate on the advancement of science. Rockefeller is a really special place that I will always hold dear to my heart.

Thank you to my committee members, Shai Shaham and Cori Bargmann for the helpful advice throughout my PhD. They were there to both give scientific feedback and suggestions and also, personal guidance in which I am extremely grateful.

I lastly want to thank my family and friends. My parents and siblings for always being there to guide me through difficult turning points and my friends for their continual support. Graduate school would not be the same without you.

Table of Contents

Acknowledgments	iv
Table of Contents	vi
List of Figures	viii
List of Tables.....	x
List of Abbreviations	xi
Chapter 1: Introduction and Overview of the Field.....	1
Rationale	1
Amyotrophic Lateral Sclerosis Prevalence and Types.....	2
Genetic and molecular underpinnings of ALS.....	5
SOD-1 function and mutations.....	8
<i>SOD-1</i> transgenic mouse models to study ALS	10
Cell autonomous mechanisms in ALS.....	15
Mechanisms of Apoptosis	19
The role of the apoptotic pathway in ALS.....	22
Anatomical features of <i>Bax</i> deletion in the <i>SOD1G93A</i> mouse model	28
The Wallerian degeneration pathway	30
Perspective and overview of thesis project.....	35
Chapter 2: Apoptosis and Wallerian degeneration affect disease onset and progression	39
Rationale	39
<i>Bax</i> , but not <i>Sarm1</i> deletion extends survival of the <i>SOD-1G93A</i> Tg mouse model.....	39
<i>Sarm1</i> involved in early stages and <i>Bax</i> involved in late stages of the disease.....	44
Elimination of both <i>Bax</i> and <i>Sarm</i> decreases symptomatic stages in ALS	46
Conclusions	47
Chapter 3: Histological analysis tracks with disease.....	48
Rationale	48
<i>Bax</i> and <i>Sarm1</i> play distinct roles in neuromuscular junction denervation	48
<i>Sarm1</i> deletion slightly delays axon degeneration in <i>SOD-1G93A</i> Tg animals.....	54
Deletion of <i>Bax</i> and <i>Sarm1</i> delays large neuron loss in ventral horn.....	57
Deletion of <i>Bax</i> and <i>Sarm1</i> delays loss of MMP-9+ neurons.....	61
Conclusions	63
Chapter 4: Non-cell autonomous SOD-1 toxicity	64
Rationale	64
Co-culture of motor neurons and astrocytes.....	64
Non-cell autonomous SOD-1 toxicity causes motor neuron cell death, but not axon degeneration.....	67
Conclusions	70
Chapter 5: Discussion and Future Directions	71
The role of <i>Sarm1</i> in the <i>SOD-1G93A</i> Tg model of ALS.....	72
The role of <i>Bax</i> in the <i>SOD-1G93A</i> Tg ALS mouse model.....	74
The synergistic role of <i>Bax</i> and <i>Sarm</i>	75
Future Directions.....	77

Chapter 6: Materials and Methods.....	80
Animal models	80
Rotorod behavioral assay	82
Tissue collection	82
Neuromuscular Junction Analysis	83
Axon counts and electron microscopy	84
Neuron number in the ventral horn of the spinal cord.....	84
Statistical analysis.....	85
Primary astrocyte culture.....	86
Astrocyte conditioned medium	86
Primary motor neuron culture	87
Ventral explant cultures	87
Appendix 1: <i>SOD-1</i>WT Histology	89
Appendix 2. MMP-9+ cells at all timepoints in <i>SOD-1G93A</i> Tg animals ..	96
Appendix 3. Treatment of infection with antibiotics.....	98
References	100

List of Figures

Figure 1.1 Illustration of areas affected in ALS.....	4
Fig 1.2 Mutations that cause familial and sporadic forms of ALS.....	5
Fig 1.3 Histological analysis of <i>SOD-1^{G93A}</i> Tg mouse model throughout disease progression.....	13
Fig 1.4 ALS includes cell autonomous and non-cell autonomous mechanisms.....	17
Figure 1.5 The role of non-cell autonomous mutant <i>SOD-1</i> on motor neurons <i>in vitro</i>	18
Figure 1.6 Apoptotic Pathway Schematic.....	21
Fig 1.7 The role of anti-apoptotic factors in a mouse model of ALS.....	23
Fig 1.8 The Role of Bax in an <i>SOD1G93A</i> mouse model of ALS.....	25
Fig 1.9 Evidence of downstream executors of apoptosis in ALS mouse models.....	27
Figure 1.10 Anatomical features of the <i>SOD-1G93A/Bax</i> KO mouse line.....	29
Figure 1.11 Conflicting results for role of <i>Wld^S</i> mouse in ALS.....	32
Fig 1.12 <i>Sarm1</i> KO protects against axon degeneration and NMJ denervation.....	34
Figure 1.13 <i>SOD-1^{G93A}</i> Tg, <i>Sarm1^{-/-}</i> has effect on disease progression, but no effect on survival.....	36
Figure 2.1 <i>SOD-1^{G93A}</i> copy number analyzed by qPCR.....	40
Figure 2.2. Survival and body weight loss of <i>SOD-1^{G93A}</i> Tg mice.....	41
Figure 2.3. Rotorod Behavioral Assay.....	43
Figure 2.4 Disease onset and progression of <i>SOD-1^{G93A}</i> Tg mice.....	45
Figure 2.5 Duration and complete progression of <i>SOD-1^{G93A}</i> Tg mice.	46
Figure 3.1 Neuromuscular junction denervation of the tibialis anterior muscle throughout disease progression.....	50
Figure 3.2 Neuromuscular junction denervation of the gastrocnemius muscle throughout disease progression.....	51
Figure 3.3 Neuromuscular junction quantification of the tibialis anterior and gastrocnemius muscle.....	53
Figure 3.4. Motor axon degeneration in ventral root.....	55
Figure 3.5. Quantification of large and small diameter axons in ventral root.....	56

Figure 3.6. Neuron cell body loss in the ventral horn of the spinal cord.....	59
Fig 3.7. MMP-expressing neuron loss in ventral horn of spinal cord.....	62
Fig 4.1 Motor neuron loss after treatment with SOD-1 astrocyte conditioned medium.....	65
Fig 4.2 Peripherin as a marker for motor neurons.....	66
Fig 4.3 SOD-1 CM causes motor neuron cell death in dissociated culture, but not ventral explant culture.....	69
Figure A1.1. Neuromuscular junction innervation at endstage.....	89
Figure A1.2. Motor axon degeneration in ventral root.....	91
Figure A1.3. Neuron cell body in ventral horn of spinal cord.....	92
Figure A1.4. MMP-9+ cell body in ventral horn of spinal cord.....	94
Figure A2.1. MMP-9+ cell body in ventral horn of spinal cord in <i>SOD-1^{G93A}</i> Tg animals.....	97
Figure A3.1 Abnormalities in disease progression of <i>SOD-1^{G93A}</i> Tg animals.....	99

List of Tables

Table 1.1 Genes known to carry ALS-causing mutations.....	6
Table 1.2 Other genes implicated in the pathogenesis of ALS.....	7
Table 6.1 Genotypes analyzed in this study.....	81
Table 6.2 Antibodies used in this study.....	85

List of Abbreviations

ALS	Amyotrophic Lateral Sclerosis
C9ORF72	Hexanucleotide repeat expansion in C9ORF72
CM	Conditioned medium
dSarm	Drosophila sterile a/Armadillo/Toll-Interleukin receptor homology domain protein
ES	Endstage
fALS	familial Amyotrophic Lateral Sclerosis
FTLD	Frontotemporal lobar dementia
FUS	Fused in sarcoma
LMN	Lower motor neuron
NMJ	Neuromuscular junction
Ntg	Non-transgenic
OPTN	Optineurin
PCD	Programmed cell death
PMN	Primary motor neuron
sALS	Sporadic Amyotrophic Lateral Sclerosis
SOD-1	Superoxide dismutase 1
TARDBP	TAR DNA-binding protein
Tg	Transgenic
UMN	Upper motor neuron
VCP	Valosin-containing protein
WT	Wild type

Chapter 1: Introduction and Overview of the Field

Rationale

Neurodegenerative disorders are characterized by the disruption and death of neuronal cells. Different neurodegenerative diseases result in a loss of distinct neuronal cell types, particularly in their early stage. For example, Alzheimer's disease is mainly characterized by the loss of cortical neurons, Parkinson's affects dopaminergic neurons in the substantia nigra, Huntington's causes death of striatal neurons in the basal ganglia, and amyotrophic lateral sclerosis (ALS) is specific to motor neurons and corticospinal neurons. While different neuronal cell types are affected, there is evidence that similar cell death pathways are active during degeneration in these unique diseases. In this study, we will focus on neuronal cell death of motor neurons in ALS, but hope that elucidation of these cell death mechanisms may be applied more broadly to neuron degeneration in neurodegenerative diseases, in general.

Amyotrophic Lateral Sclerosis (ALS) is a fatal disorder that results in degeneration of motor neurons located in the brain and spinal cord, which leads to paralysis and eventual death. Studies have described ALS as a "dying back" disorder, which begins with disruption in synaptic connections at the neuromuscular junction, followed by axon degeneration resulting in motor neuron cell death (Fischer et al, 2004). While the anatomical features of the disease

have been well documented, the underlying molecular mechanisms remain unknown.

Since axon degeneration precedes motor neuron loss, we thought by targeting mechanisms of axon degeneration we might be able to delay onset or prevent disease progression in an ALS mouse model. The work in this thesis examines an approach to target an axon degeneration mechanism known to be involved in other motor neuronopathies that is distinct from other cell death pathways. Since it is already known that the apoptotic pathway is involved in ALS, we further attempt to elucidate the interaction of these two pathways in a murine model of ALS.

Amyotrophic Lateral Sclerosis Prevalence and Types

Amyotrophic Lateral Sclerosis (ALS), sometimes referred to as Charcot's sclerosis (named after Jean-Martin Charcot who discovered the disease) or Lou Gehrig's disease, is a rapidly-progressing adult-onset neurodegenerative disorder characterized by degeneration of upper and lower motor neurons, which leads to paralysis and eventual death (Cleveland and Rothstein, 2001) (Figure 1.1). ALS has a prevalence of about 2 per 100,000 total cases each year (O'Toole et al, 2004), with multiple studies showing an increased risk in males (Vazquez et al, 2008). The average age of onset for a typical ALS patient is between 50-65 (Logroscino et al, 2008; O'Toole et al, 2008) and progression of the disease is typically very rapid with the time from disease onset until death

ranging from three to five years. While most cases of ALS have a late onset and fast progression, 5% of cases are juvenile forms where onset occurs much earlier between the ages of 20-40 (Andersen et al, 2011). These juvenile cases usually progress more slowly from onset until death and predominantly affect so called upper motor neurons (i.e., corticospinal tract neurons, with cell bodies in layer V of the cortex) (Pupillo, et al, 2014; Zoccolella et al, 2008; Sabatelli et al, 2008).

About 10% of ALS cases are inherited as an autosomal dominant trait (Leblond et al, 2014; Sreedharan et al, 2013) with the remaining 90% caused by sporadic mutations. Familial ALS (fALS) and sporadic ALS (sALS) both have similar pathological hallmarks (Boillée et al, 2006; Ferraiuolo et al, 2011) including progressive muscle weakness, atrophy, and spasticity (Amato et al, 2008) with denervation of the respiratory muscles as the fatal event for most patients. The type of mutation does seem to affect the site of onset of the disease with some sites resulting in a more aggressive form of ALS. For example, ALS patients with onset in the bulbar muscles have a mean survival of 2 years (Chiò et al, 2011). This shows that some patients do have a genetic component, however pathology at autopsy is very similar in ALS patients with different mutations (Iwanaga et al, 1997).

Patients with either fALS or sALS can develop frontotemporal lobar dementia (FTLD) as well. FTLD is characterized by degeneration of layer V neurons located in the frontotemporal lobe of the cortex, which results in behavioral changes (Figure 1.1). 25% of patients with ALS display clinical FTD

(Swinnen, et al 2014) through language abnormalities, disinhibition, delusions (Strong et al, 2011; Mioshi et al, 2014), and depression (although whether depression is caused by cognitive changes or reactive depression is difficult to tell) (Ferrari et al, 2011).

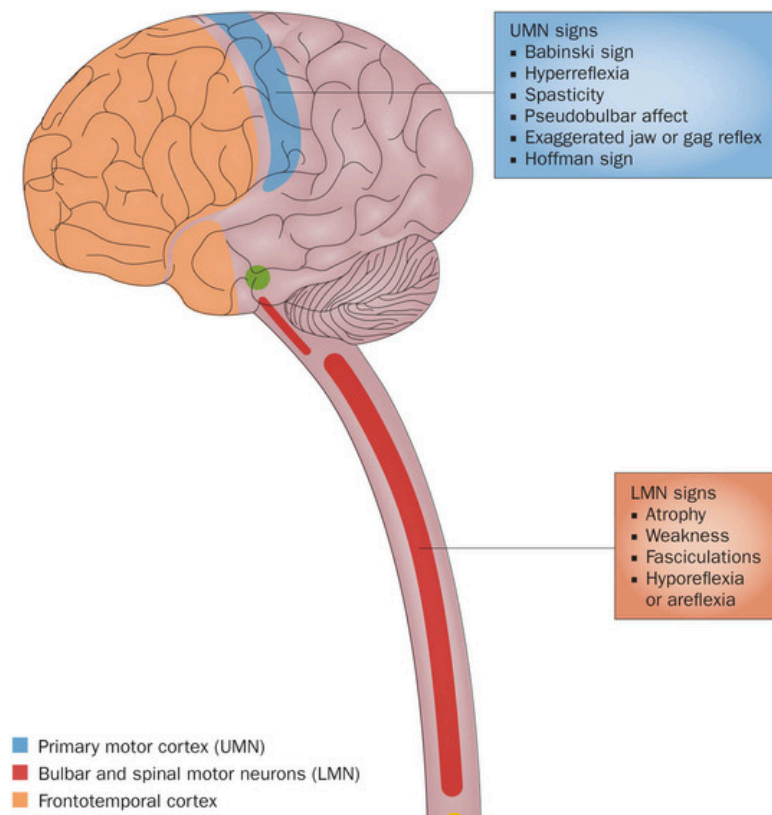


Figure 1.1 Illustration of areas affected in ALS. Upper motor neurons (UMN) (in blue) and lower motor neurons (in red) are the areas affected in both familial and sporadic ALS. 25% of these cases are associated with degeneration in layer V of the frontotemporal lobe (in orange). Degeneration of each of these components causes different phenotypes listed in the blue box for UMN degeneration and the orange box for LMN degeneration (Swinnen, et al 2014).

Genetic and molecular underpinnings of ALS

Over the past few years, great progress has been made in determining the genetic etiology of ALS, which has in turn led to insights into molecular mechanisms of neurodegeneration. ALS was thought initially to be a non-hereditary disease. It wasn't until 1955 that a hereditary form was identified (Kurland and Mulder 1955). As mentioned above, 10% of ALS cases have been identified as familial with the rest labeled as sporadic, but in part caused by identifiable mutations. Currently, the genetic etiology of two-thirds of fALS and 11% of sALS are known to be caused by genetic mutations (Figure 1.2).

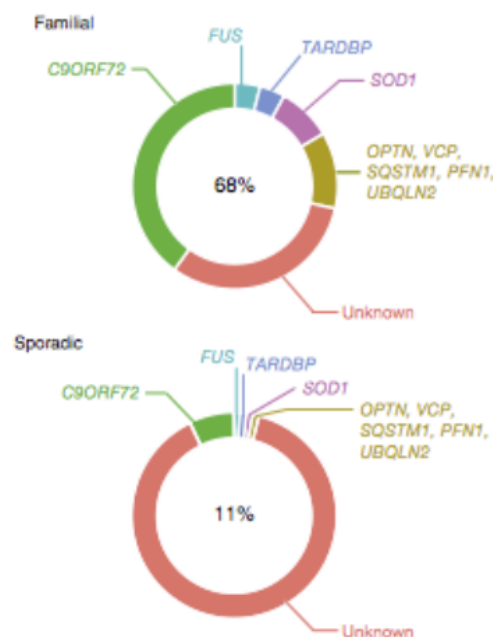


Fig 1.2 Mutations that cause familial and sporadic forms of ALS. Genes with mutations found to cause familial (top circle) or sporadic (bottom circle) forms of ALS. Each color identifies one gene including C9ORG72 (green), FUS (light blue), TARDBP (dark blue), SOD-1 (purple), other genes that contribute including OPTN, VCP, SQSTM1, PFN1, UBQLN2 (yellow) and unknown (red). The number in the middle of the circle represents the total fraction of either fALS or sALS cases (Renton et al, 2014).

The first gene mutation identified in an ALS patient was in the superoxide dismutase-1 (*SOD-1*) gene (Rosen et al, 1993). The next gene, TARDBP, was not identified until fifteen years later (Sreedharan et al, 2008). Advances in technology and computation, such as GWAS studies, have led to the discovery of many more contributing genes in recent years, including fused in sarcoma (FUS), valosin-containing protein (VCP), optineurin (OPTN), ubiquilin 2 (UBQLN2), sequestosome 1 (SQSTM1) and a hexanucleotide repeat expansion in C9ORF72 (Kwiatkowski et al, 2009; Vance et al, 2009; Johnson et al 2010; Renton et al 2011; DeJesus-Hernandez et al, 2011; Maruyama et al, 2010) (Figure 1.2 and Table 1.1).

Table 1.1 Genes known to carry ALS-causing mutations. Genes identified to be mutated in ALS (first column), location of gene on the chromosome (second column), how the gene is inherited as autosomal dominant (AD), autosomal recessive (AR) or X-linked dominant (XD) (third column), percentage of cases in which this gene has been shown to cause either fALS or sALS (fourth and fifth column, respectively), and putative protein function (sixth column) (Renton et al, 2014).

Gene	Location	Inheritance	Percentage explained		Putative protein function
			Familial ALS	Sporadic ALS	
<i>TARDBP</i>	1p36	AD	4	1	RNA metabolism
<i>SQSTM1</i>	5q35	AD	1	<1	Ubiquitination; autophagy
<i>C9ORF72</i>	9p21	AD	40	7	DENN protein
<i>VCP</i>	9p13	AD	1	1	Proteasome; vesicle trafficking
<i>OPTN</i>	10p13	AR and AD	<1	<1	Vesicle trafficking
<i>FUS</i>	16p11	AD and AR	4	1	RNA metabolism
<i>PFN1</i>	17p13	AD	<1	<1	Cytoskeletal dynamics
<i>SOD1</i>	21q22	AD and AR	12	1–2	Superoxide metabolism
<i>UBQLN2</i>	Xp11	XD	<1	<1	Proteasome

Values represent the percentage of ALS explained by each gene in populations of European ancestry. References are provided in the main text. AD, autosomal dominant; AR, autosomal recessive; XD, X-linked dominant; DENN, differentially expressed in normal and neoplasia.

Other genes have also been identified in rare cases to cause ALS or ALS-like pathology (Hadano et al, 2001; Eymard-Pierre et al 2002; Chen et al, 2004; Duquette et al, 2005) (Table 1.2).

Table 1.2 Other genes implicated in the pathogenesis of ALS. Multiple additional genes have been reported with rare mutations that can cause ALS. Most of these mutations cause a juvenile onset, slower progressing version of the disease. Column labels are similar to Table 1.1 and listed in above legend.

Gene	Location	Inheritance	Predominant clinical syndromes	Putative protein function
<i>DCTN1</i>	2p13	AD	PMA; Perry syndrome	Axonal transport
<i>ALS2</i>	2q33	AR	Juvenile PLS; infantile HSP	Vesicle trafficking
<i>CHMP2B</i>	3p11	AD	Familial ALS; sporadic ALS; FTD	Vesicle trafficking
<i>FIG4</i>	6q21	AD and AR	CMT; familial ALS	Vesicle trafficking
<i>HNRNPA2B1</i>	7p15	AD	Multisystem proteinopathy; ALS	RNA metabolism
<i>ELP3</i>	8p21	Undefined	Sporadic ALS	RNA metabolism
<i>SETX</i>	9q34	AD	Juvenile ALS; ataxia with oculomotor apraxia	RNA metabolism
<i>HNRNPA1</i>	12q13	AD	Multisystem proteinopathy; ALS	RNA metabolism
<i>ATXN2</i>	12q24	Undefined	Sporadic ALS; ataxia	Endocytosis; RNA translation
<i>ANG</i>	14q11	AD	Familial ALS; sporadic ALS	Angiogenesis
<i>SPG11</i>	15q14	AR	Juvenile ALS; HSP	DNA damage repair
<i>VAPB</i>	20q13	AD	PMA; FALS	Vesicle trafficking
<i>NEFH</i>	22q12	AD	Familial ALS; sporadic ALS	Axonal transport

AD, autosomal dominant; AR, autosomal recessive; CMT, Charcot-Marie-Tooth disease; HSP, hereditary spastic paraplegia; PLS, primary lateral sclerosis; PMA, progressive muscular atrophy.

Some commonalities between protein function of mutated genes in ALS have been found, such as RNA metabolism dysfunctions in the TARDBP and FUS genes, proteasome and vesicle transport defects in VCP, OPTN and UBQLN2, and axonal transport and vesicle trafficking defects in various slow progressing and juvenile onset forms, but there does not seem to be one overarching theme of protein function that is deregulated in motor neuron degeneration in ALS, since many different types of dysfunctions can cause ALS symptoms.

SOD-1 function and mutations

As mentioned above, the first gene mutation identified to cause familial ALS was in the gene encoding superoxide dismutase 1 (*SOD-1*) (Rosen et al, 1993). 20% of the 10% of fALS cases have been attributed to *SOD-1*, making up 2-5% of all ALS cases. *SOD-1* encodes a cytosolic, Cu/Zn-binding protein that catalyzes the conversion of toxic superoxide O_2^- to O_2 and H_2O_2 (Fridovich, 1976). SOD-1 is located in the cytosol, nucleus, peroxisomes, and mitochondrial intermembrane space (Fridovich I, 1997; Okado-Matsumoto et al, 2001; Sturtz LA et al, 2001).

Although the function of SOD-1 is known, it has been very difficult to determine the nature of its dysfunction in ALS. This is because over 100 different mutations have been identified in the *SOD-1* gene to cause ALS (Valentine et al, 2004), but these mutations vary in biochemical properties, stability, and protein

function (Hayward et al, 2002; Rodriguez et al, 2002; Tiwari et al, 2003). Mutated sites include positions in the metal-binding ligand or electrostatic loop that might perturb metal binding affinity, positions at the disulfide bond where protein stability might be affected, and truncations that would not allow dimerization to occur. On the other side of the spectrum, many SOD1 mutations occur in locations far away from critical areas of protein function. Some of the mutant forms of SOD-1 retain nearly normal SOD1 activity. It is therefore thought that mutant SOD-1 exerts its effect through a gain of function mutation. This conclusion is further supported by a lack of an ALS phenotype in SOD-1 deficient mice (Reaume et al, 1996) or mice overexpressing human wild-type SOD-1 (Gurney et al, 1994).

Mutations that affect different SOD1 functions also do not correlate with survival times. Mutations in human SOD1 that result in an activity similar to WT SOD1 show a greater than seventeen-year survival for G37R, G41D, and E100K, about ten year survival for G93C, about five years for E100G, one to three years for L38V, H43R, and G93A, and one year for A4V (Orrell et al, 1999; Parton et al 2002). Mutations in SOD1 found in the metal binding region have similar variability with a greater than seventeen-year survival for H46R (Abe et al, 1996), six years for G85R (Juneja et al, 1997), and very short survival times for H48Q and S134N.

Information on how mutations in SOD1 affected its activity levels came from studies in yeast. Human WT SOD1 and multiple SOD1 mutant proteins,

including A4V, G37R, L38V, G41D, G85R, G93A, G93C, and I113T, rescued the O_2^- negative phenotype of the *sod1 Δ* yeast strain (Rabizadeh et al, 1995; Corson et al, 1998). H46R and H48Q mutant SOD1 did not rescue this phenotype (Ratovitski et al, 1999), indicating that SOD-1 activity is not the cause of the ALS phenotype.

There is some evidence that mutated SOD-1 protein aggregates in ALS, which is similar to what is seen in other neurodegenerative disorders, such as $a\beta$ plaques in Alzheimer's disease and Lewy bodies in Parkinson's disease (Soto et al, 2003; Valentine et al, 2003). Mutated SOD-1 human patient samples have been found to have inclusions containing neurofilament, ubiquitin, and SOD1 protein aggregates. These protein aggregates are not thought to be toxic since accumulation occurs during late stages of the disease (Morrison et al, 1998). However, high molecular weight oligomers of SOD1 are found well before disease onset in mice expressing mutant SOD1 so this evidence does indicate that mutant SOD1 does differ in some feature from its wild type form to allow for oligomerization (Wang et al, 2002; Johnston et al, 2000).

***SOD-1* transgenic mouse models to study ALS**

Multiple mutant *SOD-1* transgenic mouse models have been created that reproduce the human disease phenotype (Wong et al, 1995; Bruijn et al, 1997; Ripps et al, 1995; Brännström et al, 2000). Transgene copy number of mutated *SOD-1* has been found to be important in determining disease phenotype. High

transgene copy number causes early onset and a rapidly progressive disease, whereas low transgene number causes a late onset and a slower progressing form (Dal Canto et al, 1995; Dal Canto et al, 1997). Three well-characterized transgenic *SOD1* mutant lines are the G93A (Nagai et al, 2001), G37R (Wong et al, 1995) and the G85R (Bruijn et al, 1997) mutation, each expressing a high transgene copy number.

Although disease onset and survival vary among transgenic mouse strains, many pathological features remain constant and comparable to ALS patients. Hind limb weakness and tremors usually occur at symptom onset, followed by progressive motor paralysis and eventually death. The early onset, fast progressing transgenic mouse model, *SOD1G93A*, dies around four to five months. The gray matter of the motor neuron system is most dramatically affected in mutant *SOD1* transgenic mice, specifically the ventral horn and brainstem motor nuclei, which are not affected in non-transgenic or WT *SOD-1* overexpressing mice (Wong et al, 1995; Bruijn et al, 1997; Ripps et al 1995; Gurney et al 1994; Friedlander et al 1997). In transgenic mice with high *SOD-1* copy number, lesions have also been seen to extend into other areas such as the dorsal horn of the spinal cord, vagal nerve dorsal nuclei, brainstem reticular formation, substantia nigra, cerebellum, and thalamus.

Numerous malfunctions of various biological processes have been identified in ALS mouse models including protein aggregations, mitochondrial abnormalities, axonal transport dysfunction, dysregulation of calcium metabolism,

high glutamate levels, and oxidative damage (Brujin et al, 2004, Ilieva et al, 2007, Lev et al, 2009). Interestingly, the morphological changes in lower motor neurons seem to occur in a “dying back” fashion in mice (Frey et al, 2000). This phenotype is manifested through weakening at the synapse, followed by axon degeneration, which precedes motor neuron cell body loss. This phenomenon is not unique to ALS, since this type of disease progression is also seen in progressive motor neuropathy mouse models (Schmalbruch et al, 1991). Studies have elucidated similar spatiotemporal progression of the disease in an *SOD1G93A* transgenic ALS mouse model (Fischer et al, 2003).

It has been well reported that a pathological phenotype precedes disease onset. Fischer et al. (2003) discovered that neuromuscular junction (NMJ) denervation begins at day 47, while clinical stages of the disease do not occur until day 80. This study also pointed out that ventral root motor axons were affected between these two timepoints and a loss of alpha motor neurons (the vulnerable subtype of motor neurons in ALS) did not occur until day 100 (Figure 1.3). This same study also analyzed a 58-year-old ALS patient who died unexpectedly before undergoing full progression of the disease. Samples from this patient showed atrophy in leg muscles, but very little axon degeneration. Also, motor neuron number in the spinal cord was normal. This case is anecdotal and therefore cannot be used to generalize a common pathology in mice and humans, but is an indication that something similar might be occurring.

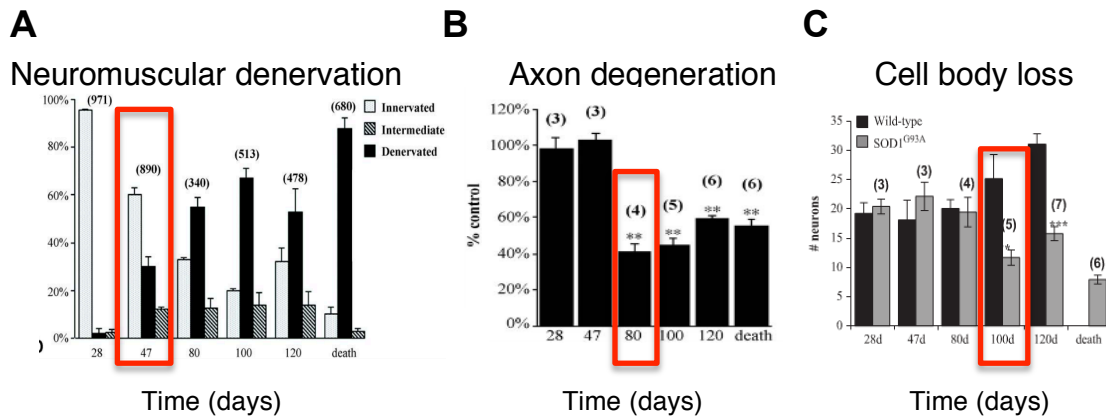


Fig 1.3 Histological analysis of *SOD-1^{G93A}* Tg mouse model throughout disease progression. A) Percentage of neuromuscular junction innervation (white), partially innervated (gray), and denervated (black) at various timepoints throughout disease. B) Percentage of axon degeneration at various timepoints. C) Number of neuron cell bodies in the ventral horn at various timepoints. Red boxes indicate the timepoint where significant loss is seen of each parameter (Fischer et al, 2003).

Other groups went on to characterize the loss of neuromuscular junction innervation in more detail. The hindlimb muscles are dramatically affected at early stages and throughout the disease and are therefore the major site analyzed in many studies. The mouse hindlimb contains three major muscles that have been analyzed extensively. These include the gastrocnemius, the tibialis anterior, and the soleus muscles. Each of these muscles contains a different composition of fast and slow twitch fibers. The gastrocnemius and tibialis anterior muscles are composed mostly of fast twitch fibers, referred to as Type IIB fibers. The soleus muscle is made up mostly of slow fibers, or Type IIA fibers.

Identification of a third category of muscle, the Type IID fibers, is intermediate between the fast and slow fibers. Fast fibers rely on more glycolytic mechanisms for metabolism, while slow fibers use oxidative mechanisms. Type IID fibers use a combination of both of these mechanisms, but are still categorized as fast fibers.

EMG recordings of whole muscle and motor unit contractile forces were taken from both fast and slow muscle fibers at different timepoints in a *SOD1G93A* transgenic mouse model (Hegedus et al, 2007). They found that there was an initial loss of fast motor unit function, but not slow motor units. Slow motor unit loss occurred later and the loss of overall motor units in the hind limb plateaued during symptomatic stages of the disease. These results are consistent with immunohistochemical evidence showing that denervation occurs in a muscle specific manner. This makes sense since fast motor units innervate fast muscle fibers and slow motor units innervate slow muscle fibers.

It is thought that clinical symptoms occur after denervation due to the ability of the remaining axons that innervate slow fibers to reinnervate muscle fibers through collateral sprouting. Motor axons that innervate fast fibers, the most vulnerable type, are not able to sprout and reinnervate target muscles, while the axons that innervate slow fibers retain this ability (Frey et al, 2000). Compensatory sprouting occurs until a critical point is reached where reinnervation is unable to substitute for the increased denervation, which is when

muscle weakness or symptomatic stages of the disease occur (Felice et al, 1997; Hayworth et al, 2009).

It has been shown that large caliber axons are the most susceptible in an *SOD1G93A* mouse model (Feinberg et al, 1999, Bendotti et al, 2001, Fischer et al, 2003). Others have provided further insight into the mechanisms underlying this vulnerability (Pun et al 2006). The large size of the axons might indicate a greater dependency on axonal transport. This is consistent with studies that show perturbations in various axonal transport proteins can cause symptoms of ALS in motor neuron diseases and have also been identified in the *SOD1G93A* mouse, specifically neurofilament aggregates. Other studies have shown enlarged mitochondria in the distal part of large axons in the sciatic nerve of the *SOD1G93A* mouse at presymptomatic stages of the disease and in sporadic ALS patients (Siklos et al, 1996, Dadon-Nachum et al, 2011).

Multiple studies identify synapses at the NMJ as a vulnerable location for motor neuron axons. A few hypotheses currently exist, but no one abnormal function has been attributed to synaptic dysfunction leading to axon degeneration. Some information is known about the mechanisms of cell body loss following axon degeneration, which will be discussed in later sections.

Cell autonomous mechanisms in ALS

Descriptive studies examining the anatomical features of motor neuron cell death in the mutant SOD-1 disease mouse model led many to believe that the

disruption was occurring in neuronal cells. The first evidence that mutant SOD-1-mediated cell death was not solely neuronal came from evidence where human mutant SOD-1 was expressed exclusively in motor neurons, but did not cause ALS symptoms (Pramatarova et al, 2001). The *SOD-1*^{G37R} high transgene copy number was driven under the neurofilament promoter and although mutant SOD-1 expression was high in motor neurons in the spinal cord, no cell body loss in the spinal cord or axon degeneration in the ventral root was observed. In addition, there was no effect on motor performance when testing motor function using the limb grip strength test.

Other work pointing to a non-cell autonomous component driving ALS was work from Clement et al, who showed that the ALS phenotype observed in the SOD-1 mutant mouse was driven by a combination of cell autonomous and non-cell-autonomous processes. In this study, researchers created mutant SOD-1 chimeric mouse lines that express both mutant SOD-1 and WT cells and showed that non-mutant SOD-1 motor neurons develop an ALS pathology, specifically SOD-1 aggregate and ubiquitin accumulation, which causes these WT cells to atrophy. This group also went on to show that nonneuronal non-mutant SOD-1 cells can delay or prevent degeneration of ventral root axons and motor neuron loss in the spinal cord and ultimately result in an extended lifespan in these chimeric lines compared to SOD-1 mutant lines (Figure 1.4) (Clement et al, 2003).

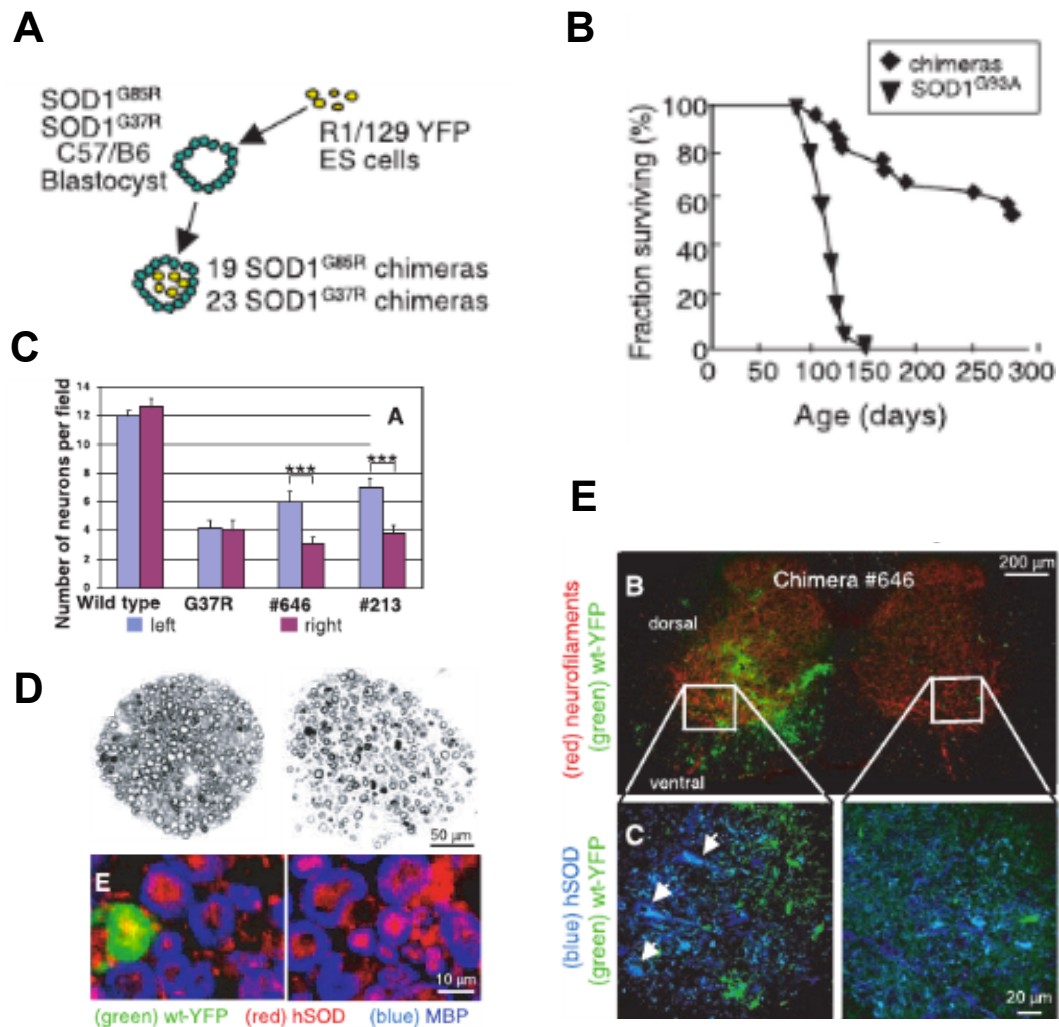


Fig 1.4 ALS includes cell autonomous and non-cell autonomous mechanisms. A) Chimeric *SOD1*^{G85R} and *SOD1*^{G37R} mutants were created by injecting WT YFP expressing ES cells into *SOD1*^{G85R} and *SOD1*^{G37R} mutant animals at the blastocyst stage. B) Survival curve showing extended survival in chimeras vs. mutant SOD-1 lines. C) Number of neurons in ventral spinal cord per field quantified for WT, *SOD-1*^{G37R}, and two chimeric lines (#646 and #213) where the left side contained WT expressing YFP cells and the right side did not. Representative image of D) motor axons in ventral root of chimeric line #646 showing degeneration in right side without WT expressing-YFP cells and E) motor neurons in spinal cord degenerated without WT non-neuronal cells present. (Clement et al, 2003)

Since this finding, other groups have tried to identify the source of the non-cell autonomous toxic effect. There are conflicting results in the field as to what is the driving factor that causes SOD-1 mediated toxic cell death. Nagai et al isolated conditioned medium from mutant SOD-1 astrocytes and found it to cause primary motor neuron cell death (Nagai et al, 2007). Other labs have identified microglia as the major contributor to motor neuron cell death *in vitro* (Fig 1.5) (de Boer et al, 2014).

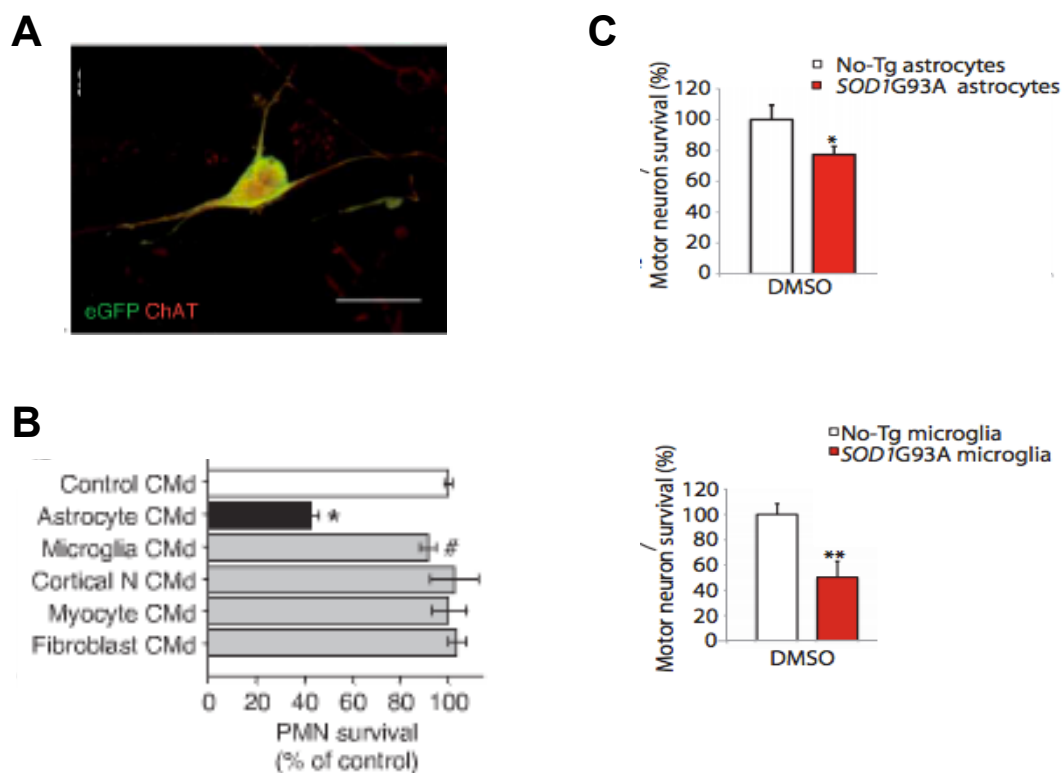


Figure 1.5 The role of non-cell autonomous mutant SOD-1 on motor neurons *in vitro*. A) Isolation and identification of motor neurons through Hb-9-GFP and ChAT staining. B) Conditioned medium from mutant SOD-1 astrocytes, but not any other cell type shows motor neuron cell death. C) Another study shows motor neurons cultured with mutant SOD-1 microglia (bottom panel) have an even greater cell death effect than when cultured with mutant SOD-1 astrocytes (top panel). Red bar = SOD-1^{G93A} treated, White bar = Non-transgenic treated (Nagai et al, 2007 A, B; de Boer et al 2014 C). PMN = primary motor neuron

Mechanisms of Apoptosis

The apoptotic pathway involves a complex series of steps that can be activated through multiple avenues. Apoptosis can proceed through the death receptor (extrinsic) or the mitochondrial (intrinsic) pathway (Figure 1.6). The death receptor mediated pathway can be initiated through ligand binding to receptors such as Fas/CD95 and tumor necrosis factor receptor 1 (TNFR1). This binding allows these receptors to aggregate “death domains” intracellularly that can then aggregate adaptor proteins, Fas associates with FADD and TNFR1 associates with FADD and TRADD. FADD and TRADD contain death domains, which are then able to recruit and activate pro-caspase 8 (Vila and Pzedborski 2003).

The mitochondrial or intrinsic pathway can be activated through a death receptor-independent mechanism. Various stimuli trigger translocation of pro-apoptotic effectors including Bax and its relative Bak, to the mitochondria. Bax

and Bak localize to the mitochondrial outer membrane to allow for permeabilization and subsequent release of cytochrome c into the cytosol. Cytochrome c is then able to interact with other proteins, specifically procaspase 9 and Apaf1 (Li et al, 1997) leading to the cleavage and activation of the initiator caspase, Caspase-9 (Hengartner et al, 2000). Catalytically active caspase-9 can then further activate downstream effector caspases, such as caspase-3 and -7 (Liu et al, 1997; Sakahira et al, 1998). Caspase-3 is the first step in the pathway that can both be activated by the intrinsic and extrinsic pathways.

In addition to activators of apoptosis, there are also known inhibitors and modulators of the apoptotic pathway. A well-known family of proteins that can inhibit apoptosis are the pro-survival Bcl-2 family members. This group consists of Bcl-2, Bcl-xL, Bcl-w, Mcl1, Bcl-B, and A1. There are also a group of pro-apoptotic family members including Bad, Bim, Bid, Hrk, Noxa, Puma, and BMF (Figure 1.6) (Adams and Cory, 1998; Youle and Strasser, 2008). The pro-survival family members, such as Bcl-2 and Bcl-xL have been shown to inhibit Bax and Bak by direct binding (Willis et al, 2007).

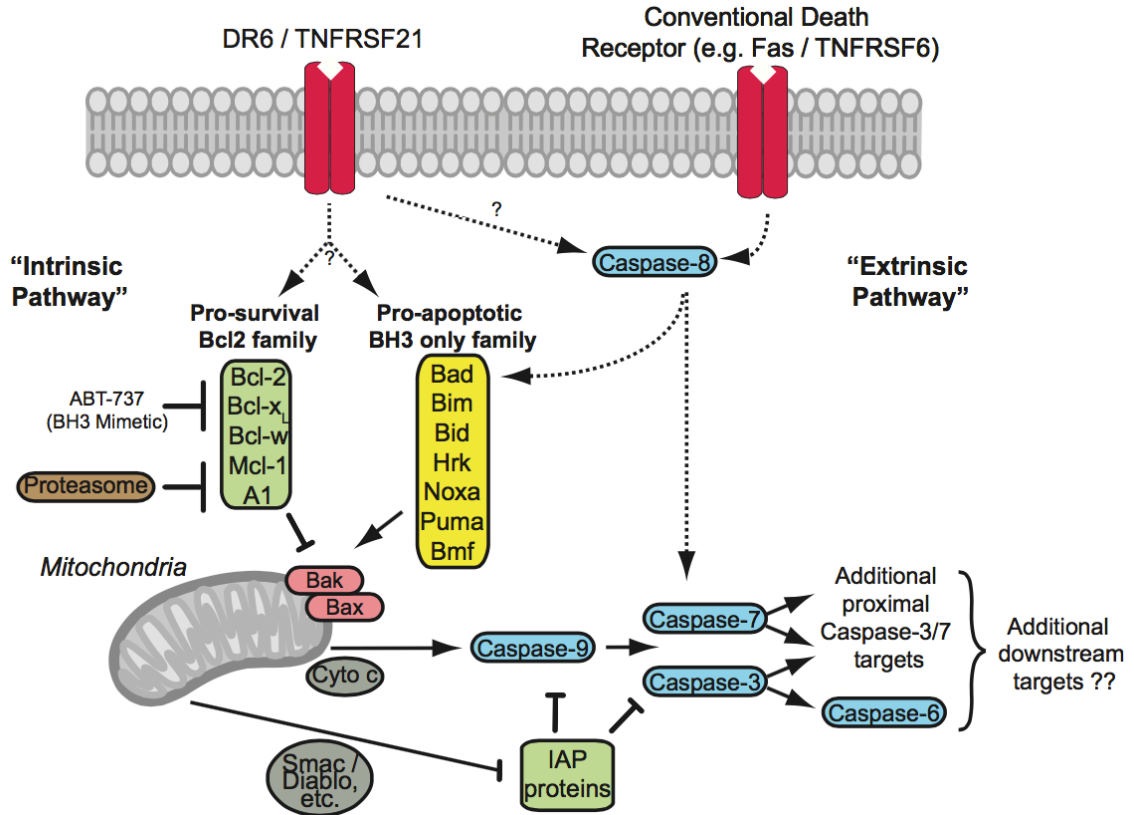


Figure 1.6 Apoptotic Pathway Schematic. The apoptotic pathway can either be initiated through the death receptor-mediated (extrinsic) or the mitochondrial (intrinsic) pathway. Both lead to downstream activation of effector caspases. The intrinsic pathway can be initiated through a number of different stress signals, which lead to colocalization of Bax and Bak to the mitochondria. This results in outer membrane permeabilization and release of cytochrome c into the cytosol. Pro-caspase-9 is then cleaved to its active initiator caspase-9 form which can then cleave downstream effector caspases such as Caspase-3 and -7 (Illustrated by David Simon).

The role of the apoptotic pathway in ALS

There is increasing evidence to suggest that motor neuron degeneration in ALS occurs at least partly by a programmed cell-death mechanism (PCD). The initial evidence that led investigators to believe that apoptosis plays a role in ALS came from observations *in vitro* of transfected neuronal cells expressing mutant SOD1 (Rabizadeh et al, 1995) and primary neurons grown from mutant *SOD1* transgenic mice (Ghadge et al, 1997) dying by apoptosis. Cells undergoing apoptosis have unique changes that occur including plasma membrane blebbing, contraction of cytoplasmic organelles and chromatin condensation and fragmentation. Interestingly, dying neurons in mutant *SOD1* transgenic lines exhibit some of the attributes of apoptosis such as the condensed chromatin, but overall the morphology is indicative of a nonapoptotic mechanism that closer resembles autophagy or necrosis (Clarke, 1999).

There are conflicting results regarding another key feature of apoptosis, that is, fragmentation of DNA. One study observed differences in DNA fragmentation in ALS patients vs. controls, but these studies were unable to be replicated in either ALS patients or animal models (Yoshiyama et al, 1994, Martin et al 1999, Migheli et al, 1999, Migheli et al, 1994, He et al, 2000). In determining the PCD mechanism, it is common that the morphology of cells lie on a spectrum, therefore a possibility is that multiple PCD pathways may be involved in ALS since the morphology of dying motor neurons does not exactly replicate traditional apoptotic morphology.

While the morphological data of whether apoptosis is involved in ALS is a little ambiguous, there are other more solid approaches that have been explored in determining the apoptotic pathway's role in ALS. One such approach is looking at expression or through genetic manipulation of apoptotic factors in mutant *SOD1* mouse models.

Vukosavic et al showed that Bcl-2 and Bcl-xL (two anti-apoptotic family members) had decreased expression levels at endstage of the disease compared to earlier asymptomatic stages and non-transgenic animals (Fig 1.7) (Vukosavic et al, 2000). Further evidence supporting the role of Bcl-2 in ALS is seen by delayed symptom onset and extended survival in a mutant *SOD-1* transgenic animal overexpressing bcl-2 (triangles in Figure 1.7) (Kostic et al, 1997).

Initiators of apoptosis were also found to play a role in ALS mouse models. Bax, a component of the apoptotic pathway that can be triggered by stress signals, has also been shown to be upregulated in an ALS mouse model at endstages of the disease compared to asymptomatic stages or in non-transgenic animals (Fig 1.8A) (Vukosavic et al, 1999). Another group examined further the localization of Bax and found that cytosolic Bax levels decreased at endstages of the disease (Fig 1.8B), while mitochondrial levels of Bax increased at endstages (Guegen et al, 2001) (Fig 1.8C). Since Bax is known to localize to the mitochondria in order to permeabilize the outer membrane to initiate apoptosis, this evidence supports an active role of Bax in apoptosis in an ALS mouse model. In addition other groups have shown this effect through a decreased ratio of anti apoptotic factors/Bax in ALS transgenic lines (Ekegren et al, 1999; Gonzalez et al, 2000).

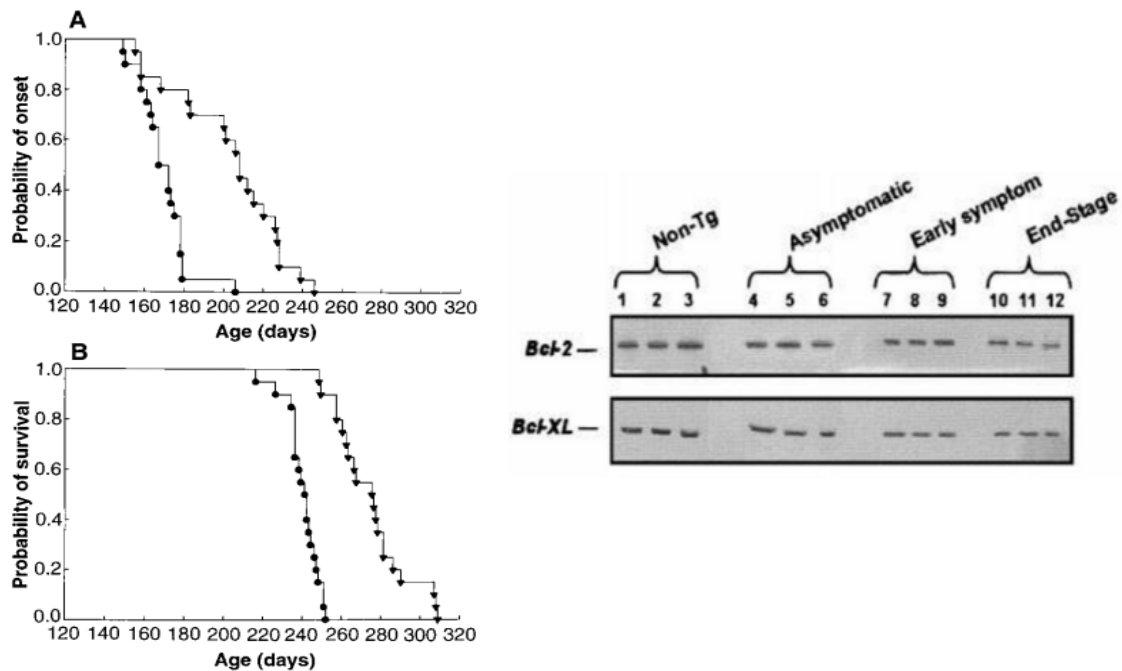


Fig 1.7 The role of anti-apoptotic factors in a mouse model of ALS. A) The age of onset is delayed and B) survival extended in a *SOD1^{G93A}/bcl-2* overexpressing (triangles) animal vs. *SOD1^{G93A}/-* (circles) animal (Kostic et al, 1997). C) Endogenous levels of anti-apoptotic factors such as Bcl-2 and Bcl-xL are reduced at endstages of the disease compared to asymptomatic and non-transgenic animals (Vukosavic et al, 2000).

All of these results were established in an *SOD1^{G93A}* transgenic mouse model, but it should be noted that Bax levels have also been shown to increase and anti apoptotic factors shown to decrease at endstages of the disease in other mutant *SOD1* transgenic animals, such as the *SOD1^{G86R}* mouse model of ALS

(Gonzalez et al, 2000). The strongest evidence for Bax involvement in ALS is seen through a genetic deletion of *Bax* in the *SOD1^{G93A}* mouse line. *SOD1/Bax* KO animals show a small extension in survival (Fig 1.8D) and better motor performance on the rotarod (Fig 1.8E) (Gould et al, 2006).

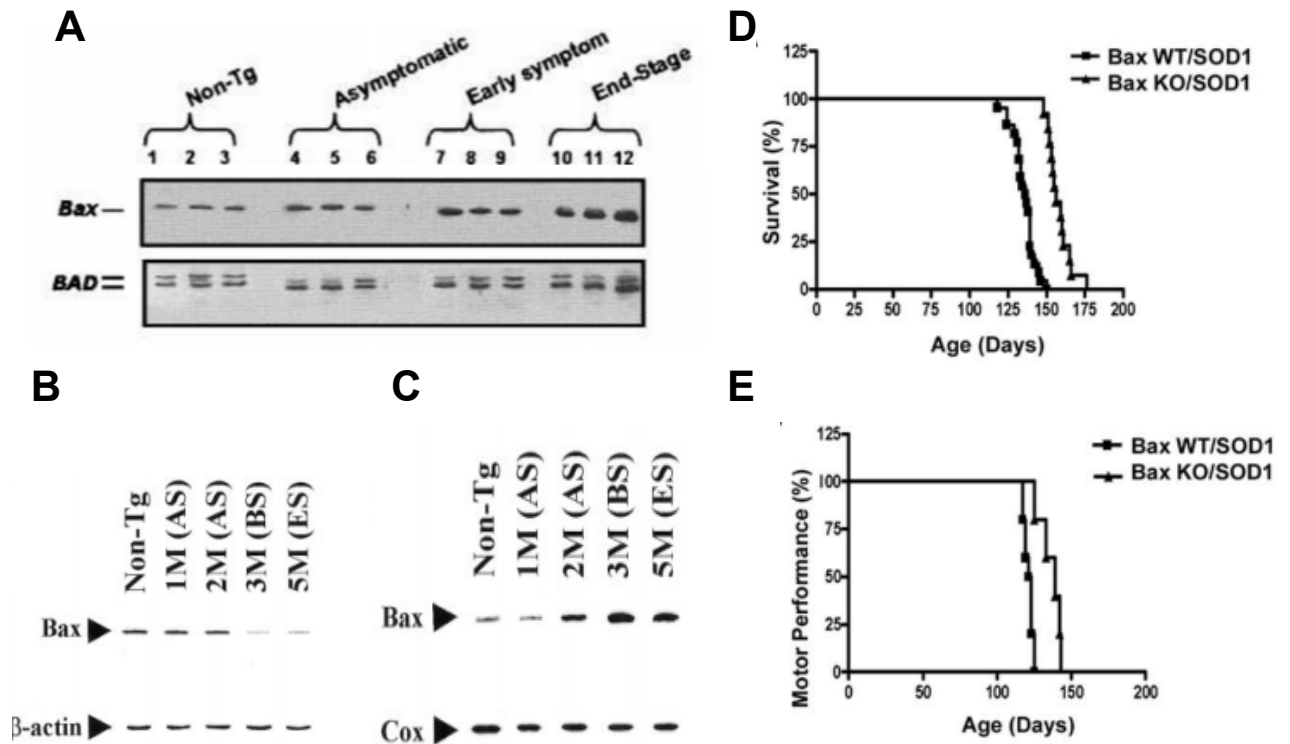


Fig 1.8 The role of Bax in an *SOD1^{G93A}* mouse model of ALS. A) Endogenous levels of Bax increase at endstage of the disease compared to asymptomatic and non-transgenic animals. Further characterization of Bax expression shows that B) cytosolic Bax decreases at endstage while C) mitochondrial Bax expression increases. A genetic deletion of *Bax* in a *SOD1^{G93A}* mouse model of ALS (triangles) compared to *Bax* WT (squares) shows a D) 20 day extension in lifespan and E) increased motor performance on the rotarod. AS = Asymptomatic, BS = Beginning of symptoms, ES = Endstage, M = Month (Vukosavic et al, 1999: panel A; Guegen et al, 2001: panel B, C; Gould et al, 2006: panel D, E)

In addition to these upstream apoptotic factors, there is also evidence for involvement of execution components of the apoptotic pathway. As mentioned above, Bax/Bak colocalization at the mitochondria causes permeabilization of its outer membrane, thus resulting in release of cytochrome c. At endstage (ES) of an *SOD1*^{G93A} mouse model, cytochrome c is shown to shift from the mitochondria to the cytosol (Fig 1.9A) (Guegen et al, 2001). Evidence from other groups has shown that minocycline (an inhibitor of cytochrome c release) is able to delay progression of ALS (Zhu et al, 2002). Cytochrome c release allows for the activation of the apoptosome and subsequent cleavage and activation of the initiator caspase, Caspase-9. At endstages in ALS mice, cleavage of Procaspase-9 to its catalytically active form is observed (Fig 1.9C) (Guegen et al, 2002).

Downstream effector caspases, caspase-3 and caspase-7 are then subsequently cleaved at late stages of the disease (Fig 1.9D&E) (Li et al, 2000, Guegen et al, 2001). Lastly, a known inhibitor of caspases, XIAP has been shown to be cleaved to its inactive form at late stages of the disease (Fig 1.9B) (Guegen et al, 2001). XIAP is the most potent inhibitor of apoptosis found in the IAP family (Deveraux and Reed, 1999) and has been implicated in other neurodegenerative diseases (Xu et al, 1999). Together, these results provide

strong evidence for the role of the apoptotic pathway in transgenic mouse models of ALS.

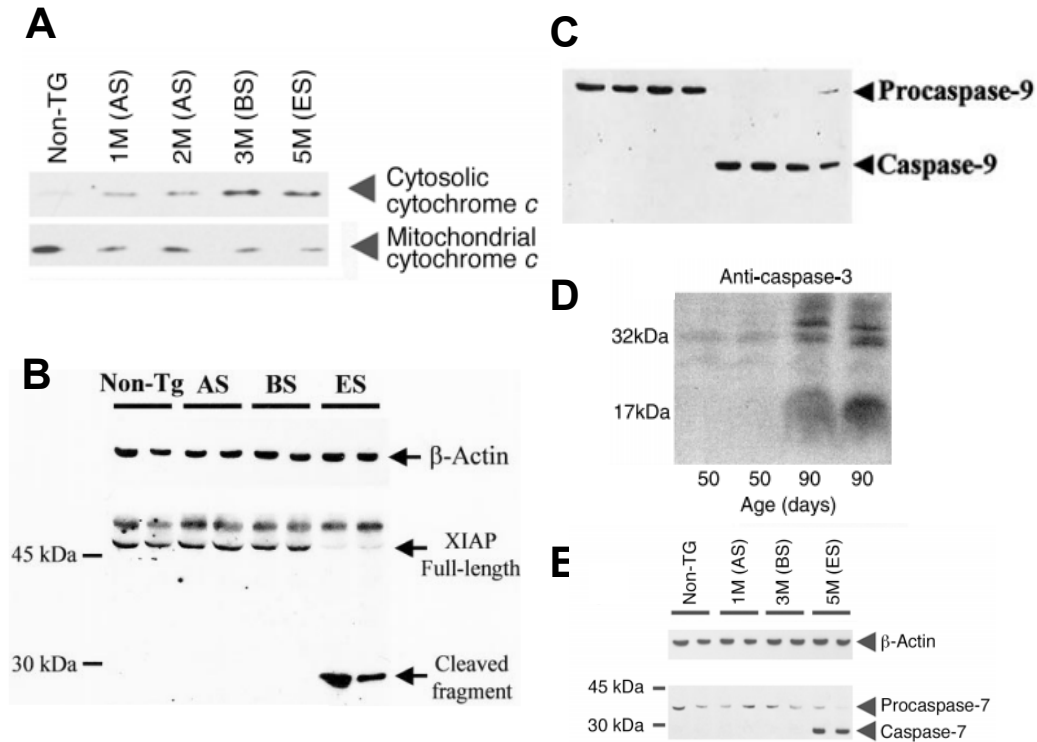


Fig 1.9 Evidence for involvement of downstream executors of apoptosis in ALS mouse models. A) Evidence of increased cytosolic cytochrome c and decreased mitochondrial cytochrome c at endstage of the disease. B) Cleavage of XIAP, a potent inhibitor of apoptosis, into its inactive form at endstages of the disease. C) Activation from inactive procaspase-9 to the catalytically active form of caspase-9 at endstages of the disease. D) Cleavage of Caspase-3 and E) Caspase-7 at symptomatic stages of the disease. AS = asymptomatic, BS = Beginning of symptoms, ES = End-stage, Non-Tg = Non-transgenic animals M = Month (Guegen et al, 2001; Guegen et al, 2002, Li et al, 2000).

It should be mentioned that although multiple apoptotic downstream factors have been implicated in ALS through expression analysis, no follow up experiments deleting these genes in *SOD1* mutant mouse models have been published. Studies with administration of zVAD-fmk, a broad caspase inhibitor, have shown delayed onset and extended survival in a mutant *SOD1* mouse model (Li et al, 2000), but there has been concern in the field whether this inhibitor exhibits off-target effects. The only concrete evidence for endogenous levels of apoptotic factors extending lifespan is the study deleting *Bax* in the mutant *SOD-1* transgenic line. Therefore, it is worth taking an in depth look at the parameters examined in the *Bax* knockout of the *SOD-1* transgenic animal.

Anatomical features of *Bax* deletion in the *SOD1*^{G93A} mouse model

Current evidence in the field suggests that the apoptotic pathway is involved in disease onset and progression of the *SOD1*^{G93A} ALS mouse model, with deletion of *Bax* having the most dramatic effect in delaying disease onset and extending lifespan. While knowledge that the apoptotic pathway plays a role in progression of the disease is useful, it is also important to understand its role in motor neuron degeneration at the anatomical level.

The main insight from this study is that the *Bax* KO/*SOD1*^{G93A} transgenic mouse line exhibits no reduction in motor neuron number at endstages of the disease (Fig 1.10A, B), but axon degeneration is similar to that seen to the *SOD1*^{G93A} mouse model (Fig 1.10D, E) (Gould et al, 2006). It should be noted

that both the motor neuron cell body somal size (Fig 1.10C) and axon diameter at endstage (Fig 1.10F) were reduced in size. Gould et al concluded in this study that while blocking the apoptotic pathway in this mouse model was able to rescue motor neuron cell body loss, it was unable to rescue fibers from axon degeneration. It is unclear whether the extension in lifespan was actually due to the preserved cell body number at endstages of the disease or rather a delay in axon degeneration.

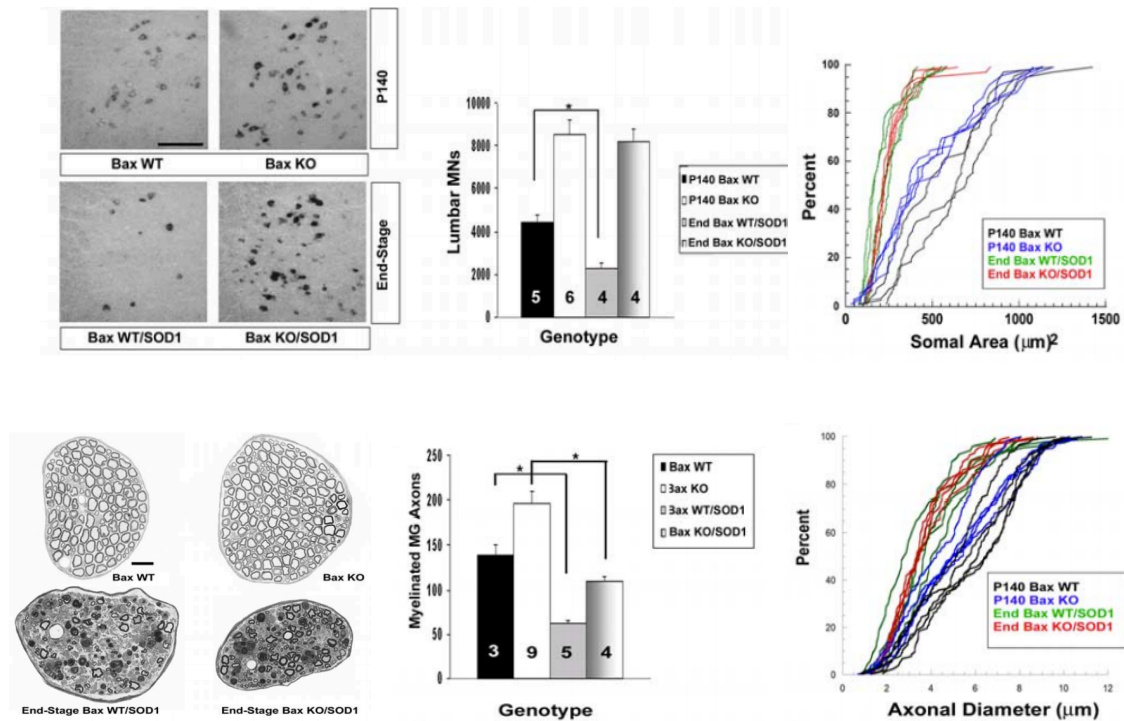


Figure 1.10 Anatomical features of the *SOD-1*^{G93A}/*Bax* KO mouse line. A) Representative images of motor neurons by vCHAT mRNA staining at P140 and Endstage in a *Bax* WT and *Bax* KO (top row) and *SOD-1* Tg/*Bax* WT and *SOD-1* Tg/*Bax* KO (bottom row). Quantification of the B) number of lumbar motor neurons and C) somal size of the motor neurons pictured in A. D) Representative images of the ventral root in a *Bax* WT and *Bax* KO (top row) and *SOD-1* Tg/*Bax* WT and *SOD-1* Tg/*Bax* KO (bottom row) with quantification of E) axon number and F) axon diameter (Gould et al, 2006).

While there is strong evidence for a role of the apoptotic pathway in ALS mouse models, it is clear that ablating the apoptotic pathway is not sufficient to prevent disease. All manipulations of the apoptotic pathway have merely delayed onset and extended lifespan. Therefore, pathways other than apoptosis are likely to be involved in ALS. This is not surprising, especially due to the lack of apoptotic morphology of motor neurons seen in ALS patients and mouse models.

Careful studies have tracked the progression of anatomical features of the disease as discussed above. It is therefore known that neuromuscular junction denervation and axon degeneration precede motor neuron cell body loss (Fischer et al, 2004) and that ablating the apoptotic pathway by a *Bax* deletion does not affect axon degeneration. We therefore, hypothesized that other molecular pathways that may play a role in neuromuscular junction denervation or axon degeneration would make good candidates to pursue in this ALS mouse model.

The Wallerian degeneration pathway

The Wallerian degeneration pathway seemed a perfect candidate for two reasons: (1) it is known to be independent of the apoptotic pathway (Whitmore et al, 2003) and (2) it is known to play a role in axon degeneration in other motor

neuron axonopathies (Ferri et al, 2003). Augustus Waller discovered Wallerian degeneration in 1850 as a process where the distal portion of the axon degenerates after insult or injury (Waller et al, 1850). The fortuitous generation of the Wallerian degeneration slow (Wld^S) mouse helped elucidate this pathway as an active degeneration process. In the Wld^S mouse, the distal axons that normally degenerate, remain intact for up to two weeks after being severed away from the cell body (Lunn et al, 1989, Tsao et al 1994).

The Wld^S gene has been shown to protect axons in many disease models such as glaucoma, peripheral neuropathy, and motor neuron disease (Beirowski et al, 2008; Ferri et al, 2003; Hasbani and O'Malley, 2006; Mi et al 2005; Sajadi et al, 2004; Wang et al, 2002), but the role of Wld^S in ALS is unclear. Fischer et al found that when the Wld^S mouse was crossed with the $SOD1^{G93A}$ mouse model, there was increased survival compared to the $SOD1^{G93A}$ line (Fischer et al, 2005). However, Vande Velde et al, did not see any difference in survival in the $Wld^S/SOD1^{G37R}$ or $Wld^S/SOD1^{G85R}$ mouse lines (Fig 1.11) (Vande Velde et al, 2004). It is unclear whether these conflicting results are due to the difference in mutant *SOD-1* transgenic lines tested, or whether there is ultimately no effect caused by the Wld^S fusion protein.

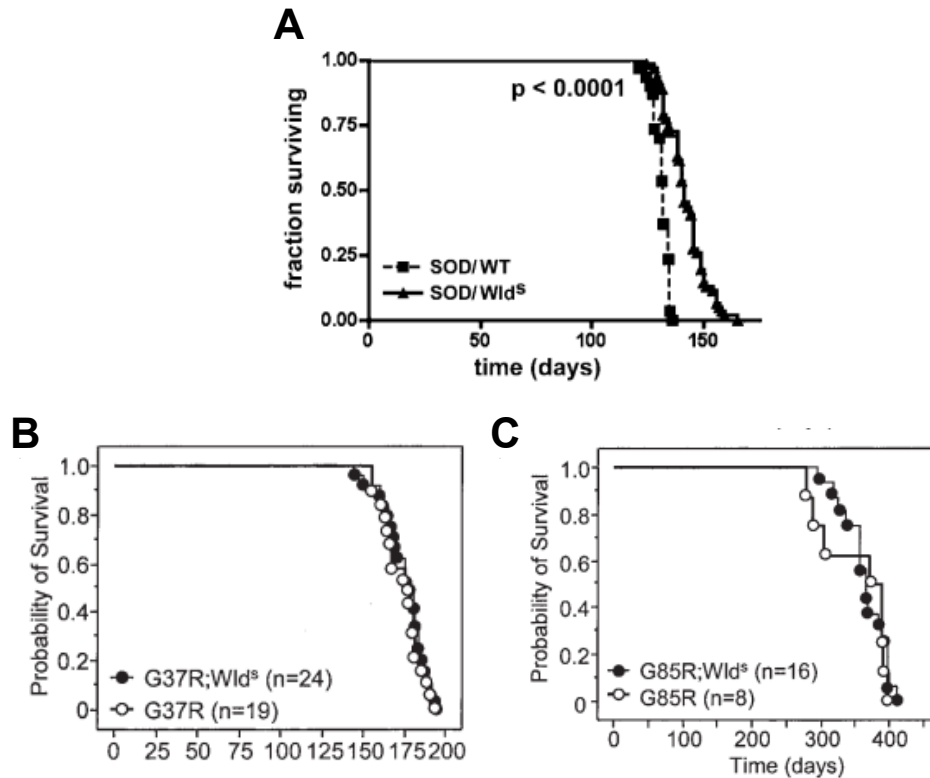


Figure 1.11 Conflicting results for the role of Wld^S in ALS. A) *Wld^S/SOD1^{G93A}* mice show increased survival compared to the *SOD1^{G93A}* line. B) No extension in survival is seen in *Wld^S/SOD1^{G37R}* or C) *Wld^S/SOD1^{G85R}* mouse lines. (Fischer et al, 2005: panel A; Vande Velde et al, 2004: panel B, C).

The *Wld^S* gene encodes a chimeric fusion protein made up of the NAD biosynthetic enzyme nicotinamide mononucleotide adenylyl-transferase (Nmnat1), which converts NAD⁺ from nicotinamide mononucleotide (NMN) and ATP, and a fragment of the ubiquitination factor UBE4B (Conforti et al, 2000). The *Wld^S* fusion protein allows for localization of nuclear Nmnat1 to the axon, and this has been shown to impart the axon protective effect (Araki et al, 2004; Babetto et al,

2010; Sasaki et al, 2009). This has been verified with direct transduction of Nmnat1 protein into cut axons *in vitro* (Sasaki and Milbrandt, 2010) that can rescue axon degeneration and resulting axon degeneration after depletion of Wld^S protein from injured axons (Wang et al, 2015).

It is thought that Nmnat1 has its axon protective effect by substituting for Nmnat2, which is normally present in the axon. Nmnat2 is supplied to the axon by continual axonal transport and thus, is blocked after injury. While the function of Nmnat2 in protecting axons after injury is not well understood, it is thought to function as a “survival factor” where its removal leads to axon degeneration, in uninjured or injured axons (Giley and Coleman, 2010).

Ultimately, the Wld^S fusion protein present in the mouse confers a gain-of-function process, overexpressing Nmnat1 in the axons of these animals. In addition to this caveat, the protective effect of the Wld^S allele against Wallerian degeneration is known to diminish with age (Gillingwater et al, 2002). For these reasons, the Wld^S mouse model is not an ideal model for assessing the role of Wallerian degeneration in ALS.

Multiple studies have followed up on the initial Wld^S result to try and elucidate the mechanism of axon protection. A role for a new component in the Wallerian degeneration pathway came from a genetic screen in *Drosophila*. A mutation in *dSarm* showed delay in degeneration after axotomy of the olfactory receptor neuron axons (Osterloh et al, 2012). Jing Yang, a post doc in our lab, also showed that *Sarm1* KO protected cortical and sensory axons from

degeneration after injury *in vitro*. He also demonstrated that *Sarm1* KO axons were protected from NMJ denervation and axon degeneration after sciatic nerve crush *in vivo* (Fig 1.12) (Osterloh et al, 2012).

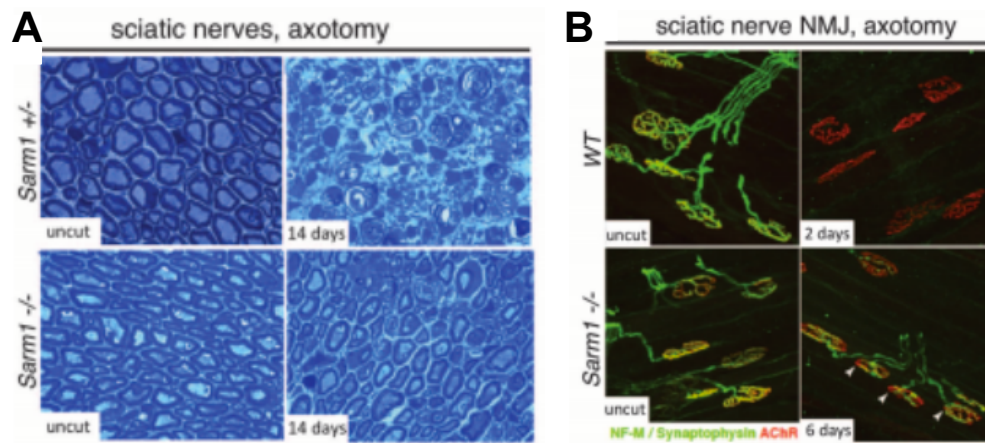


Fig 1.12 *Sarm1* KO protects against axon degeneration and NMJ denervation. A) *Sarm1* KO (bottom row) protects against axon degeneration fourteen days after sciatic nerve crush (right two panels) compared to degenerated axon in *Sarm1* heterozygotes (top row). No axon degeneration is seen in control uncut axons (left two panels). B) *Sarm1* KO (bottom row) protects against muscle denervation six days after sciatic nerve crush (right two panels) compared to complete denervation in *Sarm1* heterozygotes (top row). No NMJ denervation is seen in control uncut axons (left two panels) (Osterloh et al, 2012).

We decided to address whether deletion of *Sarm1* could protect against axon degeneration in an ALS mouse model for several reasons. 1) *Sarm1* was identified to be an active executioner of Wallerian degeneration and 2) because the *Wld^S* mouse involves a gain-of-function mutation and is not an ideal

model for studying the role of Wallerian degeneration as the protective effect of the *Wld^S* allele against Wallerian degeneration diminishes with age (Gillingwater et al, 2002).

Perspective and overview of thesis project

The overall goal of this project was to determine 1) the role of the Wallerian degeneration pathway and 2) its interaction with the apoptotic pathway in a mouse model of ALS. Establishment and characterization of a mouse model overexpressing a mutant gene, *SOD-1^{G93A}*, originally identified to cause familial ALS in human patients, has allowed for a deeper investigation into the molecular mechanisms governing ALS. Careful examination of this mouse model led to the discovery of ALS as a 'dying back' axonopathy with neuronal distal regions such as the NMJ and axon preceding the effect seen at the cell body.

The apoptotic pathway has already been identified to be involved in disease onset, progression, and survival in an *SOD1^{G93A}* mouse model of ALS and was shown specifically to prevent motor neuronal cell body death, but had no effect on axon degeneration. This led us to investigate other players that were involved in NMJ denervation and axon degeneration, initial events in ALS. The Wallerian degeneration pathway served as a great candidate since it already was shown to be involved in other motor neuron diseases, had an effect on axon degeneration and NMJ denervation after sciatic nerve crush, and is independent of the apoptotic pathway. Initial experiments done in the lab knocking out *Sarm1*

in an *SOD1^{G93A}* mouse model showed no effect on survival, but did show a difference in disease onset and progression of the disease (Fig 1.13).

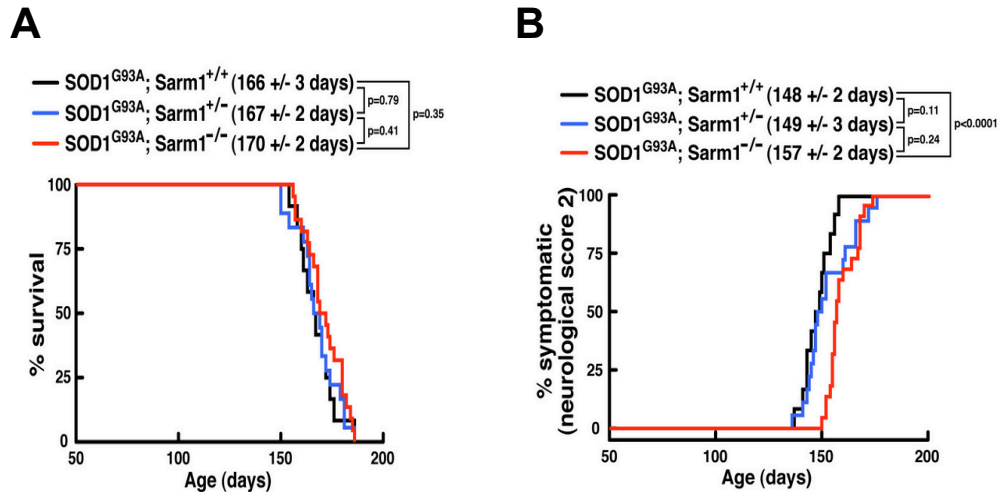


Figure 1.13 *SOD-1^{G93A}* Tg, *Sarm1^{-/-}* has effect on disease progression, but no effect on survival. A) Survival curve and B) disease progression of *SOD-1^{G93A}* Tg, *Sarm1^{+/+}* (black), *SOD-1^{G93A}* Tg, *Sarm1^{+/-}* (blue) and, *SOD-1^{G93A}* Tg, *Sarm1^{-/-}* (red). Mice are given neurological score 2 when the hind limbs start to become paralyzed (Data from Jing Yang).

Since *Sarm1^{-/-}* animals did affect disease onset and progression in the *SOD1^{G93A}* mouse, we next wanted to analyze the effect *Sarm1* was having on the anatomical features of the disease. This project will explore the *Sarm1^{-/-}* effect on neuromuscular junction denervation, axon degeneration, and motor neuron cell body death throughout disease progression. In addition to a closer histological analysis of the *SOD-1^{G93A}* Tg, *Sarm1^{-/-}* phenotype, we also wanted to explore the

interaction between this pathway and the classical apoptotic pathway, an already known regulator of disease progression and survival of the *SOD1^{G93A}* mouse model of ALS.

In Chapter 2, I will discuss the findings of disease onset, progression and survival when blocking individually the apoptotic pathway and the Wallerian degeneration pathway. I will then present the results of ablating both of these pathways together, specifically in the *SOD-1^{G93A}* Tg mouse model. We identified that these pathways play distinct roles in disease onset and progression of the disease and that they act additively to reduce symptomatic stages of the disease.

Chapter 3 explores the anatomical features of deleting each of these pathways individually and in combination. Histology was performed to examine neuromuscular junction denervation in different hindlimb muscles, motor axon degeneration in the ventral root, and cell body loss in the spinal cord. The histological results track closely with progression of the disease in the ALS mouse model. I conclude with a discussion tying the disease progression and histology results together.

Chapter 4 investigates the non-cell autonomous role that is thought to occur in the mutant *SOD-1* mouse model of ALS. Examination of this non-cell autonomous effect is pursued through the *in vitro* approaches described previously, specifically using *SOD-1* Tg astrocyte conditioned medium and microglial co-cultures with primary motor neurons to identify new factors and elucidate more fully the role of the Wallerian degeneration pathway in motor

neuron cell death. I conclude with a discussion of these results and suggestions for future experiments.

Chapter 2: Apoptosis and Wallerian degeneration affect disease onset and progression

Rationale

Previous studies showed that deletion of apoptotic pathway components slows disease progression in the *SOD-1^{G93A}* Tg mouse model of ALS, specifically exerting its effect on motor neuron cell bodies and not axon degeneration. This led us to explore other potential pathways that might mediate axon degeneration in this disease model, particularly the Wallerian degeneration pathway. We further wanted to examine the interaction between these two pathways to determine if they could act synergistically to affect disease.

To determine the role of these two pathways both individually and together, we decided to track disease onset and progression closely through daily monitoring of disease symptoms through a neurological scoring system. This allowed us to resolve the individual role of each of these pathways in the behavioral phenotype exhibited by these mice.

***Bax*, but not *Sarm1* deletion extends survival of the *SOD-1G93A* Tg mouse model**

To determine the individual and collaborative roles of the Wallerian degeneration and the classical apoptotic pathways in ALS, we assessed the effects of *Sarm1* and *Bax* on survival and disease progression in *SOD-1^{G93A}* Tg mice. We first tested *SOD-1* copy number in all of the *SOD-1* Tg animals and

removed all animals out of the range of the recommended *SOD-1* copy number used by standard Jackson Laboratory protocols (Fig 2.1).



Figure 2.1 *SOD-1*^{G93A} copy number analyzed by qPCR. *SOD-1*^{G93A} Tg animals were tested for transgene copy number using quantitative PCR. Four mice were excluded from the analysis (indicated in red boxes) since they exhibited *SOD-1* copy number outside the range of those allowed by Jackson mice protocol standards.

Consistent with previous results, blocking the apoptotic pathway by genetic deletion of *Bax* prolongs survival of *SOD-1*^{G93A} Tg mice by ~20 days compared to littermate controls (*SOD-1*^{G93A}, *Bax*^{-/-}: 187 +/- 13 days ; *SOD-1*^{G93A}, *Bax*^{+/+}: 168 days +/- 14 days , **p = 0.0052). Blocking both the Wallerian

degeneration and apoptotic pathways similarly extended lifespan, but offered no additional extension over genetic deletion of *Bax* alone (*SOD-1^{G93A},Bax^{-/-};Sarm1^{-/-}*: 182 +/- 14 days; *p =0.0495). No effect on survival was observed in mice lacking *Sarm1^{-/-}* alone (*SOD-1^{G93A},Sarm1^{-/-}*: 172 +/- 12 days, *SOD-1^{G93A},Sarm1^{+/+}*: 168 +/- 14 days). (Fig 2.2A).

Interestingly, body weight loss was significantly delayed in *SOD-1^{G93A} Tg,Bax^{-/-};Sarm1^{-/-}* mice compared to *SOD-1^{G93A} Tg* (*SOD-1^{G93A}*: 156 days +/- 13 days, *SOD-1^{G93A},Bax^{-/-}*:170 +/- 14 days; ***p =0.0006, *SOD-1^{G93A},Bax^{-/-};Sarm1^{-/-}*: 182 +/- 14 days; ***p=0.0004) and *SOD-1^{G93A} Tg ,Bax^{-/-}* mice (*p=0.0435), indicating that *SOD-1^{G93A} Tg,Bax^{-/-};Sarm1^{-/-}* animals are healthier for a longer period of time, despite the fact that their lifespan is not extended relative to *SOD-1^{G93A} Tg* lacking only *Bax^{-/-}* (Fig 2.2B).

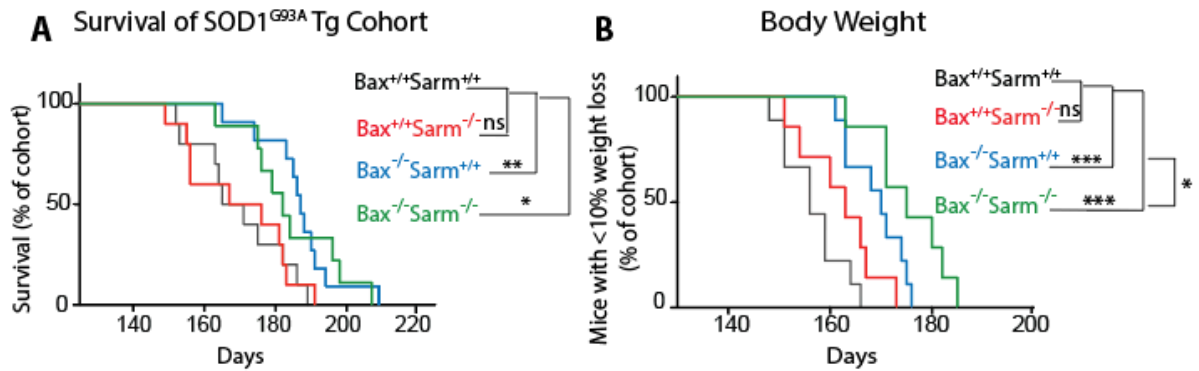


Figure 2.2. Survival and body weight loss of *SOD-1^{G93A} Tg* mice. (A) Survival and (B) body weight loss of *SOD-1^{G93A} Tg* (black), *SOD-1^{G93A} Tg,Bax^{-/-}* *Sarm^{+/+}* (blue), *SOD-1^{G93A} Tg,Bax^{+/+}Sarm^{-/-}* (red), and *SOD-1^{G93A} Tg,Bax^{-/-}Sarm^{-/-}* (green). This color scheme will be used throughout all of the figures in this paper.

In addition to tracking survival and body weight, we also performed a rotorod behavioral assay to assess motor performance of these animals. We performed the rotorod assay on a different cohort of animals because exercise is known to affect disease onset and progression. Since the size of this cohort was so large, we needed to modify the existing rotorod protocol in order to test all of the mice. The rotorod behavioral assay is normally performed every other day for the duration of the study. We decided to test each mouse monthly at different timepoints including P50, P90, P120, P150, and P180. These timepoints included asymptomatic, early stage symptomatic, and late stage symptomatic periods. We needed to test how much training was necessary to achieve results that related to motor function and not motor learning.

In order to do this, we had differently staged mice perform three days of training on the rotorod. We also slightly modified the rotorod protocol so that mice were exposed to a short training period before times were recorded. Our results showed that while training on the rotorod did slightly increase overall time the mice were able to stay on the rotorod, the significant decrease in time at late stages was observed similarly after either one, two, or three days of training (Figure 2.3A-C). This allowed us to use this newly developed protocol to measure differences seen between genotypes. Unfortunately, we were unable to distinguish a difference among genotypes (Fig 2.3D), most likely because the timepoints at which the mice were tested were too far apart to catch any key differences.

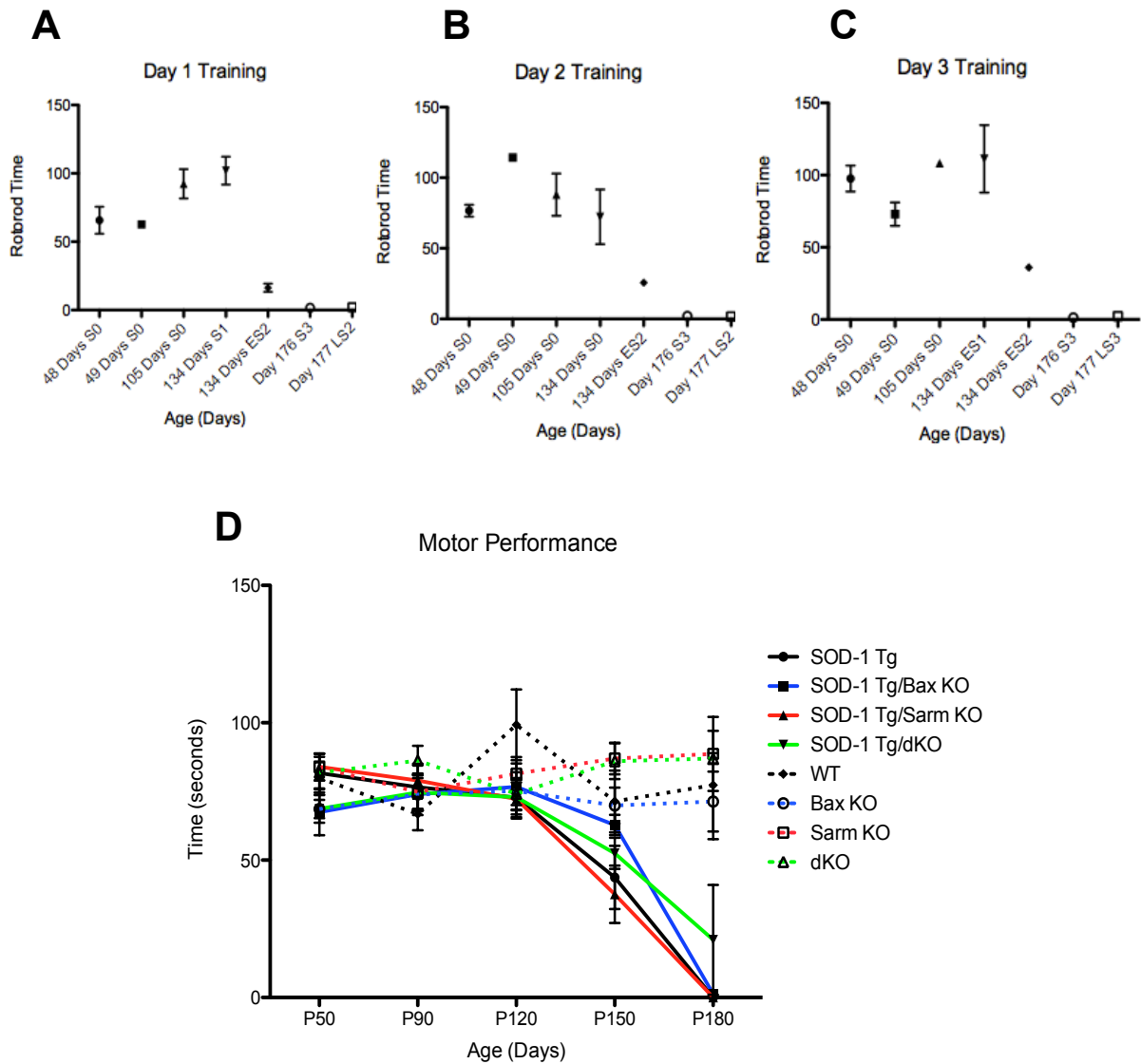


Figure 2.3. Rotorod Behavioral Assay. A new training protocol was developed to test the rotorod behavioral assay in mice. Mice at different ages and disease stages were tested using this new protocol with A) 1 day of training, B) 2 days of training, or C) 3 days of training. The age of the mice and neurological score is listed on the x-axis of the graph. S0 = Score 0, S1 = Score 1, ES2 = early stage 2, S3 = Stage 3, LS2 = late stage 2. D) Rotorod performance of *SOD-1^{G93A} Tg* (black solid line), *SOD-1^{G93A} Tg, Bax^{-/-} Sarm^{+/+}* (blue solid line), *SOD-1^{G93A} Tg, Bax^{+/+} Sarm^{-/-}* (red solid line), *SOD-1^{G93A} Tg, Bax^{-/-} Sarm^{-/-}* (green solid line), *SOD-1^{WT}* (black dotted line), *SOD-1^{WT}, Bax^{-/-} Sarm^{+/+}* (blue dotted line), *SOD-1^{WT}, Bax^{+/+} Sarm^{-/-}* (red dotted line) and *SOD-1^{WT}, Bax^{-/-} Sarm^{-/-}* (green dotted line) animals at P50 (n=15 per genotype), P90 (n=12 per genotype), P120 (n=9 per genotype), P150 (n = 6 per genotype) and P180 (n = 3 per genotype).

Sarm1 involved in early stages and Bax involved in late stages of the disease

Neurological scoring system guidelines from The Jackson Laboratory were used to track symptom onset and disease progression in mice (Fig 2.4A). *SOD-1^{G93A} Tg, Bax^{-/-}* and *SOD-1^{G93A} Tg, Bax^{-/-}; Sarm1^{-/-}* mice remained symptom free for significantly longer than *SOD-1^{G93A} Tg* controls (*SOD-1^{G93A}*: 143.8 +/- 5.26; *SOD-1^{G93A}, Bax^{-/-}*: 159.2 +/- 5.5 days, *p = 0.0291; *SOD-1^{G93A}, Bax^{-/-}, Sarm1^{-/-}*: 171.1 +/- 4.91; **p = 0.0016). Although *Sarm1^{-/-}* does not prolong survival of *SOD-1^{G93A} Tg* ALS animals, disease onset and progression were modestly affected. *SOD-1^{G93A} Tg, Sarm1^{-/-}* animals exhibit disease-associated symptoms (score 1: muscle weakness) earlier than littermate controls (*SOD-1^{G93A}, Sarm1^{-/-}*: 132.8 +/- 7.74 days). (Fig 2.4B). However, progression to score 2 is delayed, thereby prolonging the period that *SOD-1^{G93A} Tg, Sarm1^{-/-}* animals exhibit early disease symptoms compared to *SOD-1^{G93A} Tg* animals (*SOD-1^{G93A}*: 18.33 +/- 3.091 days; *SOD-1^{G93A}, Sarm1^{-/-}*: 37.55 +/- 7.056 days, * p = 0.033). In contrast, progression from score 1 to score 2 occurs more quickly in *SOD-1^{G93A} Tg, Bax^{-/-}; Sarm1^{-/-}* animals (*SOD-1^{G93A} Tg, Bax^{-/-}; Sarm1^{-/-}*: 8 +/- 1.462 days, ** p = 0.008) (Fig 2.4C).

Genetic disruption of the Wallerian and apoptotic pathways also modifies later stages of the disease. In *SOD-1^{G93A}* Tg, *Bax^{-/-}* mice, the length of time between onset of score 2 to paralysis (ES) is significantly prolonged compared to controls (*SOD-1^{G93A}*: 6.56 +/- 1.69 days; *SOD-1^{G93A},Bax^{-/-}*:12.91 +/- 1.84 days; *p=0.022) (Fig 2.4D).

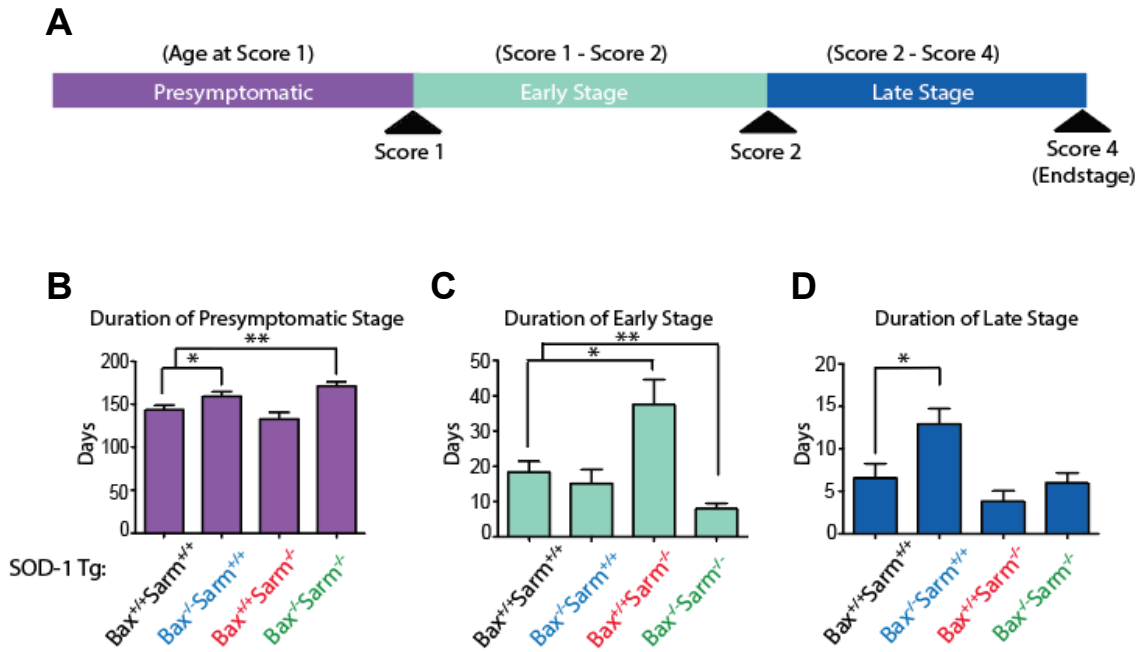


Figure 2.4 Disease onset and progression of *SOD-1^{G93A}* Tg mice. (A) Schematic of neurological scoring and corresponding disease stage of animal. Mean number of days mice in each genotype (*SOD-1^{G93A}* Tg (n=9), *SOD-1^{G93A}* Tg,*Bax^{-/-}Sarm^{+/+}*(n=11), *SOD-1^{G93A}* Tg,*Bax^{+/+}Sarm^{-/-}*(n=9), and *SOD-1^{G93A}* Tg,*Bax^{-/-}Sarm^{-/-}*(n=9)) listed above was given score 0 and termed presymptomatic (B), given score 1 and termed as early stage (C), and given score 2 or later and termed late stage (D).

Elimination of both Bax and Sarm decreases symptomatic stages in ALS

Further, total disease duration was significantly reduced in the *SOD-1^{G93A}* Tg, *Bax^{-/-};Sarm1^{-/-}* animals relative to other groups (*SOD-1^{G93A}*: 26.67 +/- 3.44 days, *SOD-1^{G93A}* Tg, *Bax^{-/-}*, 26.90 +/- 4.829 days, ; *SOD-1^{G93A}*, *Sarm1^{-/-}*: 41.55 +/- 7.91 days *SOD-1^{G93A}*, *Bax^{-/-}*, *Sarm1^{-/-}*: 13.56 +/- 2.28 days; *p =0.017, *p =0.029, **p =0.002, respectively) (Fig 2.5A). The differences in disease progression that are observed between *Bax^{-/-}* and *Sarm1^{-/-}* animals indicate that the apoptotic and Wallerian degeneration pathways play parallel and synergistic roles in ALS (Fig 2.5B).

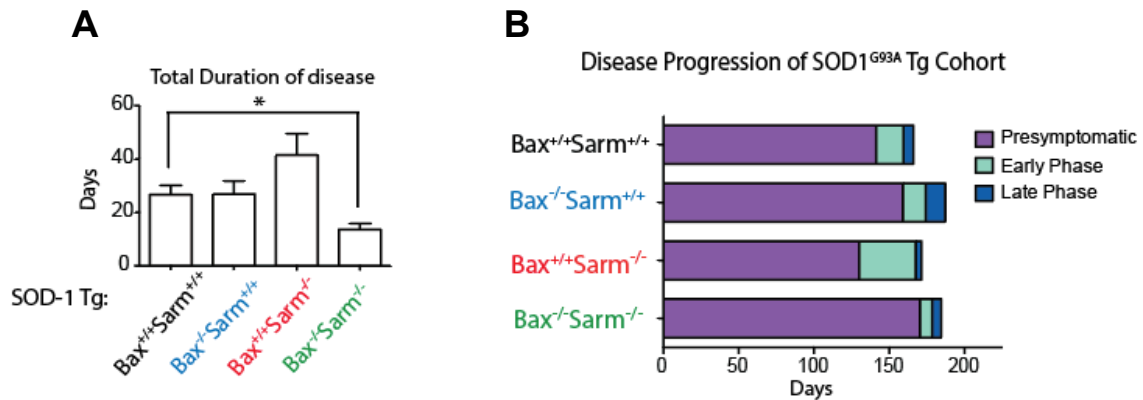


Figure 2.5 Duration and complete progression of *SOD-1^{G93A}* Tg mice. (A) Mean number of days spent in both early and late stage of disease which results in total duration of symptomatic stages of the disease (B) Mean number of days subset of animals in each genotype spent in each stage.

Conclusions

Here we showed that the apoptotic pathway and Wallerian degeneration pathway play distinct roles in disease onset and progression of the disease. By tracking disease symptoms, we were able to show that the Wallerian degeneration pathway through deletion of *Sarm1* plays a role in symptom onset of the disease, while the apoptotic pathway is involved more in late stages of the disease. We also were able to show that the apoptotic pathway can delay symptom onset, but does not decrease overall duration of the disease, whereas deletion of *Sarm1* does increase overall disease.

Interestingly, the neurological scoring and body weight loss results show that the apoptotic and Wallerian degeneration pathways function additively to control disease onset and progression, ultimately resulting in a decreased burden of symptomatic stages of the disease and an extended survival that is comparable to the individual deletion of the apoptotic pathway.

Chapter 3: Histological analysis tracks with disease

Rationale

Since the *Bax* and *Sarm* genes were found to play distinct roles in disease onset and progression, we next wanted to ask what the anatomical features throughout disease progression were when deleting these genes, both individually and together. We also wanted to determine how these histological changes tracked with disease onset and progression.

Along with a general characterization of anatomical features throughout the disease, we also were curious to investigate the role of each of these pathways in the “dying back” progression of the disease. Previous results had shown that deleting the apoptotic pathway resulted in preserved motor neuron cell body loss, but no axon degeneration at endstages of the disease. We wanted to perform a closer analysis at various timepoints to determine if this delayed onset tracked with delayed early features of the disease, such as NMJ denervation and axon degeneration. Furthermore, this is the first study to perform careful histological characterization when deleting the Wallerian degeneration pathway and with double deletion of both pathways.

Bax and Sarm1 play distinct roles in neuromuscular junction denervation

To determine how the Wallerian and apoptotic pathways affect neuromuscular junction denervation in the *SOD-1^{G93A}* Tg model of ALS, gastrocnemius and tibialis anterior muscles were examined at different disease

stages. Representative images are shown for the tibialis anterior (Fig 3.1) and the gastrocnemius muscle (Fig 3.2). In *SOD-1^{G93A}* Tg animals, NMJ denervation was first observed at P90 and was nearly complete by disease endstage (Fig 3.1, 3.2, quantified in 3.3). Denervation of both muscles was significantly delayed at P90 in both *SOD-1^{G93A}, Bax^{-/-}* and *SOD-1^{G93A}, Bax^{-/-}, Sarm1^{-/-}* (Fig 3.1, 3.2, 3.3), but only the tibialis anterior muscle showed delayed NMJ denervation in the *SOD-1^{G93A}, Sarm1^{-/-}* mice at P90 (*SOD-1^{G93A}*: 39.67 +/- 6.36 % innervated, *SOD-1^{G93A}, Bax^{-/-}*: 100 +/- 0; ***p<.0001, *SOD-1^{G93A}, Sarm1^{-/-}*: 92.33 +/- 4.09, ***p<0.001; *SOD-1^{G93A}, Bax^{-/-}, Sarm1^{-/-}*: 100 +/- 0; ***p<0.001 for tibialis anterior and *SOD-1^{G93A}*: 45 +/- 8.62 % innervated, *SOD-1^{G93A}, Bax^{-/-}*: 100 +/- 0; ***p<.0001, *SOD-1^{G93A}, Sarm1^{-/-}*: 37.33 +/- 1.202; *SOD-1^{G93A}, Bax^{-/-}, Sarm1^{-/-}*: 100 +/- 0; ***p<0.001 for gastrocnemius).

At P120 and P150, the percentages of partially and completed denervated NMJs were similar across all the genotypes for the gastrocnemius muscle (Fig 3.2, quantified in 3.3B). However, in the tibialis anterior, the number of fully innervated NMJs was significantly increased in *SOD-1^{G93A}, Bax^{-/-}, Sarm1^{-/-}* mice compared to the *SOD-1^{G93A}* Tg at P120 and P150 (Fig 3.1, 3.3A) (*SOD-1^{G93A}*: 21.33 +/- 13.74 % innervated, *SOD-1^{G93A}, Bax^{-/-}, Sarm1^{-/-}*: 53 +/- 0.58 at P120 and *SOD-1^{G93A}*: 13.67 +/- 0.89 % innervated, *SOD-1^{G93A}, Bax^{-/-}, Sarm1^{-/-}*: 36.33 +/- 6.64 at P150).

In P90 *SOD-1^{G93A}; Sarm1^{-/-}* mice, NMJ innervation is preserved in the tibialis anterior, but not the gastrocnemius muscle. Increased NMJ innervation

was also observed in the *SOD-1^{G93A},Bax^{-/-}, Sarm1^{-/-}* tibialis at later time points (P120 and P150). Denervation was decreased in *SOD-1^{G93A},Bax^{-/-}, Sarm1^{-/-}* gastrocnemius muscle relative to the *SOD-1^{G93A} Tg*, but the reduction was not significant (Fig 3.2 and quantified in 3.3B).

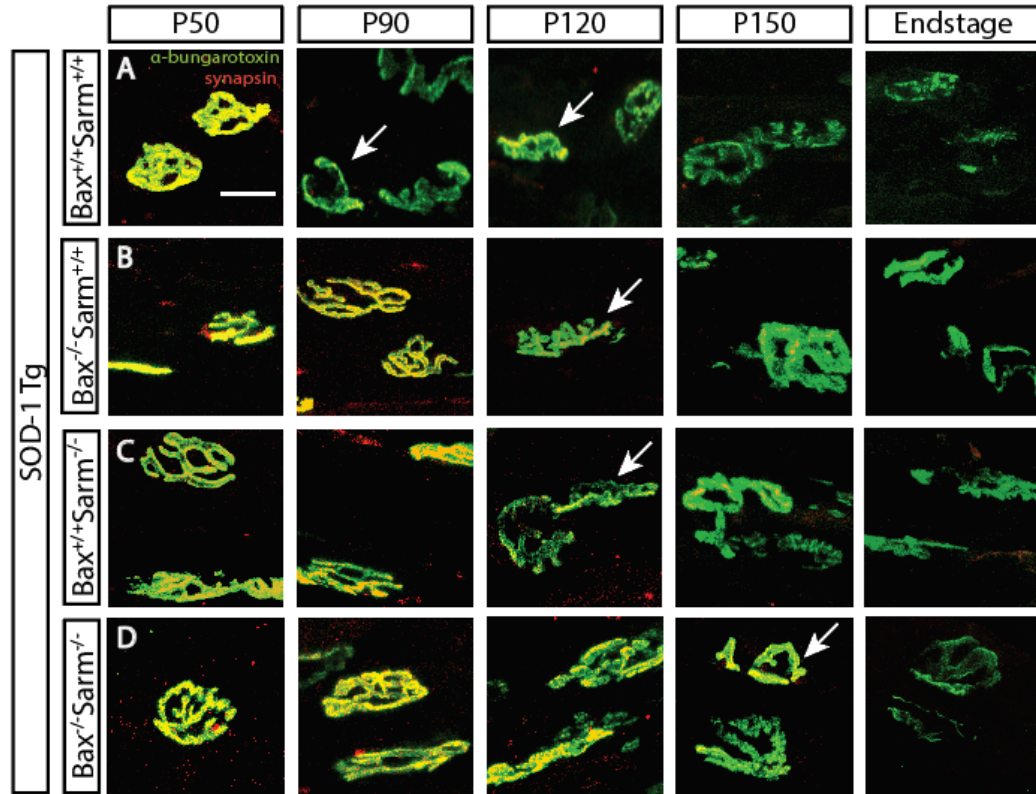


Figure 3.1 Neuromuscular junction denervation of the tibialis anterior muscle throughout disease progression. α -bungarotoxin was used to label postsynaptic sites (green) and synapsin antibody (red) labeled presynaptic sites of the neuromuscular junction in the tibialis anterior (shown above). Yellow was counted as completely innervated synapses, yellow and green (indicated by white arrows) were counted as partially innervated synapses, and green only were counted as denervated synapses. (A) *SOD-1^{G93A} Tg*, (B) *SOD-1^{G93A} Tg, Bax^{-/-} Sarm^{+/+}*, (C) *SOD-1^{G93A} Tg, Bax^{+/+} Sarm^{-/-}*, and (D) *SOD-1^{G93A} Tg, Bax^{-/-} Sarm^{-/-}* animals (n=3 for each timepoint) were dissected when each reached P50, P90, P120, P150, and when they reached score 4, or endstage. Scale bar = 20 μ m.

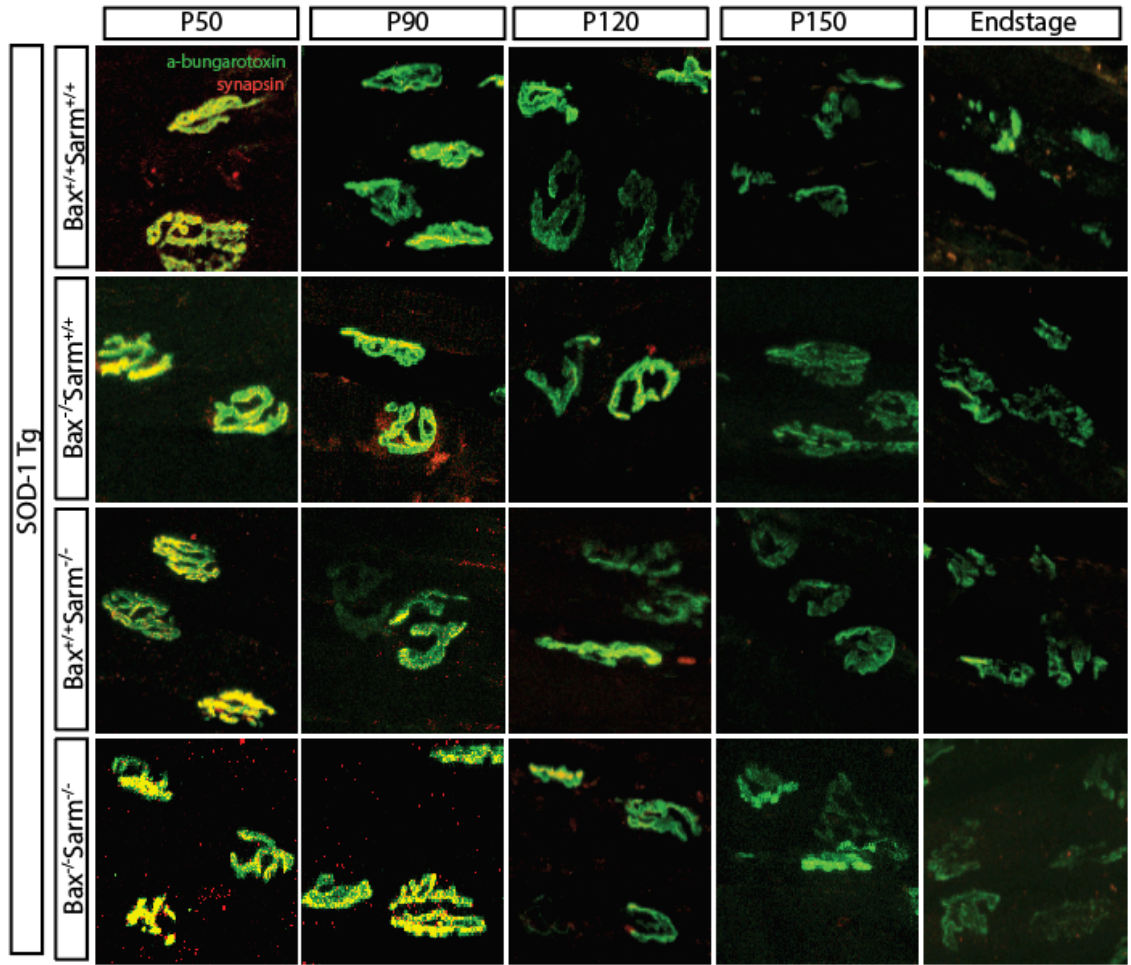
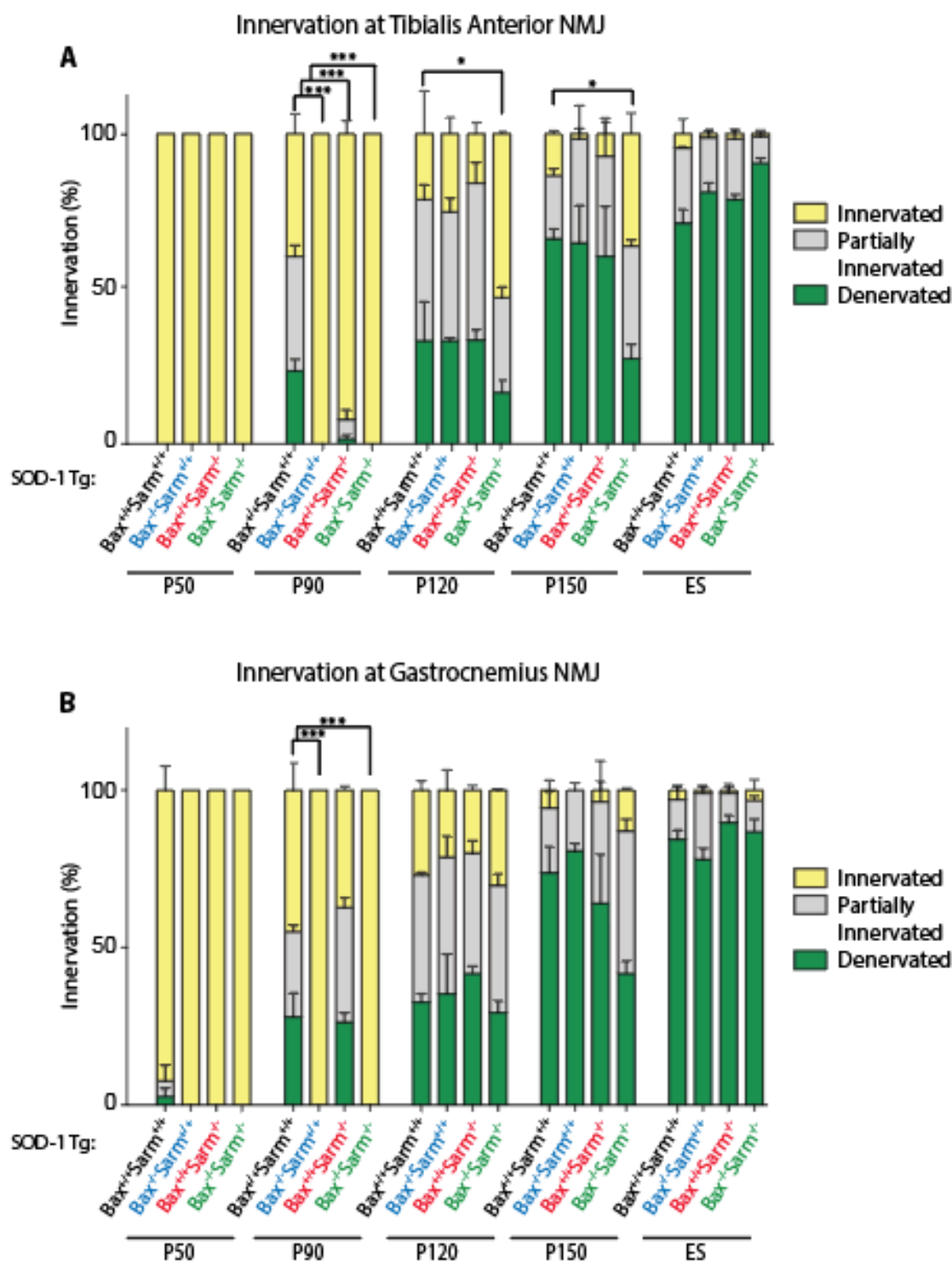


Figure 3.2 Neuromuscular junction denervation of the gastrocnemius muscle throughout disease progression. α -bungarotoxin was used to label postsynaptic sites (green) and synapsin antibody (red) labeled presynaptic sites of the neuromuscular junction in the gastrocnemius muscle. Yellow was counted as completely innervated synapses, yellow and green (indicated by white arrows) were counted as partially innervated synapses, and green only were counted as denervated synapses. (A) $SOD-1^{G93A} Tg$, (B) $SOD-1^{G93A} Tg, Bax^{-/-} Sarm^{+/+}$, (C) $SOD-1^{G93A} Tg, Bax^{+/+} Sarm^{-/-}$, and (D) $SOD-1^{G93A} Tg, Bax^{-/-} Sarm^{-/-}$ animals (n=3 for each timepoint) were dissected when each reached P50, P90, P120, P150, and when they reached score 4, or endstage.

Figure 3.3 Neuromuscular junction quantification of the tibialis anterior and gastrocnemius muscle. Synapses from Fig 3.1 and 3.2 were quantified as either innervated (yellow bars), partially innervated (grey bars) or denervated (green bars) in the (A) tibialis anterior and (B) gastrocnemius in the *SOD-1^{G93A} Tg* (black font) *SOD-1^{G93A} Tg, Bax^{-/-} Sarm^{+/+}* (blue font), *SOD-1^{G93A} Tg, Bax^{+/+} Sarm^{-/-}* (red font), and *SOD-1^{G93A} Tg, Bax^{-/-} Sarm^{-/-}* (green font) animals (n=3 for each timepoint) at P50, P90, P120, P150, and ES (endstage).



***Sarm1* deletion slightly delays axon degeneration in *SOD-1^{G93A}* Tg animals**

Ventral root samples were analyzed to determine the effect of the apoptotic and Wallerian degeneration pathways on axon degeneration. The number of large and small diameter axons that were intact or degenerated was quantified at different time points throughout the disease (Fig 3.4 and quantified in 3.5). Large diameter axons first showed signs of degeneration by P120 in *SOD-1^{G93A}* controls, with a significant decrease in the number of intact axons by P150 (Fig 3.5A). In *SOD-1^{G93A},Bax^{-/-}, Sarm1^{-/-}* mice, axon degeneration was significantly delayed, as evidenced by an increase in the number of large diameter axons at P150 (*SOD-1^{G93A}*: 42.25 +/- 23.9 large axons, *SOD-1^{G93A},Bax^{-/-}, Sarm1^{-/-}*: 161.3 +/- 12.1 at P150; *p=0.03) (Fig 3.5A). Degeneration was also modestly affected in *SOD-1^{G93A},Bax^{-/-}* and *SOD-1^{G93A}, Sarm1^{-/-}*, but not significantly.

By disease endstage, axons had degenerated to a similar extent across genotypes. Consistent with a role for *Bax* in developmental cell death, the number of small diameter axons was significantly increased in *SOD-1^{G93A},Bax^{-/-}* mice, and to a similar extent in *SOD-1^{G93A},Bax^{-/-};Sarm1^{-/-}* animals at all ages. The number of small diameter axons was modestly affected at disease endstage in all mutants, but significantly in both *SOD-1^{G93A},Bax^{-/-}* and *SOD-1^{G93A},Bax^{-/-};Sarm1^{-/-}* mice (Fig 3.5B). These results indicate that loss of motor axons in the ventral root mostly reflects the loss of large diameter axons.

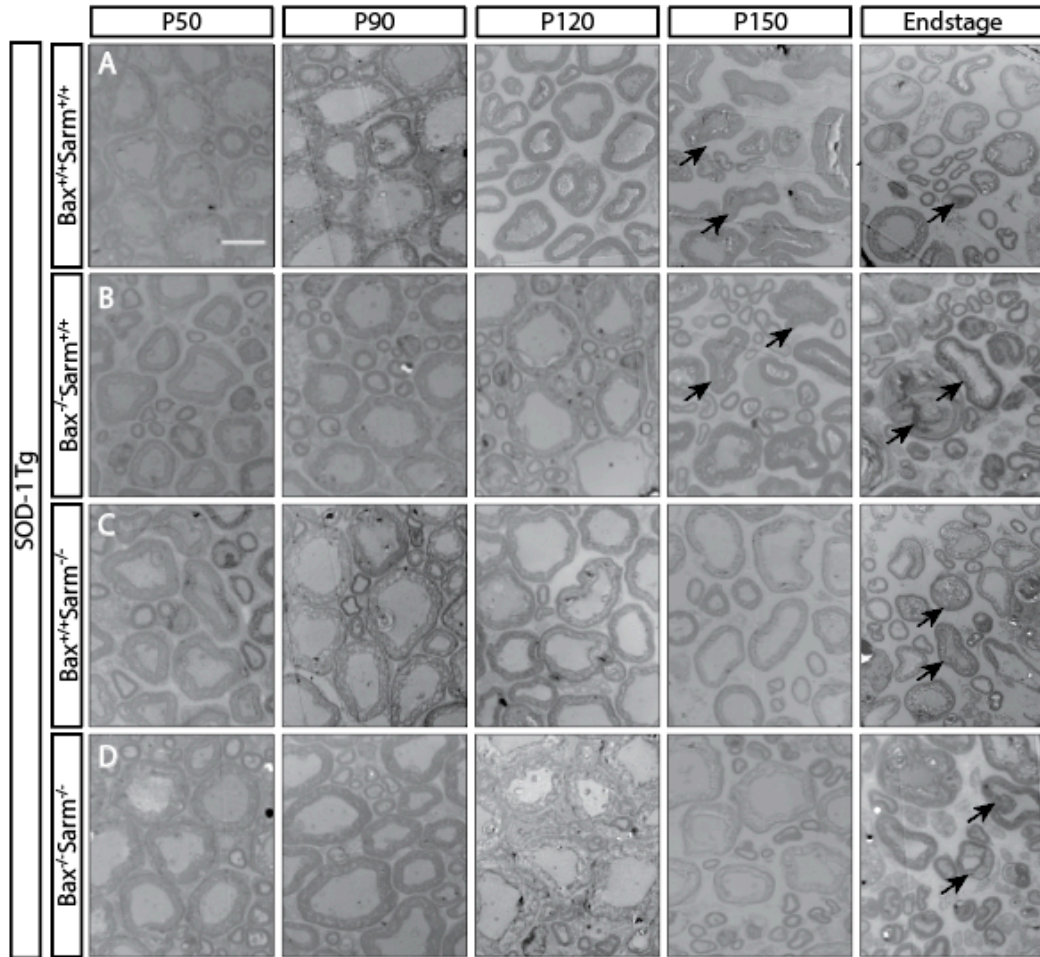


Figure 3.4. Motor axon degeneration in ventral root. Representative electron micrograph images taken of ventral root samples dissected from (A) *SOD-1^{G93A} Tg*, (B) *SOD-1^{G93A} Tg, Bax^{-/-} Sarm^{+/+}*, (C) *SOD-1^{G93A} Tg, Bax^{+/+} Sarm^{-/-}*, and (D) *SOD-1^{G93A} Tg, Bax^{-/-} Sarm^{-/-}* animals (n=3 for each timepoint) when each reached P50, P90, P120, P150, and when they reached score 4, or endstage. Black arrows indicate large degenerating axons. Scale bar = 5 μ m.

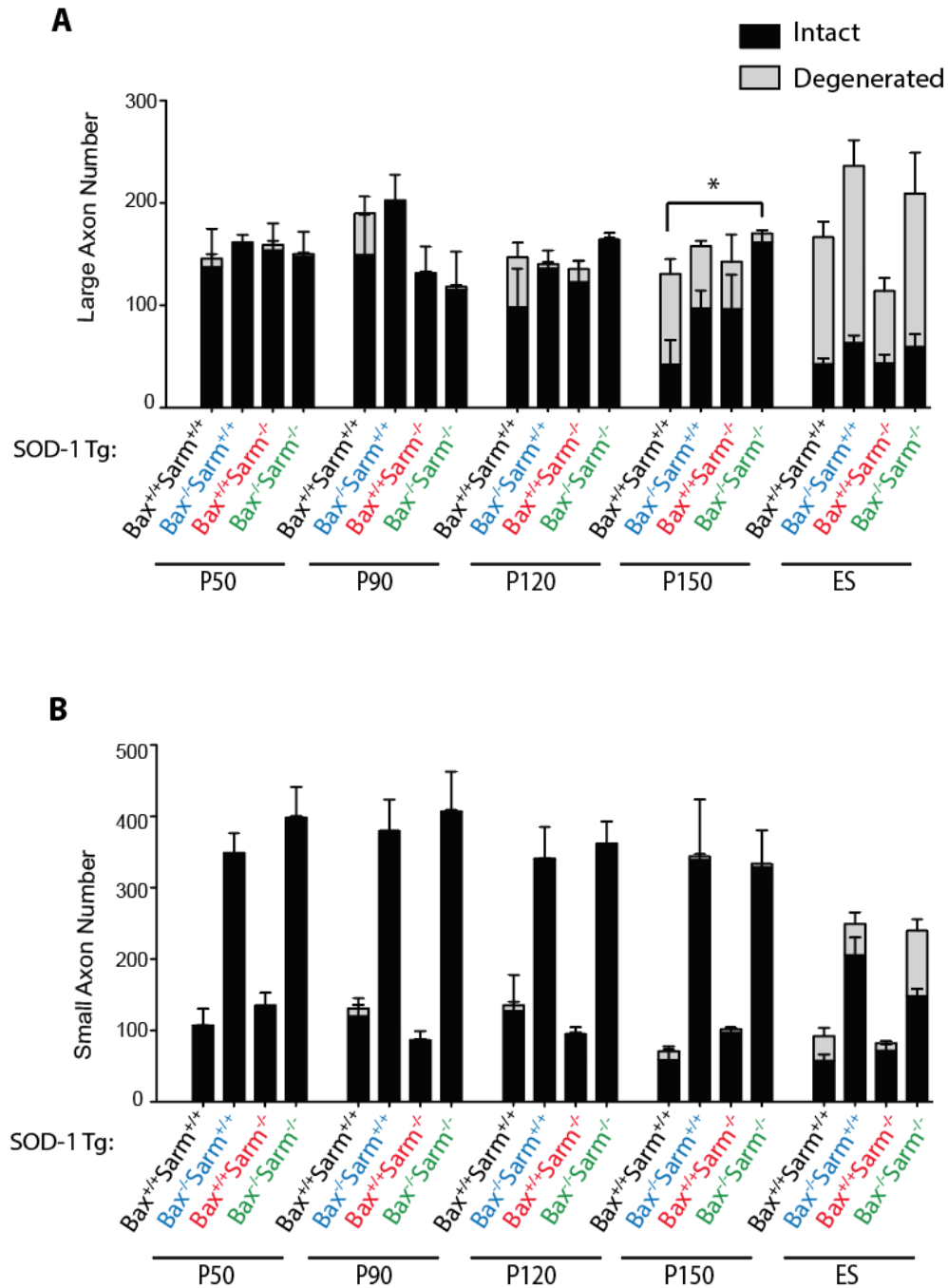


Figure 3.5. Quantification of large and small axons in ventral root. Intact (black bars) and degenerated (gray bars) (A) large and (B) small diameter axons were counted from *SOD-1*^{G93A} Tg (black font) *SOD-1*^{G93A} Tg;*Bax*^{-/-}*Sarm*^{+/+} (blue font), *SOD-1*^{G93A} Tg;*Bax*^{+/+}*Sarm*^{-/-} (red font), and *SOD-1*^{G93A} Tg;*Bax*^{-/-}*Sarm*^{-/-} (green font) animals (n=3 for each timepoint) at P50, P90, P120, P150, and ES (endstage).

Deletion of *Bax* and *Sarm1* delays large neuron loss in ventral horn

NeuN+ cell bodies were counted in the ventral horn of the spinal cord.

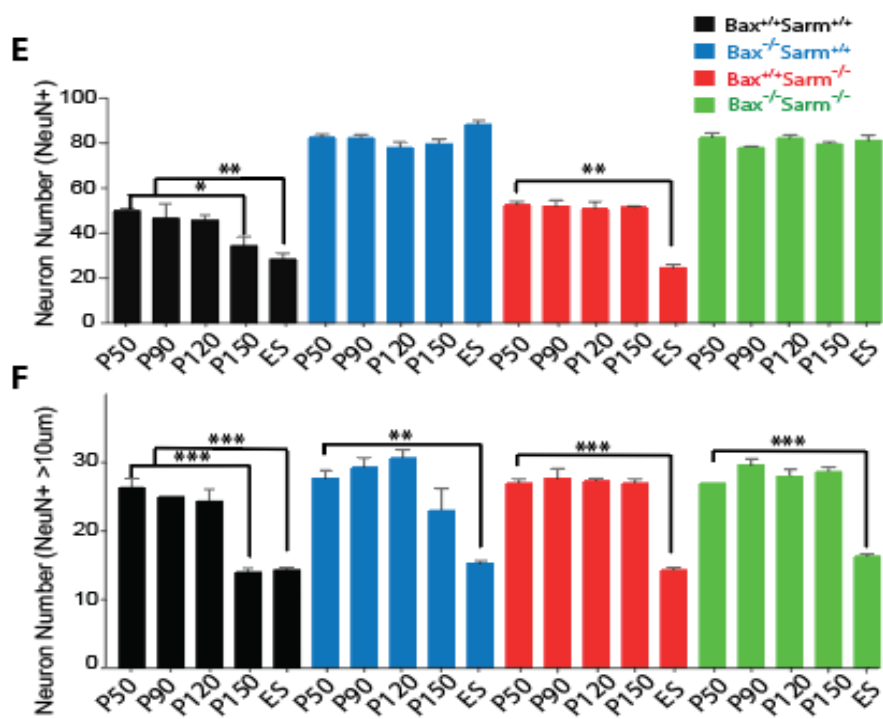
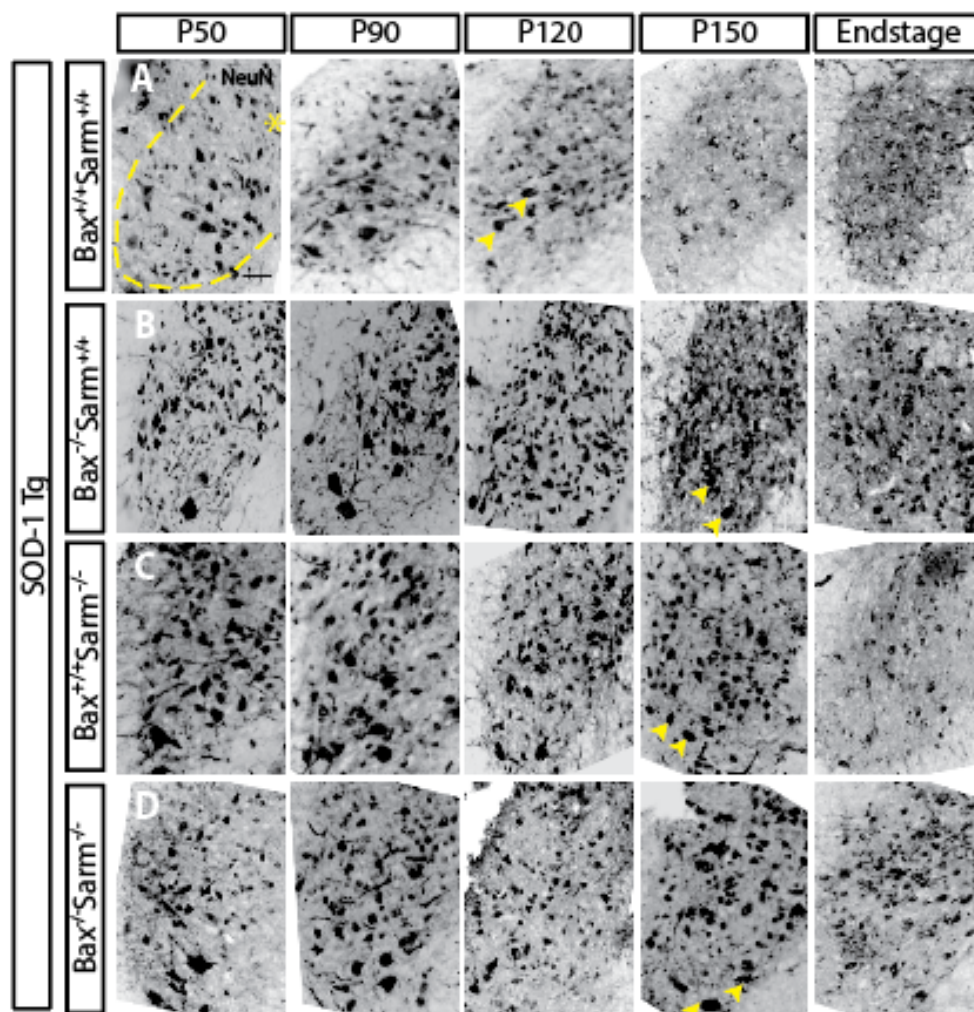
SOD-1^{G93A} Tg animals first exhibit motor neuron loss at late stages (P150) and at endstage, after NMJ denervation and axon degeneration (Fig 3.6A, 3.6E) as reported (Fischer et al, 2004). As reported previously (Gould et al., 2006), the ventral horn of *SOD-1^{G93A}*, *Bax*^{-/-} animals show an increase in neuron number (*SOD-1^{G93A}*: 50 +/- 1.0 NeuN+ neurons, *SOD-1^{G93A}*, *Bax*^{-/-}: 82.7 +/- 1.33 NeuN+ neurons at P50), reflecting both a lack of developmental neuronal cell death and protection of neuronal cell body death at disease endstage (*SOD-1^{G93A}*, *Bax*^{-/-}: 82.7 +/- 1.33 NeuN+ neurons at P50, *SOD-1^{G93A}*, *Bax*^{-/-}: 88.33 +/- 1.76 NeuN+ neurons at endstage (ES) p=ns) (Fig 3.6B and quantified in 3.6E). Large cell bodies in the ventral horn (>10µm in diameter), thought to be the more vulnerable neuron population in ALS, were also quantified. Although it was not statistically significant, a trend of large motor neuron loss was observed in the P150 *SOD-1^{G93A}*, *Bax*^{-/-} mice (*SOD-1^{G93A}*, *Bax*^{-/-}: 27.7 +/- 1.20 large NeuN+ neurons at P50, *SOD-1^{G93A}*, *Bax*^{-/-}: 23 +/- 3.22 large NeuN+ neurons at P150). Loss of large neurons in *SOD-1^{G93A}*, *Bax*^{-/-} mice was comparable to the *SOD-1^{G93A}* Tg mice at endstage (Fig 3.6) (*SOD-1^{G93A}*: 14.33 +/- 0.33 large NeuN+ neurons at ES; *SOD-1^{G93A}*, *Bax*^{-/-}: 15.33 +/- 0.33 large NeuN+ neurons at ES). There was no change in total NeuN+ neuron number in *SOD-1^{G93A}*, *Bax*^{-/-} mice at endstage, because the supernumerary large neurons atrophied and became smaller.

Numbers of ventral horn neurons were similar in *SOD-1^{G93A},Sarm1^{-/-}* mice and *SOD-1^{G93A}* Tg animals at P50 (*SOD-1^{G93A}*: 50 +/- 1.0 NeuN+ neurons; *SOD-1^{G93A},Sarm1^{-/-}*: 52.7 +/- 1.33 NeuN+ neurons) Ventral horn neuron loss (total NeuN+ neurons and large neurons (>10µm)) was delayed in P150 *SOD-1^{G93A},Sarm1^{-/-}* mice relative to *SOD-1^{G93A}* Tg animals, but neuron loss was similar at endstage (Fig 3.6C, 3.6E, 3.6F) (*SOD-1^{G93A}*: 34.33 +/- 4.096 NeuN+ neurons at P150; *SOD-1^{G93A},Sarm1^{-/-}*: 51.7 +/- 0.33 NeuN+ neurons at P150; * p = 0.02; *SOD-1^{G93A}*: 28.33 +/- 2.667 NeuN+ neurons at ES, *SOD-1^{G93A},Sarm1^{-/-}*: 24.67 +/- 1.33 NeuN+ neurons at ES, p=0.36).

The last time point (endstage) was always measured when the animal reached Score 4 (complete paralysis) and varied among genotypes. The *SOD-1^{G93A}* and *SOD-1^{G93A},Sarm1^{-/-}* animals reached this stage around P165, whereas the *SOD-1^{G93A},Bax^{-/-}* and *SOD-1^{G93A},Bax^{-/-};Sarm1^{-/-}* mice reached this stage around P185. Thus, *Sarm1^{-/-}* protection of both large and total ventral horn neuron number at P150 is closer to the time when the animals reach Score 4, suggesting that deletion of *Sarm1* causes the late stage of the disease to progress rapidly. This is consistent with the neurological scoring phenotype in which the *SOD-1^{G93A},Sarm1^{-/-}* animals get the disease later (Score 2) and progress very rapidly to endstage (Fig 2.4B).

Figure 3.6. Neuron cell body loss in ventral horn of spinal cord.

Representative images of NeuN+ stained 12 μ m spinal cord sections labeling cell bodies in (A) *SOD-1^{G93A} Tg*, (B) *SOD-1^{G93A} Tg, Bax^{-/-} Sarm^{+/+}*, (C) *SOD-1^{G93A} Tg, Bax^{+/+} Sarm^{-/-}*, and (D) *SOD-1^{G93A} Tg, Bax^{-/-} Sarm^{-/-}* animals (n=3 for each timepoint) were dissected when each reached P50, P90, P120, P150, and when they reached score 4, or endstage. Yellow dotted line indicates ventral horn where cell bodies were counted and * indicates midline of spinal cord. Quantification of (E) total NeuN+ neurons and (F) large NeuN+ neurons (>10 μ m) located in the ventral horn at timepoints listed above. Scale bar = 50 μ m



Deletion of *Bax* and *Sarm1* delays loss of MMP-9+ neurons

MMP-9 is a marker for the type of large motor neurons most susceptible to degeneration in ALS (Kaplan et al, 2014). MMP-9+ expressing neurons in the *SOD-1^{G93A}* animals degenerated at P120 (Fig 3.7A, quantified in 3.7E) (*SOD-1^{G93A}*: 4.65 +/- 0.43 MMP-9+ neurons at P50; *SOD-1^{G93A}*: 2.08 +/- 0.63 MMP-9+ neurons at P120; * p = 0.05). *Sarm1* knockout, and *Bax*;*Sarm1* double knockout protected MMP-9+ expressing ventral horn neurons up to P150 (Fig 3.7B-D)) (*SOD-1^{G93A}*: 1.51 +/- 0.44 MMP-9+ neurons; *SOD-1^{G93A},Bax^{-/-}*: 3.07 +/- 0.70; p=0.4 ; *SOD-1^{G93A}, Sarm1^{-/-}*: 3.28 +/- 0.06, *p=0.05; *SOD-1^{G93A},Bax^{-/-}, Sarm1^{-/-}*: 4.13 +/- 0.13 ; *p=0.03 at P150). MMP-9+ expressing neurons were lost similarly in all genotypes at endstage (Fig 3.7E) (*SOD-1^{G93A}*: 1.01 +/- 0.20 MMP-9+ neurons; *SOD-1^{G93A},Bax^{-/-}*: 1.11 +/- 0.11; *SOD-1^{G93A}, Sarm1^{-/-}*: 1.00 +/- 0.17; *SOD-1^{G93A},Bax^{-/-}, Sarm1^{-/-}*: 1.34 +/- 0.21 ; at ES).

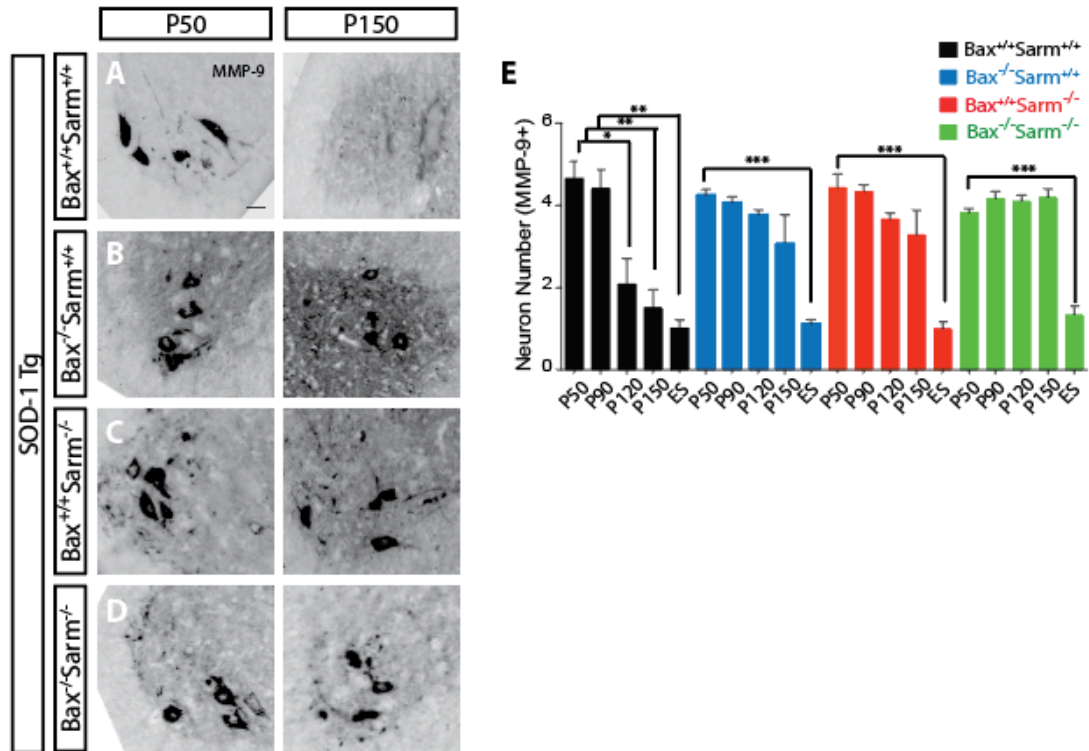


Fig 3.7. MMP-expressing neuron loss in the ventral horn of the spinal cord.

Representative images of MMP-9+ stained 12 μ m spinal cord sections labeling motor neuron cell bodies in (A) *SOD-1^{G93A} Tg*, (B) *SOD-1^{G93A} Tg, Bax^{-/-} Sarm^{+/+}*, (C) *SOD-1^{G93A} Tg, Bax^{+/+} Sarm^{-/-}*, and (D) *SOD-1^{G93A} Tg, Bax^{-/-} Sarm^{-/-}* animals (n=3 for each timepoint) were dissected when each reached P50, P90, P120, P150, and when they reached score 4, or endstage (ES). P50 and P150 representative images are shown. (E) Quantification for MMP-9+ motor neurons in P50, P90, P120, P150, and ES ventral spinal cords.

Conclusions

The results of histological analysis in *Bax*^{-/-} and *Sarm1*^{-/-} animals tracked closely with disease progression. Apoptotic and Wallerian degeneration pathways played distinct roles in the dying back phenotype. Symptom onset did not correlate strictly with the start of neuromuscular junction denervation, but rather occurred about thirty days after the start of NMJ denervation. However, delay in NMJ denervation did correlate with a delayed symptom onset.

Interestingly, the *SOD-1*^{G93A}, *Bax*^{-/-} *Sarm1*^{-/-} animals showed improved neuronal morphology phenotype in all parameters, including a delayed denervation at the NMJ, delayed axon degeneration, and motor neuron cell body preservation which aligned with a delayed symptom onset. These differences were even stronger even further than the *Bax*^{-/-} strain alone.

Chapter 4: Non-cell autonomous SOD-1 toxicity

Rationale

In parallel with the *in vivo* studies described above, we also took an *in vitro* approach to identify novel factors that might play a role in SOD-1-mediated cell death and to elucidate further the mechanism of neuronal cell death observed *in vivo*. We attempted to replicate the previously reported co-culture assay of WT motor neurons and conditioned medium from mutant SOD-1 astrocytes. The goal of this project was to 1) screen through other factors of the apoptotic pathway to determine their role in motor neuron cell death and 2) elucidate further the mechanism between the apoptotic and Wallerian degeneration pathway *in vitro*.

Co-culture of motor neurons and astrocytes

In order to screen through other potential players that were involved in causing motor neuron cell death in this SOD-1-mediated toxicity assay, we needed to first replicate the assay. I first dissected motor neurons from the E12.5 spinal cords of the Hb9-GFP mouse line and co-cultured them with astrocytes (Fig 4.1A). I then treated WT primary motor neurons with collected conditioned medium (CM) from either *SOD-1*^{G93A} Tg astrocytes or Non-transgenic littermate controls (Ntg). After 7 days in culture, I observed a small decline in motor neuron number in cultures conditioned with *SOD-1* Tg CM compared to Ntg conditioned medium (Fig 4.1B)

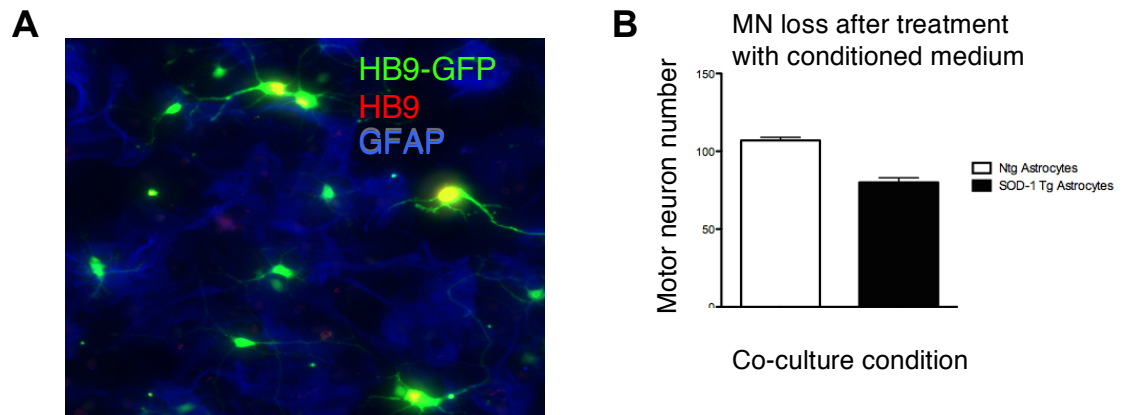


Fig 4.1 Motor neuron loss after treatment with SOD-1 astrocyte conditioned medium. A) Motor neurons isolated from the HB9-GFP mouse line stained with GFP (green) and HB9 antibody (red) co-cultured with an astrocyte monolayer, stained with the marker astrocyte-specific marker, GFAP (blue). B) Motor neuron number after 7 days cultured with either CM from non-transgenic Ntg astrocytes (white bar) or *SOD-1*^{G93A} Tg astrocytes, MN = motor neuron (black bar).

However, we found that not every Hb9-GFP expressing cell stained with the Hb9 antibody (Fig 4.2A). This led to an investigation of the Hb9-GFP line that we were using in the lab. Although Hb9 is a post mitotic marker of motor neurons, we had discovered the Hb9-GFP line was not specific to motor neurons both by observing E12.5 sections from spinal cord stained with Hb9 antibody and either stained with GFP antibody (Fig 4.2B) or just looking at endogenous GFP (Fig 4.2C). This led us to try to determine a new marker for motor neurons. A marker that labeled motor neurons more specifically was peripherin, which we showed successful labeling both *in vivo* (Fig 4.2E) and *in vitro* (Fig 4.2F).

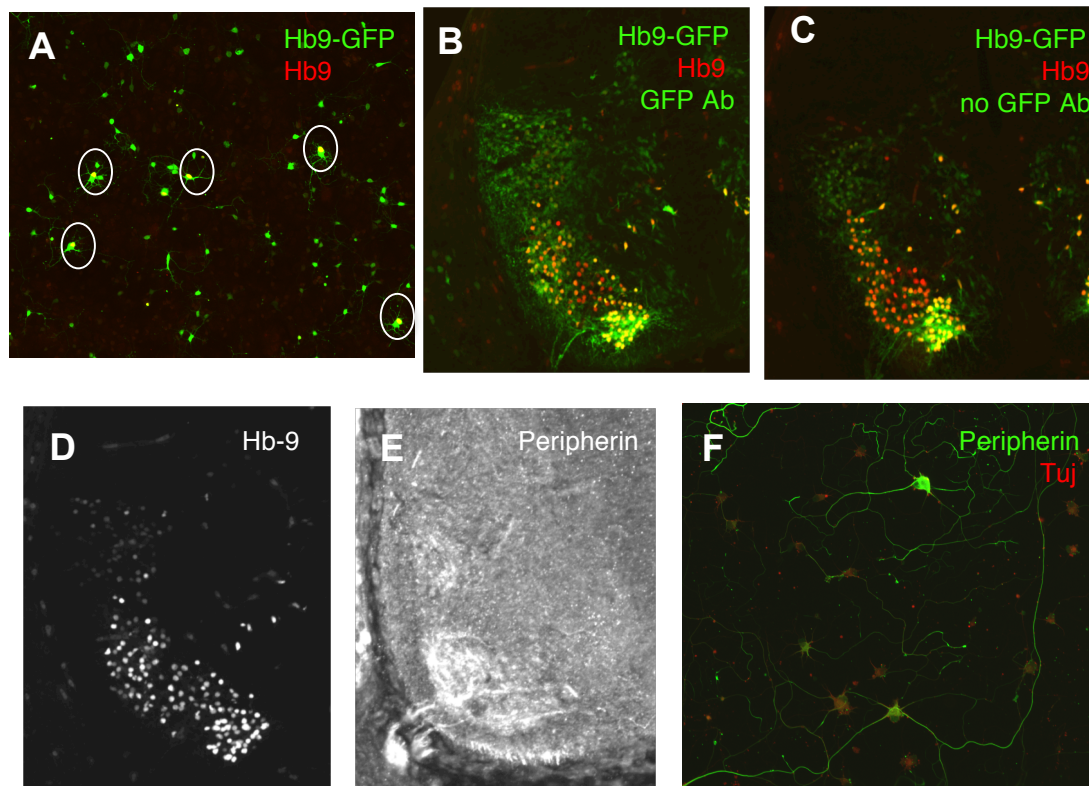


Fig 4.2 Peripherin as a marker for motor neurons. A) Motor neurons dissected and dissociated from spinal cords at E12.5 from the Hb9-GFP mouse line. Circled motor neurons also labeled with the Hb9 antibody stain. B) Unspecific staining of non motor neurons of E12.5 spinal cords in the Hb9-GFP mouse line co-labeled with Hb9 and either GFP antibody (green) or C) endogenous GFP. Serial sections of E12.5 spinal cord stained with D) Hb9 and E) peripherin. F) Peripherin (green) and Tuj (red) staining *in vitro*.

Non-cell autonomous SOD-1 toxicity causes motor neuron cell death, but not axon degeneration

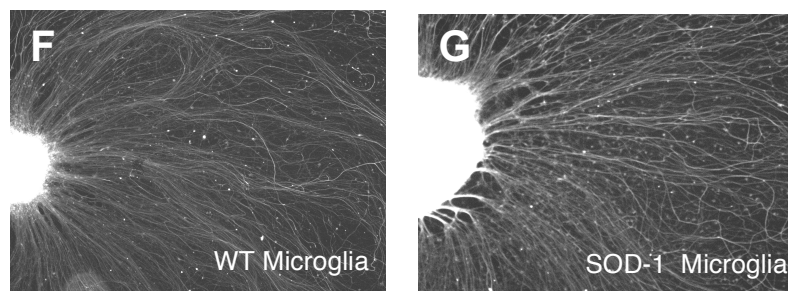
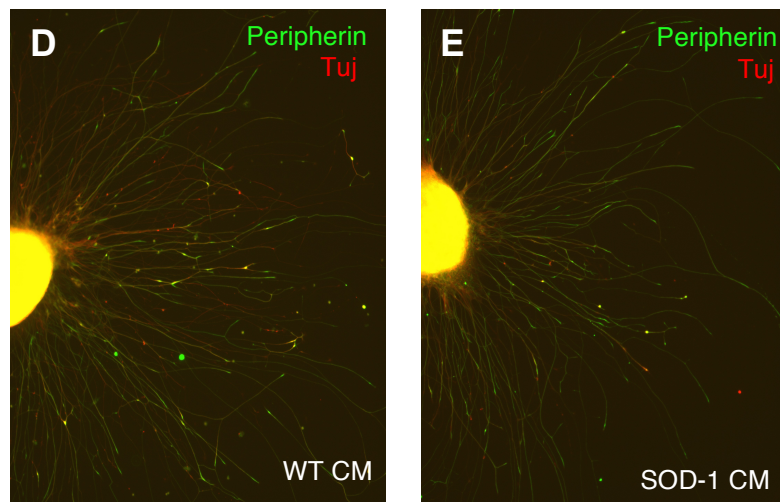
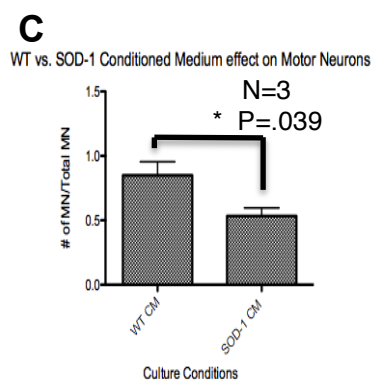
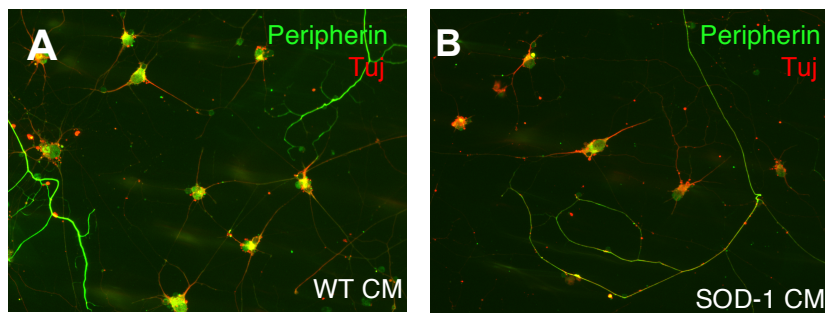
Once we determined a marker for motor neurons *in vitro*, we attempted to reproduce the *SOD-1* Tg astrocyte-mediated toxicity of primary WT motor

neurons (Nagai et al, 2007). We collected conditioned medium (CM) from both *SOD-1^{G93A}* Tg astrocytes and their nontransgenic littermate controls and placed the CM on dissociated motor neuron cultures for 7 days. We saw a decline of motor neuron number (i.e. peripherin+ neurons) conditioned with *SOD-1^{G93A}* Tg CM compared to WT CM (Fig 4.3A-C).

We next wanted to determine the effect of *SOD-1^{G93A}* Tg CM on axon degeneration since deletion of *Sarm1* slightly delayed axon degeneration *in vivo*. We utilized an assay using a spinal cord explant developed in the lab by Zhu hao Wu. The ventral section of the spinal cord was isolated and allowed to adhere to PDL/laminin coated cover slides. These explants grow their axons in a concentric fashion. We treated these ventral explants with either WT or *SOD-1* Tg CM. We did not observe axon degeneration of the ventral explants cultured with *SOD-1* Tg CM compared to WT CM either after 2 days (Fig 4.3D-E) or 7 days (data not shown).

We next tried to co-culture microglia with the ventral explant cultures since microglia were shown by others to cause more motor neuron death than either the *SOD-1* Tg astrocyte monolayer or CM (Nagai et al, 2007). We isolated cortical microglia from P0 pups and allowed microglia to adhere for three to four days before plating ventral explant cultures. Ventral explant cultures were grown on microglia either isolated from *SOD-1* Tg animals or littermate controls (WT) for seven days. Axons from ventral explant cultures did not show any difference in degeneration cultured with WT vs. *SOD-1* Tg microglia (Fig 4.3 F & G).

Fig 4.3 Mutant *SOD-1* CM causes motor neuron cell death in dissociated culture, but not ventral explant culture. Dissociated motor neurons labeled with tuj (red) and peripherin (green) treated with CM from A) WT astrocytes or B) *SOD-1*^{G93A} Tg astrocytes. C) Quantification of motor neurons shows significant loss of motor neuron number cultured with *SOD-1* CM compared to WT CM. No axon degeneration is seen in E12.5 ventral explants cultured with D) WT astrocyte CM vs. E) *SOD-1* astrocyte CM. No axon degeneration is seen in E12.5 ventral explants cultured with F) WT microglia vs. G) *SOD-1* microglia.



Conclusions

While we were able to replicate the cell death phenotype attributed by *SOD-1* Tg astrocyte conditioned medium, the effect was not robust enough to identify novel factors. We sought an enhanced phenotype in ventral explant cultures, specifically looking for an axon degeneration phenotype that we could study *in vitro*. We were unable to observe any effect of either *SOD-1* Tg astrocyte-conditioned medium or microglia monolayers. These negative results could have been caused by a number of different factors. For example, astrocytes and microglia are not present in the peripheral nervous system and therefore direct contact with these factors might not effect axon degeneration; more natural sources of regulators would be Schwann cells.

Chapter 5: Discussion and Future Directions

Before this study, there were conflicting reports as to the role of the Wallerian degeneration pathway in mouse models of ALS. By deleting an active executor of this pathway, *Sarm1*, we were able to definitively determine this pathway's role in a mouse model of ALS. This study answers whether deleting the Wallerian degeneration pathway from the *SOD-1^{G93A}* Tg mouse model would extend lifespan as previously seen in the *Wld^S/SOD-1^{G93A}* Tg mouse (Fischer et al, 2004). We determined that knocking out *Sarm1* and therefore ablating this pathway does not further extend lifespan in an *SOD-1^{G93A}* mouse model. Therefore, the effect seen by *Wld^S* is likely caused by a gain of function independent of *Sarm1*. Through careful characterization, we determined that the Wallerian degeneration pathway plays a role in disease onset and progression.

In this study we completed a deeper analysis than had been done previously on deleting the apoptotic pathway in the *SOD-1^{G93A}* mouse model. We were able to reproduce the previously reported results of cell body preservation at endstage in the spinal cord, delayed neuromuscular junction denervation, and extended lifespan (Gould et al, 2006). In addition to these results, we showed a delayed onset in symptoms of the disease, a prolonged late stage of the disease, and a specific loss of large axon and cell bodies at endstage.

This study is the first to show that deleting the Wallerian degeneration pathway and the apoptotic pathway together resulted in an additive phenotype,

more dramatic than deleting each of these pathways individually. We found further delayed onset of symptoms, which tracked with histological effects indicating delayed NMJ denervation, protection of axons at late stages of the disease, and preservation of cell bodies at endstage. Most interestingly, all of this resulted in a decreased duration of symptomatic stages of the disease.

The role of *Sarm1* in the *SOD-1^{G93A}* Tg model of ALS

In this study, we explored the role of the Wallerian degeneration pathway and its interaction with the classical apoptotic pathway in a *SOD-1^{G93A}* transgenic ALS mouse model. Each of these pathways plays a unique role in disease progression. Deletion of *Sarm1* did not extend lifespan, but it did affect disease onset and progression. *SOD-1^{G93A}* Tg, *Sarm1^{-/-}* mice tended to show trembling of the hindlimbs during a tail suspension test (an early sign of the disease; neurological score 1) before *SOD-1^{G93A}* Tg animals. Combined with delayed late stage development, this led to a prolonged duration of the early stage of the disease in *SOD-1^{G93A}* Tg, *Sarm1^{-/-}* mice.

NMJ alterations present prior to symptom onset in the *SOD-1^{G93A}* Tg mouse line (Mancuso et al 2011; Casas et al 2013). NMJ denervation in the tibialis anterior muscle is delayed in *SOD-1^{G93A}* Tg, *Sarm1^{-/-}* animals compared to *SOD-1^{G93A}* Tg animals. By P120, however, near the onset of symptoms, partial and total denervation is similar. Therefore, it is not surprising that delayed NMJ denervation in the tibialis does not track with symptom onset. There are two

waves of denervation that occur: first, the fast fibers are denervated, followed by a second wave of the more resistant fast fibers and some slow fibers (Hegedus et al, 2007). Delayed denervation of the tibialis, but not the gastrocnemius, suggests that deletion of *Sarm1* may be protective for vulnerable fast fibers, specifically intermediate type IID fast fibers, since there is a significantly increased amount of these fibers in the tibialis compared to the gastrocnemius (Allen et al, 2001).

The extended duration of the early phase is most likely due to delayed axon degeneration in *Sarm1* knockouts at late time points. It should be noted that the number of animals in this cohort for each time point was small (n=3) and that delayed axonal degeneration was seen in two out of the three animals. Axon degeneration in one of the three P150 *SOD-1^{G93A}* Tg, *Sarm1^{-/-}* animals was similar to the *SOD-1^{G93A}* Tg animals, while the other two were intact. These results point to P150 as a sensitive time point for axon degeneration in the *SOD-1^{G93A}* Tg ;*Sarm1^{-/-}* and speaks to the rapid progression of axon degeneration in these animals.

Sarm1^{-/-} mice also showed a delayed ventral horn neuron cell body loss compared to the *SOD-1^{G93A}* Tg mice at P150. The dying back hypothesis suggests that motor neuron cell death follows axon degeneration. Although *Sarm1* does delay ventral horn neuron cell body loss, it is possible that this protection reflects delayed axon degeneration. This hypothesis seems likely because (1) *Sarm1* knockout delays axon degeneration in a number of different

contexts and (2) ventral horn neuron cell body loss proceeds very quickly (P150 - P165) in *SOD-1^{G93A}* Tg, *Sarm1^{-/-}* animals. Delayed NMJ denervation, axon degeneration, and neuronal cell body loss, without an extension in lifespan follows closely with the more rapidly progressing late phase seen in the *SOD-1^{G93A}* Tg, *Sarm1^{-/-}* animals.

The role of Bax in the *SOD-1G93A* Tg ALS mouse model

We replicated results seen previously when blocking the apoptotic pathway through a *Bax* deletion in the *SOD-1^{G93A}* Tg mouse (Gould et al, 2006). Lifespan of *SOD-1^{G93A}* Tg animals was extended by ~20 days, NMJ denervation was delayed, and an increased number of motor neuron cell bodies persisted until endstage. That study was the first to identify the specific loss of large diameter motor neuron axons and cell bodies and specific preservation of small diameter motor neuron axons and cell bodies at endstage. The total number of neuronal cell bodies did not decrease at endstage, whereas large ventral horn NeuN+ cell bodies did. Thus, the ventral horn neurons remaining at endstage included both pre-existing small diameter neurons and large diameter neurons that atrophied and shrank in diameter. This suggests that although ventral horn neuron cell bodies are protected by deletion of the apoptotic pathway, the neurons that remain at endstage of the disease are most likely non-functional. This interpretation is consistent with the fact that even though cell bodies remain

in the *SOD-1^{G93A}* Tg, *Bax^{-/-}* animals, the animals still proceed through all stages of disease progression, including complete paralysis.

The lifespan of *SOD-1^{G93A}* Tg, *Bax^{-/-}* animals correlates best with the delayed disease onset, which likely reflects delayed NMJ denervation. Duration of the disease is similar in *SOD-1^{G93A}* Tg, *Bax^{-/-}* and *SOD-1^{G93A}* Tg animals (Fig 2.4A). We found that the late stage of the disease is significantly extended in the *SOD-1^{G93A}* Tg, *Bax^{-/-}* compared to the *SOD-1^{G93A}* Tg. One possibility is that this extended late phase is due to an increased amount of collateral axonal sprouting. Small fibers retain the ability to regenerate (Frey et al, 2000; Pun et al, 2006) and *SOD-1^{G93A}* Tg, *Bax^{-/-}* mice have an increased number of small diameter axons, which may be able to sprout and reinnervate the muscle. Therefore, we cannot rule out the possibility that the NMJ phenotype observed in P90 *SOD-1^{G93A}* Tg ;*Bax^{-/-}* mice reflects reinnervation by an increased number of collateral axons rather than delayed denervation. The reinnervation hypothesis may be a better explanation for the prolonged late phase, but because these effects happen long before disease onset, it is difficult to infer from these results which hypothesis is correct.

The synergistic role of Bax and Sarm

Most interestingly, we were able to explore the synergistic role of both these pathways in the *SOD-1^{G93A}* Tg animal through a double genetic deletion of *Bax* and *Sarm1*. Surprisingly, the *SOD-1^{G93A}* Tg, *Bax^{-/-}* *Sarm1^{-/-}* was able to further

delay disease onset significantly from both the *SOD-1^{G93A}* Tg and more interestingly, from the *SOD-1^{G93A}* Tg, *Bax^{-/-}* mice. The *SOD-1^{G93A}* Tg, *Bax^{-/-} Sarm1^{-/-}* mice had an extended lifespan similarly to the *SOD-1^{G93A}* Tg, *Bax^{-/-}* mice (Fig 2.2A), but a duration of symptomatic stages that was half that of the *SOD-1^{G93A}* Tg and *SOD-1^{G93A}* Tg, *Bax^{-/-}* animals (Fig 2.4A). The delayed symptom onset correlated with the delay in neuromuscular junction denervation similar to the *SOD-1^{G93A}* Tg, *Bax^{-/-}* mice in the gastrocnemius and further in the tibialis anterior. It is unclear at this time what the reason is for the further delay in denervation attributed by *Sarm1* deletion alone in the tibialis, but it is consistent with the even greater effect seen in the *Bax^{-/-} Sarm1^{-/-}* mice in the tibialis.

Double knockout of *Bax* and *Sarm1* delays large motor neuron axon degeneration better than *Bax* or *Sarm1* knockout alone. This likely reflects a *Bax^{-/-}* mediated delay in neuromuscular denervation and *Sarm1^{-/-}* mediated axonal protection. Small diameter ventral horn neuron cell bodies were equally well protected in *SOD-1^{G93A}* Tg, *Bax^{-/-} Sarm1^{-/-}* and *SOD-1^{G93A}* Tg, *Bax^{-/-}* mice at endstage of the disease. It is worth noting that while not significant, P150 *SOD-1^{G93A}* Tg, *Bax^{-/-}* mice had a trend towards a decreased number of large cell bodies in the ventral horn. It seems, therefore, that the *SOD-1^{G93A}* Tg, *Bax^{-/-} Sarm1^{-/-}* mice had better protection of large cell bodies at this timepoint. If *SOD-1^{G93A}* Tg, *Bax^{-/-}* and *SOD-1^{G93A}* Tg, *Bax^{-/-} Sarm1^{-/-}* mice had been analyzed at another time point closer to endstage, we may have been able to discern a difference in a ventral

horn neuron cell body protection. All of these results are consistent with the more rapidly progressing symptomatic stage seen in the *SOD-1^{G93A}* Tg, *Bax^{-/-}* *Sarm1^{-/-}*.

These results support other groups' findings of the importance of denervation at the NMJ in the onset of ALS disease. Axon degeneration plays an important role in disease progression and in determining lifespan. Ventral horn neuron cell bodies can be preserved, even at endstage of the disease, whereas axon degeneration always occurs. This points to the importance of determining the underlying causes of neuromuscular denervation and axon degeneration. *Sarm1* was able to delay degeneration of the axon slightly, but its inability to completely protect axons implies that other molecular pathways are involved in axon degeneration in the *SOD-1^{G93A}* Tg mouse model of ALS.

Future Directions

While this study elucidates the roles of *Bax* and *Sarm1* genes in phenotypic disease onset and progression as well as anatomical features of the “dying back” of motor neurons in the *SOD-1^{G93A}* mouse model, there are still some outstanding questions in the field. These studies addressed the role of the apoptotic and Wallerian degeneration pathways in this disease, but the cellular site at which the genes act remains unknown. While it is thought that deleting *Bax* and *Sarm1* prevents neuronal cell death in a neuron specific manner, there is also a known non-cell autonomous role of mutant *SOD-1* in these mouse models. The experiment to answer whether this effect occurs cell autonomously

would be to knock out both of these genes conditionally in motor neurons using either a Chat-Cre or Hb9-Cre mouse line. These experiments have obvious limitations that crossing another allele would make getting the number of mice needed for statistical analysis challenging, however, this approach would answer whether deletion of these two pathways exhibit its effects in a cell autonomous manner.

Also, in addition to the histological characterization that was already done, further experiments would be able to answer what is occurring on a finer scale in the ventral root and neuromuscular junction synapses. With the current results, we are unable to determine the effect of deleting the apoptotic and Wallerian degeneration pathways on reinnervation at the NMJ. Electron micrograph analysis at the neuromuscular junction would answer which of the synapses are reinnervated. Since this balance of denervation/reinnervation of synapses at the NMJ regulates symptom onset, it is possible by enhancing reinnervation, one could delay symptom onset further. Targeting this mechanism might be another potential way to mitigate disease symptoms.

Another experiment to do would be to look at the later time points (around P170-180) in the *Bax*^{-/-} and *Bax*^{-/-}/*Sarm1*^{-/-} animals. It is likely, since the histological analysis of *Bax*^{-/-}/*Sarm1*^{-/-} animals showed an even greater effect compared to *Bax*^{-/-} alone, that this later time point may show an even further protection, specifically of large neurons and MMP-9 expressing cells in the ventral spinal cord, and possibly even axons in the ventral root. Based on

symptomatic stage data from the neurological scoring, it is likely that this late time point would be a sensitive one for the *Bax*^{-/-}/*Sarm1*^{-/-} animals with either all animals showing protection or a subset of them showing protection. Addressing these questions would provide a clearer role for each of these pathways in the mechanism of the 'dying back' nature of motor axons in the *SOD-1*^{G93A} mouse model of ALS.

Chapter 6: Materials and Methods

Animal models

All experiments using animals were performed in accordance with NIH guidelines and approved by the Institutional Animal Care and Use Committee at the Rockefeller University. Mice null for *Bax* (Knudson et al, 1995) and *SOD-1^{G93A}* Tg mice (B6.Cg-Tg(SOD1-G93A)1Gur/J) were obtained from The Jackson Laboratory. *SOD-1^{G93A}* mice expressed a high copy number of the human *SOD-1* gene, which harbors a glycine to alanine mutation at the 93rd codon of the *SOD-1* gene. *Bax^{-/-}* and *Sarm^{-/-}* mice were mated to generate *Bax^{+/-}/Sarm^{+/-}* females. The *Bax/Sarm* heterozygotes were then cross with Tg[*SOD-1-G93A*] male mice to yield the following genotypes for analysis: *SOD-1^{WT}Bax^{+/+},Sarm^{+/+}*; *SOD-1^{WT} Bax^{-/-},Sarm^{+/+}*; *SOD-1^{WT}Bax^{+/+},Sarm^{-/-}*; *SOD-1^{WT}Bax^{-/-},Sarm^{-/-}*; *SOD-1^{G93A} Tg,Bax^{+/+},Sarm^{+/+}*; *SOD-1^{G93A} Tg,Bax^{-/-},Sarm^{+/+}*; *SOD-1^{G93A} Tg,Bax^{+/+},Sarm^{-/-}* and *SOD-1^{G93A} Tg,Bax^{-/-},Sarm^{-/-}*. All comparisons in this study were between littermates and housed together to minimize environmental factors. Mice were genotyped using PCR protocols from the Jackson Laboratory. The mice were housed with free access to water and SulfaTrim rodent chow. The mice were divided into two cohorts. One was dedicated to determining survival, symptom onset and progression through neurological scoring, body weight loss, and endstage histology. The other was used for histological analysis at various time points during disease progression: P50, P90, P120, and P150.

Table 6.1 Genotypes analyzed in this study:

Genotype:

$SOD-1^{WT} Bax^{+/+} Sarm^{+/+}$	$SOD-1^{G93A} Tg; Bax^{+/+} Sarm^{+/+}$
$SOD-1^{WT} Bax^{-/-} Sarm^{+/+}$	$SOD-1^{G93A} Tg; Bax^{-/-} Sarm^{+/+}$
$SOD-1^{WT} Bax^{+/+} Sarm^{-/-}$	$SOD-1^{G93A} Tg; Bax^{+/+} Sarm^{-/-}$
$SOD-1^{WT} Bax^{-/-} Sarm^{-/-}$	$SOD-1^{G93A} Tg; Bax^{-/-} Sarm^{-/-}$

Survival, symptom onset, ALS disease progression

Survival, symptom onset, disease progression, and body weight loss were assessed in one cohort (n= 8-9 for each genotype; 8 different genotypes listed above). Symptom onset and disease progression were assayed using the neurological scoring system guidelines from The Jackson Laboratory (http://jackson.jax.org/rs/444-BUH-304/images/Working_with_ALS_Mice.pdf).

Mice were assessed by two experimenters every other day starting at P50 for the duration of their lifespan. Mice were scored as follows: Score 1: trembling of the hind legs during a tail suspension test; Score 2: toes curl under foot during walking; Score 3: hind limb paralysis; Score 4: terminally paralyzed (unable to right themselves after 30 seconds of being placed on each side). Animals were euthanized upon reaching score 4. Body weight measurements were collected daily beginning at P50 and through score 4 for mice carrying the $SOD-1^{G93A}$ allele or until P200 for $SOD-1^{WT}$ controls.

Rotorod behavioral assay

Motor performance of mice was tested using the rotorod behavioral assay. A modified protocol was created and tested to accommodate a large cohort. Each mouse was tested when they reached P50, P90, P120, P150 and P180. This cohort was also used for histological analysis, so three mice were removed at each timepoint resulting in P50 (n = 15 per genotype), P90 (n = 12 per genotype), P120 (n = 9 per genotype), P150 (n = 6 per genotype), and P180 (n = 3 per genotype). The modified protocol to test the behavioral function was to (1) place the mice on the rotorod at a non-accelerating speed until each mouse stayed on successfully for 1 minute, (2) run three trials with an acceleration of 5 RPM, (3) give the mice a 1 minute break, and (4) run three trials with an acceleration of 5 RPM and record these three times. The average of the three trials was plotted for each mouse.

Tissue collection

Mice were anesthetized and perfused with PBS followed by 4% paraformaldehyde-PBS. For cohort 1, *SOD-1^{G93A}* Tg mice were euthanized when they reached score 4 and *SOD-1^{WT}* animals were euthanized at P200 to represent endstage. A second cohort was used to collect histological samples at P50, P90, P120 and P150 (n=3 per time point per genotype). Whole mice were placed on ice for 20 minutes after perfusion for further fixation. The sacral spinal

cord, sacral ventral root, tibialis anterior and gastrocnemius muscles were dissected and postfixed.

Neuromuscular Junction Analysis

Following dissection, the gastrocnemius and tibialis anterior muscles were postfixed in 4% paraformaldehyde-PBS overnight, then washed 3x with 1x PBS and transferred to a 2:1 OCT:30% sucrose-PBS solution for 3 days. Samples were frozen in OCT using an isopropanol/dry ice bath and the cryopreserved samples were sectioned longitudinally (80 μ m). The tissue was permeabilized in 1% Triton X-100/PBS for 1 hour and then blocked overnight in 0.1% Triton X-100/PBS containing 10% donkey serum at 4°C. Muscles were stained with rabbit anti-synapsin (1:200, Synaptic Systems) in blocking buffer at 4°C for at least 24 hours. After four 1-hour washes using 0.1% Triton X-100/PBS, muscles were incubated with donkey anti-rabbit Alexa 594 antibody (1:1000, Invitrogen) and α -bungarotoxin, fluorescein conjugated (1:1000, Invitrogen) for 24 hours. Sections were then washed in PBS four times and coverslips were mounted using Fluoromount-G (SouthernBiotech). Imaging of samples was performed with a LSM 510 laser scanning confocal microscope (Leica). To analyze presynaptic terminals, maximum-intensity projections of z-stack images for each muscle sample were generated using FIJI software. Postsynaptic AChR (α -bungarotoxin-positive) sites not apposed by synapsin were counted as denervated. Synapses with less than 50% overlap were described as partially denervated. Approximately

100 neuromuscular junctions were examined for both gastrocnemius and tibialis anterior muscles for all time points and genotypes.

Axon counts and electron microscopy

Ventral roots were stored in 4% paraformaldehyde/2.5% glutaraldehyde in 0.1 M sodium cacodylate buffer overnight at 4°C. Subsequently, the samples were post-fixed in 1% osmium tetroxide for one hour on ice, stained with 1% Uranyl acetate for 30 minutes at room temperature, dehydrated with increasing concentrations of ethanol, and infiltrated/embedded in Eponate12 resin. Ultrathin 70 nm sections were cut and examined on the electron microscope (100CX JEOL, Tokyo, Japan) at 80 kV with a digital imaging system (XR41-C, Advantage Microscopy Technology Corp, Denver, MA). For quantification, large and small diameter axons were counted as either intact or degenerated if any sign of fragmentation was observed.

Neuron number in the ventral horn of the spinal cord

The sacral level of the spinal cord was fixed overnight in 4% paraformaldehyde-1XPBS solution. Samples were then washed 3x with PBS and transferred to a 2:1 OCT:30% sucrose/PBS solution. Spinal cords were frozen in OCT in an isopropanol/dry ice bath and then sectioned into 12 µm thick sections. Spinal cord sections were stained with antibodies: mouse anti-NeuN (1:1000, Chemicon) and goat anti-MMP-9 (1:200, Sigma-Aldrich). The average number of

NeuN+, large NeuN+ (>10µm) and MMP-9+ expressing neurons in the ventral horn of eight spinal cord sections per animal is reported.

Statistical analysis

Statistical significance of survival and body weight loss was determined using a Log-rank test and is represented as median days of survival +/- SEM. A one-way ANOVA statistical test was used to test differences between genotypes in the duration of different stages of the disease, neuromuscular junction innervation (comparing different genotypes at various timepoints), and large and small axon number (comparing genotypes at various timepoints). A one-way ANOVA statistical test was used to determine differences in neuron number (NeuN+, large NeuN+, and MMP-9+) within one genotype at the different timepoints.

Table 6.2 Antibodies used in this study

Antibody	Source
Rabbit anti-synapsin	Synaptic systems
Alexa 488-conjugated a-bungarotoxin	Invitrogen
Mouse anti-NeuN	Chemicon
Goat anti-MMP-9	Sigma Aldrich
Rabbit anti-peripherin	Millipore

Mouse anti-tuj	Invitrogen
Mouse anti-GFAP	Millipore
Rabbit anti-GFP	Abcam
Rabbit anti-HB9	Sam Phaff

Primary astrocyte culture

Glial monolayers were prepared from *SOD-1^{G93A}* Tg or their nontransgenic littermate (WT) cortex P0 pups. Cortices were triturated 20-25x with a pipetman to cells were plated in glial medium: DMEM (Invitrogen) containing 10% FBS (Invitrogen) and 100 U of penicillin and streptomycin antibiotics (Invitrogen). Cells were allowed to grow for ~2 weeks to reach confluency.

Astrocyte conditioned medium

After glial cells became confluent, cells were shaken for 1 hour at room temperature at 100 rpm to remove microglia. The supernatant was then removed and replaced with motor neuron cell medium. At 7 days, we collected the conditioned medium, centrifuged it for 1000g for 5 minutes to eliminate floating cells. The conditioned medium was filtered and frozen down at -80°C. Before use on motor neurons, penicillin/streptomycin/glutamine plus cocktail of trophic factors was supplemented into the conditioned medium.

Primary motor neuron culture

Spinal cords from E12.5 WT CD-1 mice or HB9-GFP1 Tmj transgenic mice were dissected from embryos in Hibernate-E medium. Spinal cords were trypsinized with 0.05% trypsin (Invitrogen) for five minutes, run through 4% filtered BSA cushion at 500 rpm for 5 minutes, centrifuged through a 5.2% sucrose gradient made with optiprep solution in 4.4% Tricine buffer for 15 minutes at 800 rpm. The cells were then washed once with neurobasal medium (Invitrogen) and spun down at 1000 rpm for 5 minutes. The supernatant was removed and cells were resuspended in motor neuron medium containing B27, penicillin/streptomycin/glutamine, and a cocktail of neurotrophic factors including 10 ng/mL of brain-derived neurotrophic factor, 10 ng/mL of glia-derived neurotrophic factor, 10 ng/mL of NT-3, and 25 ng/mL of ciliary neurotrophic factor. Motor neurons were plated on plastic 8-well slides at 1500 cells/cm² coated with poly-D-lysine/laminin.

Ventral explant cultures

Spinal cords from E12.5 WT CD-1 mice were dissected carefully out of the embryo in Hibernate-E medium. The spinal cords were cut along the dorsal horn so as to flatten out the spinal cord. The dorsal section of the spinal cord was then cut from the ventral section of the spinal cord. The ventral spinal cord was then cut into 8 even sections horizontally and each section was cut another 8 times

horizontally and vertically. These ventral explants were then plated on plastic 8-well slides coated in poly-D-lysine/laminin.

Appendix 1: *SOD-1*^{WT} Histology

In parallel with all of the *SOD-1* Tg histological samples that were collected, control *SOD-1*^{WT} samples were also collected at the neuromuscular junction, ventral root, and spinal cord at all of the different timepoints analyzed above (P50, P90, P120, P150, and ES). Representative images of endstage *SOD-1*^{WT} and *SOD-1*^{G93A} Tg animals and quantification of innervated synapses is shown in A1.1. Motor axons in the ventral root at each timepoint are shown in A1.2 and neuron cell body number is shown in A1.3 and A1.4.

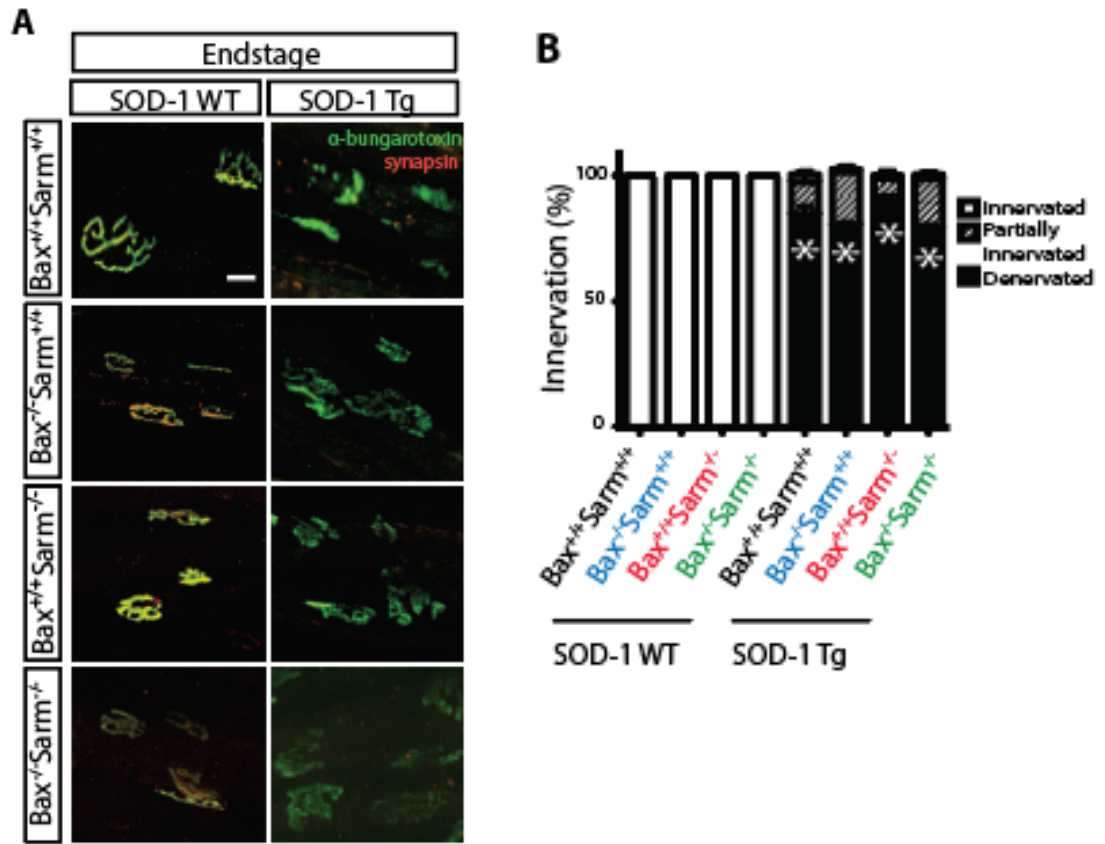


Figure A1.1. Neuromuscular junction innervation at endstage. Representative images of neuromuscular junction of ventral root samples dissected from *SOD-1*^{WT}, *SOD-1*^{WT},*Bax*^{-/-}*Sarm*^{+/+}, *SOD-1*^{WT},*Bax*^{+/+}*Sarm*^{-/-}, and *SOD-1*^{WT},*Bax*^{-/-}*Sarm*^{-/-}, *SOD-1*^{G93A} Tg, *SOD-1*^{G93A} Tg, *Bax*^{-/-}*Sarm*^{+/+}, *SOD-1*^{G93A} Tg, *Bax*^{+/+}*Sarm*^{-/-}, and *SOD-1*^{G93A} Tg, *Bax*^{-/-}*Sarm*^{-/-} animals (n=3 for each timepoint) at endstage (P200 for *SOD-1*^{WT} animals and when the animals reached score 4, or paralysis for *SOD-1* Tg animals). α -bungarotoxin was used to label postsynaptic sites (green) and synapsin antibody (red) labeled presynaptic sites of the neuromuscular junction in the gastrocnemius muscle. Yellow was counted as completely innervated synapses, yellow and green (indicated by white arrows) were counted as partially innervated synapses, and green only were counted as denervated synapses.

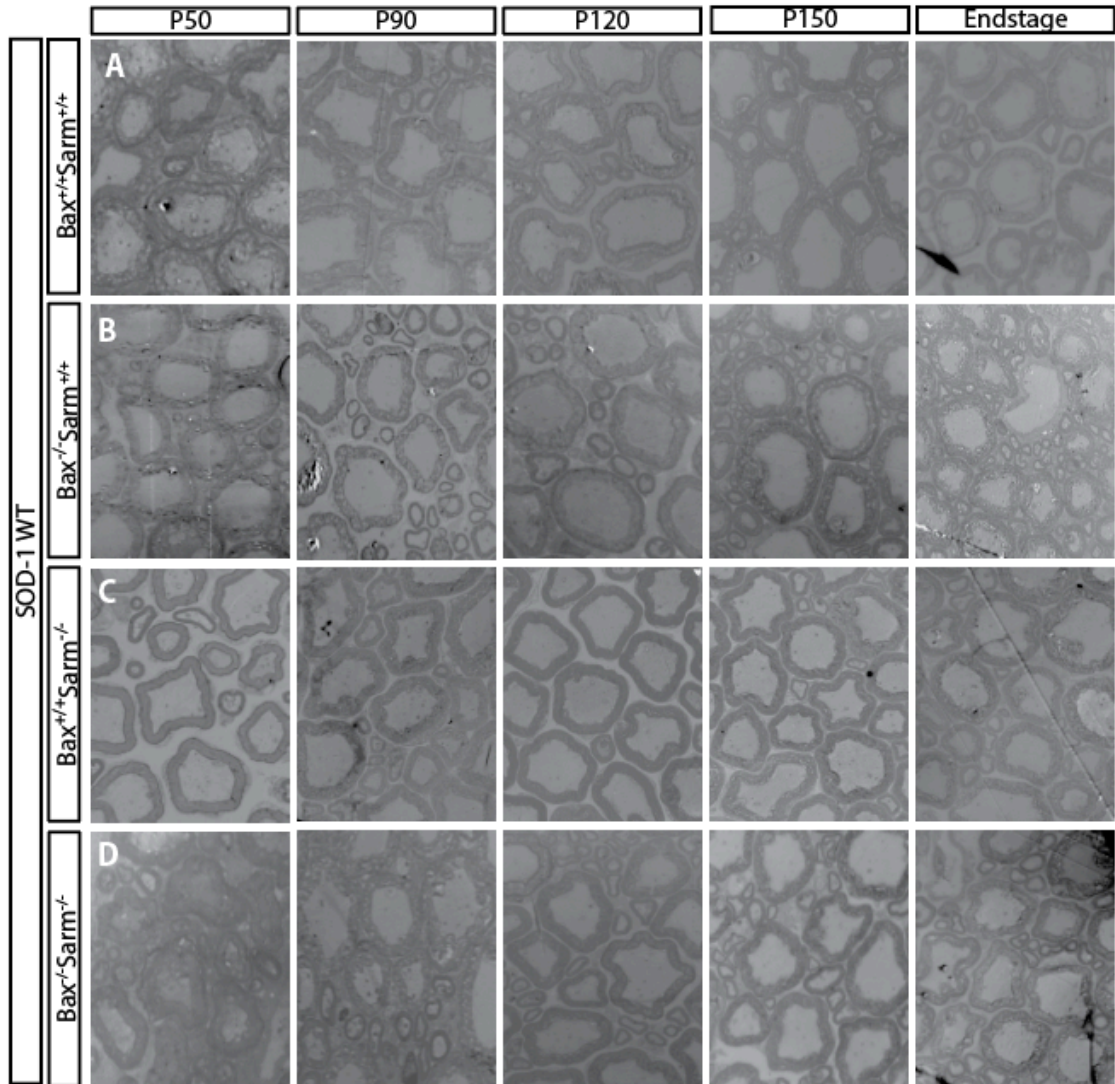


Figure A1.2. Motor axon degeneration in ventral root. Representative electron micrograph images taken of ventral root samples dissected from (A) *SOD-1^{WT}*, (B) *SOD-1^{WT},Bax^{-/-}Sarm^{+/+}*, (C) *SOD-1^{WT},Bax^{+/+}Sarm^{-/-}*, and (D) *SOD-1^{WT},Bax^{-/-}Sarm^{-/-}* animals (n=3 for each timepoint) when each reached P50, P90, P120, P150, and P200 (ES).

Figure A1.3. Neuron cell body in ventral horn of spinal cord. Representative images of NeuN+ stained 12 μ m spinal cord sections labeling cell bodies in (A) *SOD-1^{WT}*, (B) *SOD-1^{WT},Bax^{-/-}Sarm^{+/+}*, (C) *SOD-1^{WT},Bax^{+/+}Sarm^{-/-}*, and (D) *SOD-1^{WTg},Bax^{-/-}Sarm^{-/-}* animals (n=3 for each timepoint) were dissected when each reached P50, P90, P120, P150, and P200, or endstage. Quantification of (E) total NeuN+ neurons and (F) large NeuN+ neurons (>10 μ m) located in the ventral horn at timepoints listed above.

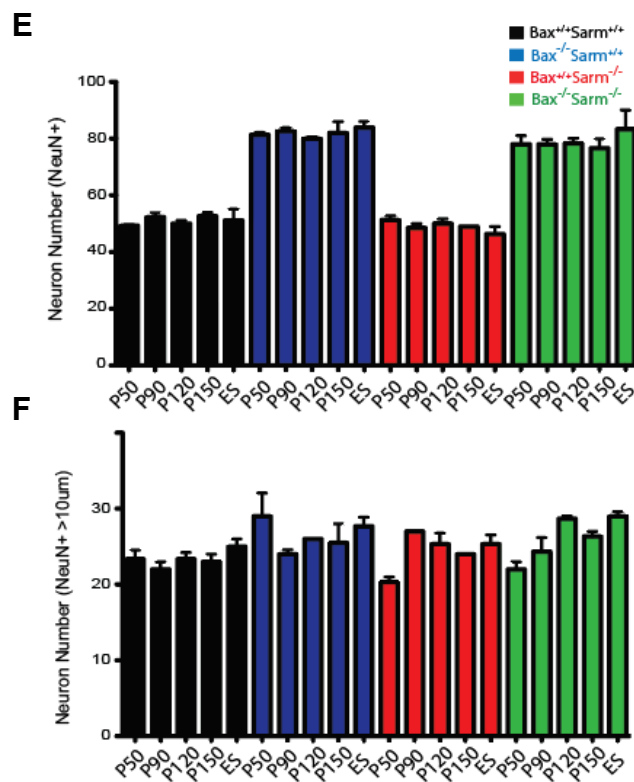
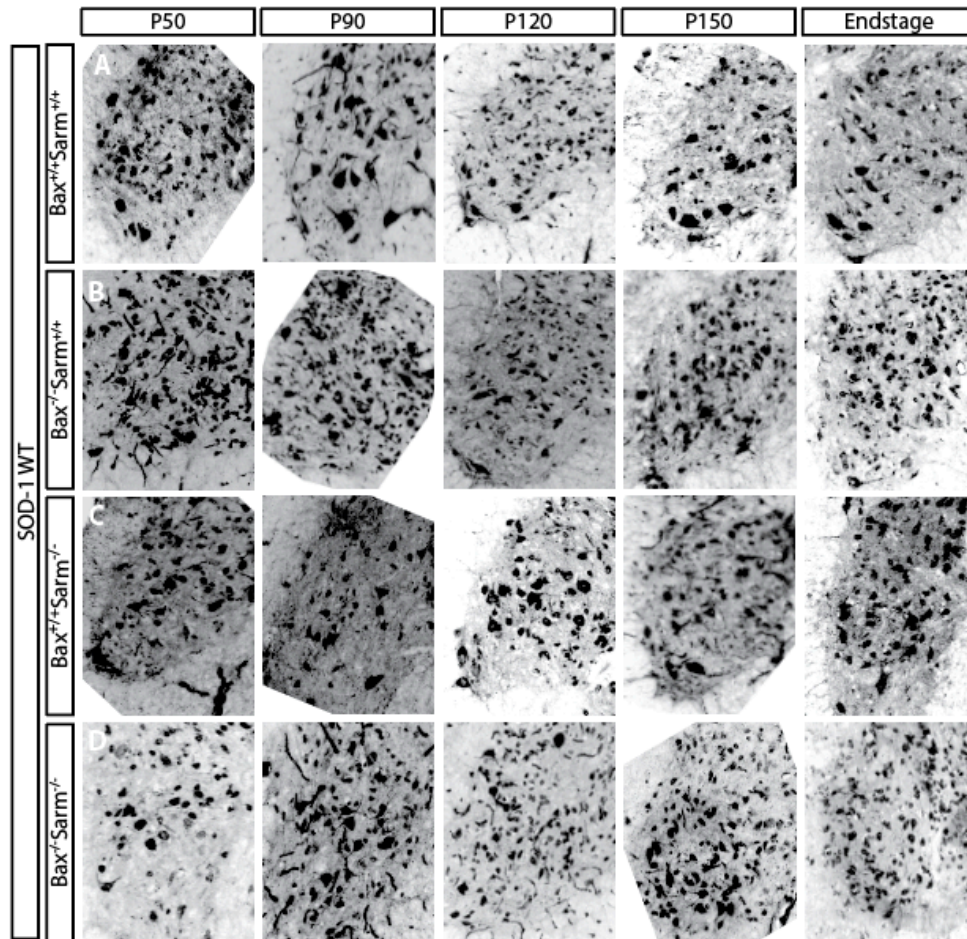
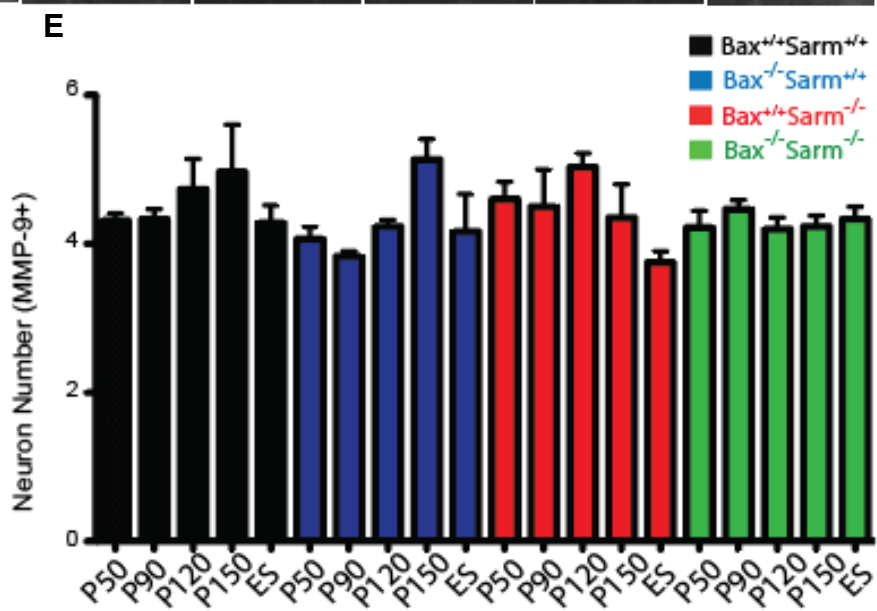
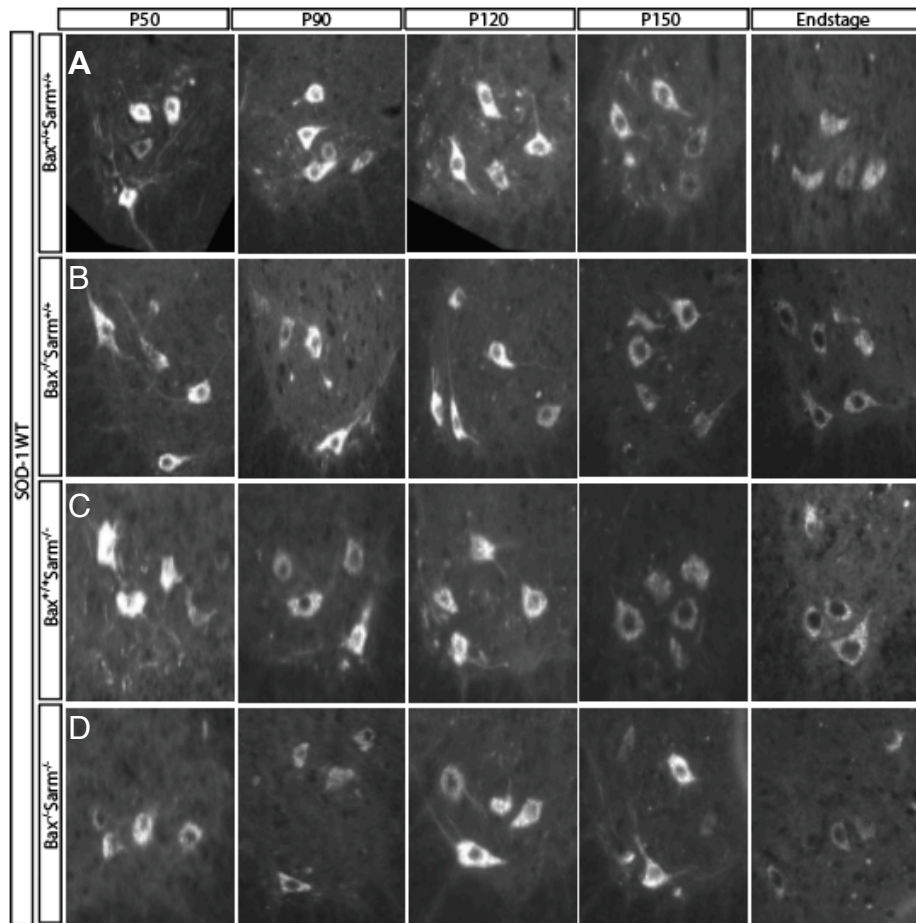


Figure A1.4. MMP-9+ cell body in ventral horn of spinal cord. Representative images of MMP-9+ stained 12 μ m spinal cord sections labeling cell bodies in (A) *SOD-1^{WT}*, (B) *SOD-1^{WT},Bax^{-/-}Sarm^{+/+}*, (C) *SOD-1^{WT},Bax^{+/+}Sarm^{-/-}*, and (D) *SOD-1^{WT},Bax^{-/-}Sarm^{-/-}* animals (n=3 for each timepoint) were dissected when each reached P50, P90, P120, P150, and P200, or endstage. (E) Quantification of MMP-9+ neurons .



Appendix 2. MMP-9+ cells at all timepoints in *SOD-1G93A* Tg animals

MMP-9 labeled cells were shown for P150 and endstage timepoints in the results section of this thesis to indicate the latest timepoint that showed protection in *Bax* KO, *Sarm* KO, and *Bax/Sarm* dKO lines. Shown below are all of the other earlier timepoints that showed protection (P50, P90, and P120). All results in A2.1 showed similar protection at these timepoints comparatively to the P150 timepoint in the genetic knockouts.

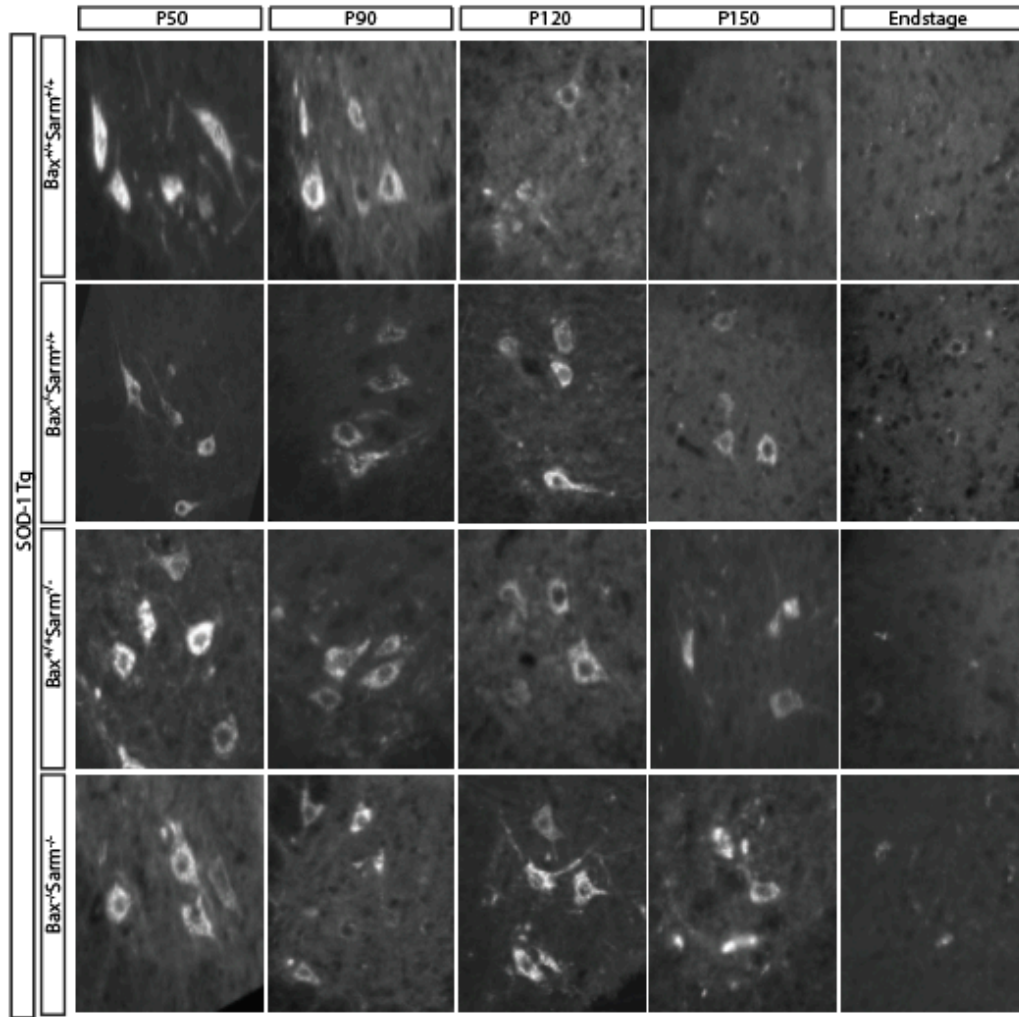


Figure A2.1. MMP-9+ cell body in ventral horn of spinal cord. Representative images of MMP-9+ stained 12 μ m spinal cord sections labeling cell bodies in (A) *SOD-1^{G93A} Tg*, (B) *SOD-1^{G93A} Tg, Bax^{-/-} Sarm^{+/+}*, (C) *SOD-1^{G93A} Tg, Bax^{+/+} Sarm^{-/-}*, and (D) *SOD-1^{G93A} Tg, Bax^{-/-} Sarm^{-/-}* animals (n=3 for each timepoint) were dissected when each reached P50, P90, P120, P150, and endstage.

Appendix 3. Treatment of infection with antibiotics

In the middle of the study we were conducting, we noticed something odd occurring. The mice that contained the *SOD-1*^{G93A} transgene were dying earlier than their expected lifespan of ~P165 and they were progressing very rapidly from Score 2 to Score 4, irrespective of genotype (Figure A3.1). This phenomenon was ensuing with all animals that reached late stage, while WT animals were unaffected. Blood samples were collected and pathological analysis was done on these mice that died early. No extreme abnormalities were discovered from this analysis.

We decided that it was possible that the mice may be harboring some sort of infection, so we treated the mice with broad-spectrum antibiotics. The problem resolved itself in mice treated with two weeks of SulfaTrim rodent chow. All mice without two weeks of treatment were removed from the analysis and some mice from Cohort 2 were added to this cohort to compensate for the loss of mice.

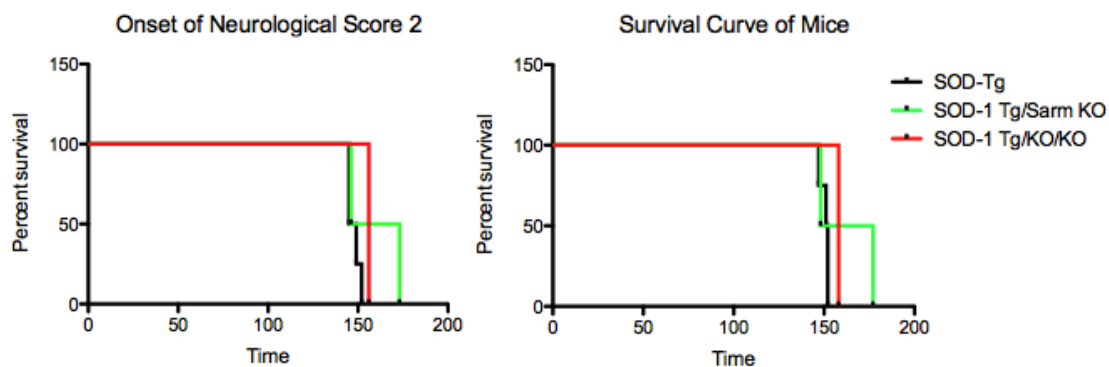


Figure A3.1 Abnormalities in disease progression of *SOD-1^{G93A}* Tg animals.

A) Time when mice reached neurological score 2 and B) reached score 4, the phenotype at which they were sacrificed. *SOD-1^{G93A}* Tg animals (black line) (n=3), *SOD-1^{G93A}* Tg/*Sarm* KO (green line) (n=2), and *SOD-1* Tg/*Bax* KO/*Sarm* KO (red line) (n=1). Survival of mice correlated with onset of Score 2.

References

- Abe K, Aoki M, Ikeda M, Watanabe M, Hirai S, Itoyama Y. (1996) Clinical characteristics of familial amyotrophic lateral sclerosis with Cu/Zn superoxide dismutase gene mutations. *J. Neurol. Sci.* 136:108–16
- Amato, A. & Russell, J. *Neuromuscular Disorders* 97–113 (McGraw-Hill, 2008).
- Andersen, P. M. & Al-Chalabi, A. (2011). Clinical genetics of amyotrophic lateral sclerosis: what do we really know? *Nat. Rev. Neurol.* 7, 603–615.
- Araki, T., Sasaki, Y., and Milbrandt, J. (2004). Increased nuclear NAD biosynthesis and SIRT1 activation prevent axonal degeneration. *Science* 305, 1010– 1013.
- Babetto, E., Beirowski, B., Janeckova, L., Brown, R., Gilley, J., Thomson, D., Ribchester, R.R., and Coleman, M.P. (2010). Targeting NMNAT1 to axons and synapses transforms its neuroprotective potency in vivo. *J. Neurosci.* 30, 13291–13304.
- Bendotti C, Calvaresi N, Chiveri L et al (2001) Early vacuolization and mitochondrial damage in motor neurons of FALS mice are not associated with apoptosis or with changes in cytochrome oxidase histochemical reactivity. *J Neurol Sci* 191:25–33
- Beirowski, B., Babetto, E., Coleman, M.P., and Martin, K.R. (2008). The WldS gene delays axonal but not somatic degeneration in a rat glaucoma model. *Eur. J. Neurosci.* 28, 1166–1179.
- Boillée S, Vande Velde C, Cleveland DW (2006) ALS: a disease of motor neurons and their nonneuronal neighbors. *Neuron* 52: 39-59.
- Brännström T, Ernhill K, Jonsson A, Nilsson A, Marklund S. (2000). SOD1 immunoreactive precipitates in mice transgenic for human SOD1 with and without mutations. *Brain Pathol*; 10: 775.
- Brujin LI, Becher MW, Lee MK et al. (1997). ALS-linked SOD1 mutant G85R mediates damage to astrocytes and promotes rapidly progressive disease with SOD1-containing inclusions. *Neuron*; 18: 327-338
- Brujin L, Miller TM, Cleveland DW (2004) Unraveling the mechanisms involved in motor neuron degeneration in ALS. *Annu Rev Neurosci* 27:723–749

Chen, Y.Z. et al. (2004). DNA/RNA helicase gene mutations in a form of juvenile amyotrophic lateral sclerosis (ALS4). *Am. J. Hum. Genet.* 74, 1128–1135.

Chiò, A., Calvo, A., Moglia, C., Mazzini, L. & Mora, G. (2011). Phenotypic heterogeneity of amyotrophic lateral sclerosis: a population based study. *J. Neurol. Neurosurg. Psychiatry* **82**, 740–746.

Clarke, P.G.H. (1999) Apoptosis versus necrosis. In *Cell death and diseases of the nervous system*. V.E. Koliatsos and R.R. Ratan, editors. Humana Press. Totowa, New Jersey, USA. 3–28.

Clement A. M., Nguyen M. D., Roberts E. A., Garcia M. L., Boillee S., Rule M., et al. . (2003). Wild-type nonneuronal cells extend survival of SOD1 mutant motor neurons in ALS mice. *Science* 302, 113–117.

Conforti, L., Tarlton, A., Mack, T.G., Mi, W., Buckmaster, E.A., Wagner, D., Perry, V.H., and Coleman, M.P. (2000). A Ufd2/D4Cole1e chimeric protein and overexpression of Rbp7 in the slow Wallerian degeneration (WldS) mouse. *Proc. Natl. Acad. Sci. U S A* 97, 11377–11382.

Corson LB, Strain JJ, Culotta VC, Cleveland DW (1998). Chaperone-facilitated copper binding is a property common to several classes of familial amyotrophic lateral sclerosis-linked superoxide dismutase mutants. *Proc. Natl. Acad. Sci. USA* 95:6361-66.

Dadon-Nachum M, Melamed E, Offen D (2011) The “dying-back” phenomenon of motor neurons in ALS. *J Mol Neurosci* **43**: 470–477

Dal Canto MC, Gurney ME. (1995). Neuropathological changes in two lines of mice carrying a transgene for mutant human Cu,Zn SOD, and in mice overexpressing wild-type human SOD: A model of familial amyotrophic lateral sclerosis (FALS). *Brain Res*; 676: 25-40.

Dal Canto MC, Gurney ME. (1997). A low expressor line of transgenic mice carrying a mutant human Cu,Zn superoxide dismutase (SOD1) gene develops pathological changes that most closely resemble those in human amyotrophic lateral sclerosis. *Acta Neuropathol*; 93: 537-550.

de Boer AS, Koszka K, Kiskinis E, Suzuki N, Davis-Dusenbery BN, Eggan K. (2014) Genetic validation of a therapeutic target in a mouse model of ALS. *Sci Transl Med.*;6(248):248ra104.

- DeJesus-Hernandez, M. et al. Expanded GGGGCC hexanucleotide repeat in noncoding region of C9ORF72 causes chromosome 9p-linked FTD and ALS. *Neuron* 72, 245–256 (2011).
- Deveraux QL, Reed JC (1999) IAP family proteins—suppressors of apoptosis. *Genes Dev* 13:239–252.
- Duquette, A. et al. Mutations in senataxin responsible for Quebec cluster of ataxia with neuropathy. *Ann. Neurol.* 57, 408–414 (2005).
- Ekegren, T., Grundstrom, E., Lindholm, D. & Aquilonius, S. M. Upregulation of Bax protein and increased DNA degradation in ALS spinal cord motor neurons. *Acta Neurol. Scand.* 100, 317–321 (1999).
- Eymard-Pierre, E. et al. Infantile-onset ascending hereditary spastic paralysis is associated with mutations in the alsin gene. *Am. J. Hum. Genet.* 71, 518–527 (2002).
- Feinberg DM, Preston DC, Shefner JM, Logigian EL (1999) Amplitude dependent slowing of conduction in amyotrophic lateral sclerosis and polyneuropathy. *Muscle Nerve* 22:1646– 1651
- Felice KJ (1997) A longitudinal study comparing thenar motor unit number estimates to other quantitative tests in patients with amyotrophic lateral sclerosis. *Muscle Nerve* 20(2):179–185
- Ferraiuolo L, Kirby J, Grierson AJ, Sendtner M, Shaw PJ (2011) Molecular pathways of motor neuron injury in amyotrophic lateral sclerosis. *Nat Rev Neurol* 7: 616-630.
- Ferri, A., Sanes, J. R., Coleman, M. P., Cunningham, J. M., and Kato, A. C. (2003). Inhibiting axon degeneration and synapse loss attenuates apoptosis and disease progression in a mouse model of motoneuron disease. *Curr. Biol.* 13, 669–673. doi: 10.1016/s0960-9822(03)00206-9
- Ferrari, R., Kapogiannis, D., Huey, E. D. & Momeni, P. FTD and ALS: a tale of two diseases. *Curr. Alzheimer Res.* 8, 273–294 (2011).
- Fischer LR, Culver DG, Tennant P et al (2004) Amyotrophic lateral sclerosis is a distal axonopathy: evidence in mice and man. *Exp Neurol* 185(2):232–240
- Fridovich, I. (1976) Superoxide dismutases: studies of structure and mechanism. *Adv. Exp. Med. Biol.* 74:530-39.

Fridovich I. 1997. Superoxide anion radical (O₂⁻), superoxide dismutases, and related matters. *J. Biol. Chem.* 272: 18515-17

Frey D, Schneider C, Xu L, Borg J, Spooren W, Caroni P (2000) Early and selective loss of neuromuscular synapse subtypes with low sprouting competence in motoneuron diseases. *J Neurosci* 20:2534–2542

Ghadge, GD, et al. Mutant superoxide dismutase-1-linked familial amyotrophic lateral sclerosis: molecular mechanisms of neuronal death and protection. *J. Neurosci.* 1997.**17**:8756-8766.

Gilley, J., and Coleman, M.P. (2010). Endogenous Nmnat2 is an essential survival factor for maintenance of healthy axons. *PLoS Biol.* 8, e1000300.

Gillingwater, T. H. et al. Age-dependent synapse withdrawal at axotomised neuromuscular junctions in WldS mutant and Ube4b/Nmnat transgenic mice. *J. Physiol. (Lond.)* 543, 739–755 (2002).

Gonzalez de Aguilar, J. L. et al. Alteration of the Bcl-x/Bax ratio in a transgenic mouse model of amyotrophic lateral sclerosis: evidence for the implication of the p53 signaling pathway. *Neurobiol. Dis.* 7, 406–415 (2000).

Gould, T.W., Buss, R.R., Vinsant, S., Prevette, D., Sun, W., Knudson, C.M., Milligan, C.E., Oppenheim, R.W., 2006. Complete dissociation of motor neuron death from motor dysfunction by *Bax* deletion in a mouse model of ALS. *J. Neurosci.* 26, 8774–8786.

Guegan, C., Vila, M., Rosoklija, G., Hays, A. P. & Przedborski, S. Recruitment of the mitochondrial-dependent apoptotic pathway in amyotrophic lateral sclerosis. *J. Neurosci.* 21, 6569–6576 (2001).

Guegan, C. et al. Instrumental activation of Bid by caspase-1 in a transgenic mouse model of ALS. *Mol. Cell. Neurosci.* 20, 553 (2002).

Gurney ME, Pu H, Chiu AY, Dal Canto MC, Polchow CY, et al. Motor neuron degeneration in mice that express a human Cu,Zn superoxide dismutase mutation 1994. *Science* 264:1772–75

Hadano, S. et al. A gene encoding a putative GTPase regulator is mutated in familial amyotrophic lateral sclerosis 2. *Nat. Genet.* 29, 166–173 (2001).

Hasbani, D.M., and O'Malley, K.L. (2006). Wld(S) mice are protected against the Parkinsonian mimetic MPTP. *Exp. Neurol.* 202, 93–99.

Hayward LJ, Rodriguez JA, Kim JW, Tiwari A, Goto JJ, et al. 2002. Decreased metallation and activity in subsets of mutant superoxide dismutases associated with familial amyotrophic lateral sclerosis. *J. Biol. Chem.* 277:15923–31

Hayworth CR, Gonzales-Lima F (2009) Pre-symptomatic detection of chronic motor deficits genotype prediction in congenic B6. SOD1G93A ALS mouse model. *Neuroscience* 164:975–85

He, BP, Strong, MJ. Motor neuronal death in sporadic amyotrophic lateral sclerosis (ALS) is not apoptotic. A comparative study of ALS and chronic aluminium chloride neurotoxicity in New Zealand white rabbits. *Neuropathol. Appl. Neurobiol.* 2000. **26**:150-160.

Hegedus J, Putman CT, Gordon T (2007) Time course of preferential motor unit loss in the SOD1G93A mouse model of amyotrophic lateral sclerosis. *Neurobiol Dis* 28:154–164

Hengartner, M.O. (2000). The biochemistry of apoptosis. *Nature* 407, 770–776.

Ilieva EV, Ayala V, Jové M et al (2007) Oxidative and endoplasmic reticulum stress interplay in sporadic amyotrophic lateral sclerosis. *Brain* 130:3111–23

Iwanaga, K. *et al.* Neuropathology of sporadic amyotrophic lateral sclerosis of long duration. *J. Neurol. Sci.* **146**, 139–143 (1997).

Johnston JA, Dalton MJ, Gurney ME, Kopito RR. Exome sequencing reveals VCP mutations as a cause of familial ALS. 2000. *Proc. Natl. Acad. Sci. USA* 97:12571–76

Johnson, J.O. et al. Exome sequencing reveals VCP mutations as a cause of familial ALS. *Neuron* 68, 857–864 (2010).

Juneja T, Pericak-Vance MA, Laing NG, Dave S, Siddique T. Prognosis in familial amyotrophic lateral sclerosis: progression and survival in patients with glu100gly and ala4val mutations in Cu, Zn superoxide dismutase. 1997. *Neurology* 48: 55–57

Kostic, V., Jackson-Lewis, V., De Bilbao, F., Dubois-Dauphin, M. & Przedborski, S. Bcl-2: prolonging life in a transgenic mouse model of familial amyotrophic lateral sclerosis. *Science* 277, 559–562 (1997).

Kurland, L.T., Mulder, D.W., 1955. Epidemiologic investigations of amyotrophic lateral sclerosis. 2. Familial aggregations indicative of dominant inheritance II. *Neurology* 5, 249–268.

Kwiatkowski, T.J. Jr. et al. Mutations in the FUS/TLS gene on chromosome 16 cause familial amyotrophic lateral sclerosis. *Science* 323, 1205–1208 (2009).

Leblond CS, Kaneb HM, Dion PA, Rouleau GA. Dissection of genetic factors associated with amyotrophic lateral sclerosis. *Exp Neurol*. 2014;262(pt B):91–101.

Lev N, Ickowicz D, Barhum Y, Melamed E, Offen D (2009) DJ-1 changes in G93A-SOD1 transgenic mice: Implications for oxidative stress in ALS. *J Mol Neurosci* 38:94–102

Li, P. et al. Cytochrome c and dATP-dependent formation of Apaf-1/caspase-9 complex initiates an apoptotic protease cascade. *Cell* 91, 479–489 (1997).

Li, M. et al. Functional role of caspase-1 and caspase-3 in an ALS transgenic mouse model. *Science* 288, 335–339 (2000)

Liu, X., Zou, H., Slaughter, C. & Wang, X. DFF, a heterodimeric protein that functions downstream of caspase-3 to trigger DNA fragmentation during apoptosis. *Cell* 89, 175–184 (1997).

Logroscino G, Traynor BJ, Hardiman O, Chio' A, Couratier P, Mitchell JD, et al. Descriptive epidemiology of amyotrophic lateral sclerosis: New evidence and unsolved issues. *J Neurol Neurosurg Psychiatry*. 2008;79:6–11.

Lunn, E.R., Perry, V.H., Brown, M.C., Rosen, H., and Gordon, S. (1989). Absence of Wallerian Degeneration does not Hinder Regeneration in Peripheral Nerve. *Eur. J. Neurosci*. 1, 27–33.

Martin, LJ. Neuronal death in amyotrophic lateral sclerosis is apoptosis: possible contribution of a programmed cell death mechanism. *J. Neuropathol. Exp. Neurol*. 1999;**58**:459-471.

Maruyama, H. et al. Mutations of optineurin in amyotrophic lateral sclerosis. *Nature* 465, 223–226 (2010).

Mi, W., Beirowski, B., Gillingwater, T.H., Adalbert, R., Wagner, D., Grumme, D., Osaka, H., Conforti, L., Arnhold, S., Addicks, K., et al. (2005). The slow Wallerian degeneration gene, *WldS*, inhibits axonal spheroid pathology in gracile axonal dystrophy mice. *Brain* 128, 405–416.

Migheli, A, Cavalla, P, Marino, S, Schiffer, D. A study of apoptosis in normal and pathologic nervous tissue after in situ end-labeling of DNA strand breaks. *J. Neuropathol. Exp. Neurol.* 1994. **53**:606-616

Migheli, A, et al. Lack of apoptosis in mice with ALS. *Nat. Med.* 1999. **5**:966-967.

Mioshi, E. *et al.* Neuropsychiatric changes precede classic motor symptoms in ALS and do not affect survival. *Neurology* **82**, 149–155 (2014).

Morrison BM, Morrison JH, Gordon JW. 1998. Superoxide dismutase and neurofilament transgenic models of amyotrophic lateral sclerosis. *J. Exp. Zool.* 282:32–47

Nagai M, Aoki M, Miyoshi I, Kato M, Pasinelli P, et al. 2001. Rats expressing human cytosolic copper-zinc superoxide dismutase transgenes with amyotrophic lateral sclerosis: associated mutations develop motor neuron disease. *J. Neurosci.* 21: 9246–54

Nagai M, Re DB, Nagata T, Chalazonitis A, Jessell TM, Wichterle H, Przedborski S. Astrocytes expressing ALS-linked mutated SOD1 release factors selectively toxic to motor neurons. *Nat Neurosci.* 2007;10:615–622.

Okado-Matsumoto A, Fridovich I. 2001. Subcellular distribution of superoxide dismutases (SOD) in rat liver: Cu, Zn-SOD in mitochondria. *J. Biol. Chem.* 276: 38388-93

Orrell RW, Habgood JJ, Malaspina A, Mitchell J, Greenwood J, et al. (1999) Clinical characteristics of SOD1 gene mutations in UK families with ALS. *J. Neurol. Sci.* 169:56–60

Osterloh, J.M., Yang, J., Rooney, T.M., Fox, A.N., Adalbert, R., Powell, E.H., Sheehan, A.E., Avery, M.A., Hackett, R., Logan, M.A., et al. (2012). dSarm/ Sarm1 is required for activation of an injury-induced axon death pathway. *Science* 337, 481–484.

O'Toole O, et al. Epidemiology clinical features of amyotrophic lateral sclerosis in Ireland between 1995 and 2004. *J Neurol Neurosurg Psychiatry.* 2008;79(1):30–32.

Parton MJ, Broom W, Andersen PM, AlChalabi A, Nigel Leigh P, et al. (2002) D90A-SOD1 mediated amyotrophic lateral sclerosis: a single founder for all cases with evidence for a Cis-acting disease modifier in the recessive haplotype. *Hum. Mutat.* 20:473

Pramatarova A.; Laganière J.; Roussel J.; Brisebois K.; Rouleau G. A. (2001) Neuron-specific expression of mutant superoxide dismutase 1 in transgenic mice does not lead to motor impairment. *J. Neurosci.* 21:3369–3374

Pun S, Santos AF, Saxena S, Xu L, Caroni P (2006) Selective vulnerability and pruning of phasic motoneuron axons in motoneuron disease alleviated by CNTF. *Nat Neurosci* 9:408–419

Pupillo, E., Messina, P., Logroscino, G. & Beghi, E. (2014) Long-term survival of amyotrophic lateral sclerosis: a population-based study. *Ann. Neurol.* **75**, 287–297.

Rabizadeh S, Gralla EB, Borchelt DR, Gwinn R, Valentine JS, et al. (1995). Mutations associated with amyotrophic lateral sclerosis convert superoxide dismutase from an antiapoptotic gene to a proapoptotic gene: studies in yeast and neural cells. *Proc. Natl. Acad. Sci. USA* 92:3024–28

Ratovitski T, Corson LB, Strain J, Wong P, Cleveland DW, et al. (1999) Variation in the biochemical/biophysical properties of mutant superoxide dismutase 1 enzymes and the rate of disease progression in familial amyotrophic lateral sclerosis kindreds. *Hum. Mol. Genet.* 8:1451–60

Reaume, A.G. et al. (1996) Motor neurons in Cu/Zn superoxide dismutase-deficient mice develop normally but exhibit enhanced cell death after axonal injury. *Nat. Genet.* 13, 43–47

Renton, A.E. et al. A hexanucleotide repeat expansion in C9ORF72 is the cause of chromosome 9p21-linked ALS-FTD. *Neuron* 72, 257–268 (2011).

Renton, A.E., Chio, A., Traynor, B.J., 2014. State of play in amyotrophic lateral sclerosis genetics. *Nat. Neurosci.* 17 (1), 17–23.

Ripps ME, Huntley GW, Hor PR et al. Transgenic mice expressing an altered murine superoxide dismutase gene provide an animal model of amyotrophic lateral sclerosis. *Proc Natl Acad Sci USA* 1995; 92: 689-693

Rodriguez JA, Valentine JS, Eggers DK, Roe JA, Tiwari A, et al. (2002) Familial amyotrophic lateral sclerosis-associated mutations decrease the thermal stability of distinctly metallated species of human copper/zinc superoxide dismutase. *J. Biol. Chem.* 277:15932–37

Rosen, D.R. et al. Mutations in Cu/Zn superoxide dismutase gene are associated with familial amyotrophic lateral sclerosis. *Nature* 362, 59–62 (1993).

- Sabatelli, M. *et al.* Natural history of young-adult amyotrophic lateral sclerosis. *Neurology* **71**, 876–881 (2008).
- Sajadi, A., Schneider, B.L., and Aebischer, P. (2004). Wlds-mediated protection of dopaminergic fibers in an animal model of Parkinson disease. *Curr. Biol.* **14**, 326–330.
- Sakahira, H., Enari, M. & Nagata, S. Cleavage of CAD inhibitor in CAD activation and DNA degradation during apoptosis. *Nature* **391**, 96–99 (1998).
- Sasaki, Y., Vohra, B.P.S., Baloh, R.H., and Milbrandt, J. (2009). Transgenic mice expressing the Nmnat1 protein manifest robust delay in axonal degeneration in vivo. *J. Neurosci.* **29**, 6526–6534.
- Schmalbruch H., Jensen H.J., Bjaerg M., Kamieniecka Z., Kurland L. (1991). A new mouse mutant with progressive motor neuronopathy. *J. Neuropathol. Exp. Neurol.* **50**:192-204.
- Siklos L, Engelhardt J, Harati Y, Smith RG, Joo F, Appel SH (1996) Ultrastructural evidence for altered calcium in motornerve terminals in amyotrophic lateral sclerosis. *Ann Neurol.* **39**(2). 203-16
- Soto C. 2003. Unfolding the role of protein misfolding in neurodegenerative diseases. *Nat. Rev. Neurosci.* **4**:49– 60
- Strong, M. J. & Yang, W. The frontotemporal syndromes of ALS. Clinicopathological correlates. *J. Mol. Neurosci.* **45**, 648–655 (2011).
- Sreedharan, J. et al. TDP-43 mutations in familial and sporadic amyotrophic lateral sclerosis. *Science* **319**, 1668–1672 (2008).
- Sreedharan J, Brown RH Jr. Amyotrophic lateral sclerosis: Problems and prospects. *Ann Neurol.* **2013**;74(3):309–316.
- Sturtz LA, Diekert K, Jensen LT, Lill R, Culotta VC. 2001. A fraction of yeast Cu, Zn-superoxide dismutase and its metallochaperone, CCS, localize to the intermembrane space of mitochondria. A physiological role for SOD1 in guarding against mitochondrial oxidative damage. *J. Biol. Chem.* **276**: 38084-89.
- Swinnen B, Robberecht W. The phenotypic variability of amyotrophic lateral sclerosis. *Nat Rev Neurol.* **2014**;10(11):661–670.

Tiwari A, Hayward LJ. (2003). Familial amyotrophic lateral sclerosis mutants of copper/zinc superoxide dismutase are susceptible to disulfide reduction. *J. Biol Chem.* 278:5984-92.

Tsao, J.W., Brown, M.C., Carden, M.J., McLean, W.G., and Perry, V.H. (1994). Loss of the compound action potential: an electrophysiological, biochemical and morphological study of early events in axonal degeneration in the C57BL/Ola mouse. *Eur. J. Neurosci.* 6, 516–524.

Valentine JS, Hart PJ. 2003. Misfolded CuZnSOD and amyotrophic lateral sclerosis. *Proc. Natl. Acad. Sci. USA* 100:3617–22

Valentine, J.S. et al. (2004) Copper–zinc superoxide dismutase and amyotrophic lateral sclerosis. *Annu. Rev. Biochem.* 74, 563– 593

Vance, C. et al. Mutations in FUS, an RNA processing protein, cause familial amyotrophic lateral sclerosis type 6. *Science* 323, 1208–1211 (2009).

Vande Velde, C., Garcia, M. L., Yin, X., Trapp, B. D., and Cleveland, D. W. (2004). The neuroprotective factor Wlds does not attenuate mutant SOD1-mediated motor neuron disease. *Neuromolecular Med.* 5, 193–203.

Vazquez MC, Ketzoian C, Legnani C, Rega I, Sanchez N, Perna A, et al. Incidence and prevalence of amyotrophic lateral sclerosis in Uruguay: A population-based study. *Neuroepidemiology.* 2008;30:105-11.

Vila, M., and Przedborski, S. (2003). Neurological diseases: Targeting programmed cell death in neurodegenerative diseases. *Nat Rev Neurosci* 4, 365–375

Vukosavic, S. et al. (2000) Delaying caspase activation by Bcl-2: a clue to disease retardation in a transgenic mouse model of amyotrophic lateral sclerosis. *J. Neurosci.* 20, 9119–9125.

Wang J, Xu G, Borchelt DR. (2002). Fibrillar inclusions and motor neuron degeneration in transgenic mice expressing superoxide dismutase 1 with a disrupted copper-binding site. *Neurobiol. Dis.* 9:139-48.

Wang, M.S., Davis, A.A., Culver, D.G., and Glass, J.D. (2002). WldS mice are resistant to paclitaxel (taxol) neuropathy. *Ann. Neurol.* 52, 442–447.

Wang, J.T., Medress, Z.A., Vargas, M.E., and Barres, B.A. (2015). Local axonal protection by WldS as revealed by conditional regulation of protein stability. *Proc. Natl. Acad. Sci. U S A* 112, 10093–10100.

Whitmore, A.V., Lindsten, T., Raff, M.C. & Thompson, C.B. (2003). The proapoptotic proteins Bax and Bak are not involved in Wallerian degeneration. *Cell Death Differ* **10**, 260-261.

Willis, S. N. et al. (2007). Apoptosis initiated when BH3 ligands engage multiple Bcl-2 homologs, not Bax or Bak. *Science* 315, 856–859.

Wong PC, Pardo CA, Borchelt DR et al. (1995). An adverse property of a familial ALS-linked SOD1 mutation causes motor neuron disease characterized by vacuolar degeneration of mitochondria. *Neuron*; 14: 1105-1116

Xu D, Bureau Y, McIntyre DC, Nicholson DW, Liston P, Zhu Y, Fong WG, Crocker SJ, Korneluk RG, Robertson GS (1999) Attenuation of ischemia-induced cellular and behavioral deficits by X chromosomelinked inhibitor of apoptosis protein overexpression in the rat hippocampus. *J Neurosci* 19:5026–5033.

Yoshiyama, Y, Yamada, T, Asanuma, K, Asahi, T. (1994). Apoptosis related antigen, Le(Y) and nick-end labeling are positive in spinal motor neurons in amyotrophic lateral sclerosis. *Acta Neuropathol. (Berl.)* **88**:207-211.

Youle, R.J., and Strasser, A. (2008). The BCL-2 protein family: opposing activities that mediate cell death. *Nat Rev Mol Cell Biol* 9, 47–59.

Zhu, S. et al. (2002). Minocycline inhibits cytochrome c release and delays progression of amyotrophic lateral sclerosis in mice. *Nature* 417, 74–78.

Zoccolella, S. *et al.* (2008). Analysis of survival and prognostic factors in amyotrophic lateral sclerosis: a population based study. *J. Neurol. Neurosurg. Psychiatry* **79**, 33–37.